

# UNCLASSIFIED

AD NUMBER
AD916280
NEW LIMITATION CHANGE
TO Approved for public release, distribution unlimited
FROM Distribution authorized to U.S. Gov't. agencies only; Test and Evaluation; OCT 1973. Other requests shall be referred to Naval Underwater Systems Center, New London, CT 06320.
AUTHORITY
usnusc, ltr, 23 aug 1974

THIS PAGE IS UNCLASSIFIED

AD 916280

NUC Technical Publication 372

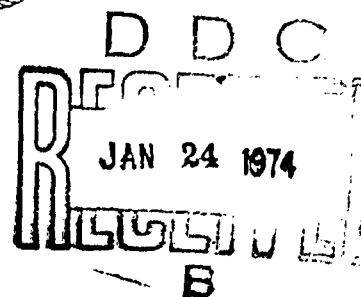
NUSC Technical Report 4527

## Navy Interim Surface Ship Model (NISSM) II

HENRY WEINBERG  
*Computer Laboratory*  
*Naval Underwater Systems Center*



14 November 1973



NAVAL UNDERWATER SYSTEMS CENTER  
and  
NAVAL UNDERSEA CENTER


Distribution limited to U. S. Government agencies only; Test and Evaluation;  
14 November 1973. Other requests for this document must be referred to the  
Naval Underwater Systems Center.

## PREFACE

This report was prepared under Project Nos. A-914-03 and B-914-03, "NISSM II Documentation" (U), Principal Investigator, H. Weinberg (Code PA4), and Navy Subproject and Task No. NIF. The coordinating activity is the Naval Undersea Center, Project Coordinator, L. K. Arndt (Code 502), and the sponsoring activity is the Naval Ship Systems Command, Program Manager, C. D. Smith (Code PMS-302-44).

The Technical Reviewer for this report was L. K. Arndt (Code 502), Naval Undersea Center.

REVIEWED AND APPROVED: 14 November 1973



R. M. Dunlap  
Director for Plans and Analysis

Inquiries concerning this report may be addressed to the author,  
New London Laboratory, Naval Underwater Systems Center,  
New London, Connecticut 06320

UNCLASSIFIED

SECURITY CLASSIFICATION OF THIS PAGE (When Data Entered)

REPORT DOCUMENTATION PAGE		READ INSTRUCTIONS BEFORE COMPLETING FORM	
1. REPORT NUMBER NUSC      NUC TR 4527    TP 372		2. GOVT ACCESSION NO.	3. RECIPIENT'S CATALOG NUMBER
4. TITLE (and Subtitle)  NAVY INTERIM SURFACE SHIP MODEL (NISSM) II		5. TYPE OF REPORT & PERIOD COVERED	
		6. PERFORMING ORG. REPORT NUMBER	
7. AUTHOR(s)  Henry Weinberg		8. CONTRACT OR GRANT NUMBER(s)	
9. PERFORMING ORGANIZATION NAME AND ADDRESS Naval Underwater Systems Center, New London Laboratory, New London, Connecticut 06320 and Naval Undersea Center, San Diego, California 92132		10. PROGRAM ELEMENT, PROJECT, TASK AREA & WORK UNIT NUMBERS A-914-03 B-914-03 NIF	
11. CONTROLLING OFFICE NAME AND ADDRESS Naval Undersea Center San Diego, California 92132		12. REPORT DATE 14 November 1973	
		13. NUMBER OF PAGES 128	
14. MONITORING AGENCY NAME & ADDRESS (if different from Controlling Office)		15. SECURITY CLASS. (of this report)  UNCLASSIFIED	
		15a. DECLASSIFICATION/DOWNGRADING SCHEDULE	
16. DISTRIBUTION STATEMENT (of this Report) Distribution limited to U. S. Government agencies only; Test and Evaluation; October 1973. Other requests for this document must be referred to the Naval Underwater Systems Center.			
17. DISTRIBUTION STATEMENT (of the abstract entered in Block 20, if different from Report)			
18. SUPPLEMENTARY NOTES			
19. KEY WORDS (Continue on reverse side if necessary and identify by block number) Active Sonar Systems      FORTRAN V Computer Program Boundary Reverberation    Geometrical Spreading Loss Continuous Function of Depth    Navy Interim Surface Ship Model (NISSM) II False-Alarm Rate      Probability of Detection False Caustics      Propagation Losses			
20. ABSTRACT (Continue on reverse side if necessary and identify by block number) A computer program, Navy Interim Surface Ship Model (NISSM) II, has been developed to predict the performance of active sonar systems. Thereby acoustic ray trajectories, propagation-loss curves, boundary and volume reverberation, signal-to-noise ratios, and the probability of detection are determined using continuous-gradient ray-tracing techniques. Caustic, shadow zone, and surface-duct corrections modify the classical ray theory. The major limitations of the model are that the ocean bottom must be horizontal and the velocity of sound may not vary with range.			

DD FORM 1473 JAN 73 EDITION OF 1 NOV 65 IS OBSOLETE

UNCLASSIFIED  
SECURITY CLASSIFICATION OF THIS PAGE (When Data Entered)



UNCLASSIFIED

SECURITY CLASSIFICATION OF THIS PAGE(When Data Entered)

19. (Cont'd)

Ray-Tracing Techniques

Ray Trajectories

Target Range

Velocity of Sound

Volume-Scattering Strength

Volume Reverberation

Volume-Reverberation Computation

UNCLASSIFIED

SECURITY CLASSIFICATION OF THIS PAGE(When Data Entered)

## TABLE OF CONTENTS.

	Page
LIST OF ILLUSTRATIONS . . . . .	iii
LIST OF TABLES . . . . .	v
INTRODUCTION . . . . .	1
Part I. THEORY	
NUMERICAL INTEGRATION OF RAY-TRACING INTEGRALS . . . . .	3
TEMPERATURE-SALINITY-DEPTH TO VELOCITY CONVERSION . . . . .	7
CORRECTION FOR EARTH'S CURVATURE . . . . .	8
PROPAGATION LOSS ALONG A RAY . . . . .	9
Surface Loss . . . . .	10
Bottom Loss . . . . .	11
Absorption Coefficient . . . . .	18
EIGENRAYS . . . . .	19
SHADOW-ZONE PROPAGATION . . . . .	21
UNIFORM ASYMPTOTIC EXPANSION AT A CAUSTIC . . . . .	24
PHASE SHIFTS. . . . .	26
SURFACE-DUCT PROPAGATION . . . . .	28
PROPAGATION LOSS VERSUS RANGE AT A CONSTANT DEPTH . . . . .	28
REVERBERATION THEORY . . . . .	29
Volume Reverberation . . . . .	32
Surface Reverberation . . . . .	34
Bottom Reverberation . . . . .	35
Total Reverberation . . . . .	35
TARGET ECHO . . . . .	36
NOISE . . . . .	36
TARGET ECHO TO MASKING BACKGROUND . . . . .	37
PROBABILITY OF DETECTION . . . . .	39
REMARKS . . . . .	40

## TABLE OF CONTENTS (Cont'd)

	Page
Part II. USER'S MANUAL	
HARDWARE AND SOFTWARE REQUIREMENTS . . . . .	41
PARAMETER CARDS . . . . .	47
INPUT TABLES . . . . .	56
CALCOMP AXIS CARDS . . . . .	59
PROCESS CARD . . . . .	59
INITIAL INCLINATION ANGLES . . . . .	60
END CARD . . . . .	60
INPUT DECK . . . . .	61
RAY DIAGRAMS, EXAMPLE 1 . . . . .	62
PROPAGATION LOSS VEPSUS RANGE, EXAMPLE 2 . . . . .	68
REVERBERATION, EXAMPLE 3 . . . . .	78
PROBABILITY OF DETECTION, EXAMPLE 4 . . . . .	85
REMARKS . . . . .	99
LIST OF REFERENCES . . . . .	101
APPENDIX A -- CONTINUOUS-GRADIENT CURVE-FITTING TECHNIQUE . . . . .	A-1
APPENDIX B -- EVALUATION OF RAY-TRACING INTEGRALS . . . . .	B-1
APPENDIX C -- AMOS SURFACE DUCT EQUATIONS . . . . .	C-1

## LIST OF ILLUSTRATIONS

Figure		Page
1	Inclination Angle Along a Ray . . . . .	3
2	Piecewise Constant-Gradient Approximation of a Sound- Velocity Profile . . . . .	5
3	Ray Diagram Plotted Using Piecewise Constant- Gradient Techniques . . . . .	6
4	Ray in an Isovelocity Medium Plotted Using Rectilinear Coordinates . . . . .	8
5	Ray in an Isovelocity Medium Plotted Using Range-Depth Coordinates . . . . .	9
6	Intersection of a Ray with the Ocean Surface . . . . .	11
7	Intersection of a Ray with the Ocean Bottom . . . . .	11
8	NUC Bottom-Loss Curves at 1.0 kHz . . . . .	13
9	NUC Bottom-Loss Curves at 3.5 kHz . . . . .	14
10	NUC Bottom-Loss Curves at 0.5 Porosity . . . . .	15
11	NUC Bottom-Loss Curves at 0.6 Porosity . . . . .	16
12	MGS Bottom-Loss Curves . . . . .	17
13	Absorption Coefficient versus Frequency for the Two Models . . . . .	19
14	Principal Ray Types . . . . .	20
15	Half-Space in Which the Velocity Decreases with Depth . . . . .	22
16	Formation of a Shadow Zone . . . . .	22
17	Propagation into a Shadow Zone . . . . .	23
18	Half-Space Within Which $(\text{Velocity})^{-2}$ Increases Linearly With Depth . . . . .	25
19	Formation of a Smooth Caustic . . . . .	25
20	Propagation Loss versus Range in the Vicinity of a Smooth Caustic . . . . .	27
21	Closed Ray Path . . . . .	30
22	Insonified Region . . . . .	33
23	Ambient Noise versus Frequency . . . . .	37
24	Narrowband Detector . . . . .	39
25	Velocity Profile for Example 1 . . . . .	66
26	Ray Diagram Corresponding to a Sonar Placed on the Sound-Channel Axis, Example 1 . . . . .	67
27	Ray Diagram Corresponding to a Sonar Placed Above the Sound-Channel Axis, Example 1 . . . . .	67
28	Velocity Profile for Example 2 . . . . .	74
29	Ray Diagram for Example 2 . . . . .	75
30	Propagation Loss for a 25-ft Target Depth, Example 2 . . . . .	76
31	Propagation Loss for a 150-ft Target Depth, Example 2 . . . . .	77

## LIST OF ILLUSTRATIONS (Cont'd)

Figure		Page
32	Velocity Profile for Example 3 . . . . .	82
33	Ray Diagram for Example 3 . . . . .	83
34	Reverberation versus Time for Example 3 . . . . .	84
35	Velocity Profile for Example 4 . . . . .	89
36	Ray Diagram for Example 4 . . . . .	90
37	Propagation Loss for Case 1 of Example 4 . . . . .	91
38	Reverberation versus Time for Case 1 of Example 4 . . . . .	92
39	Signal-to-Noise Ratio for Case 1 of Example 4 . . . . .	93
40	Probability of Detection for Case 1 of Example 4 . . . . .	94
41	Propagation Loss for Case 2 of Example 4 . . . . .	95
42	Reverberation versus Time for Case 2 of Example 4 . . . . .	96
43	Signal-to-Noise Ratio for Case 2 of Example 4 . . . . .	97
44	Probability of Detection for Case 2 of Example 4 . . . . .	98
C-1	Surface-Reflection-Loss Curve . . . . .	C-4
C-2	Imaginary Eigenvalues for the First Mode . . . . .	C-7
C-3	Propagation Losses at 10 kyd Resulting from Surface-Duct Cutoff Adjusted to FNWC Maximum Propagation Losses . . .	C-7

## LIST OF TABLES

Table		Page
1	Subroutines . . . . .	42-45
2	Input Units and Conversion Factors . . . . .	46-47
3A	Input Parameter Cards . . . . .	49-50
3B	Input Tables . . . . .	51-53
3C	Input Axis Cards . . . . .	54
4	Input Deck for Constructing Ray Diagrams, Example 1 . .	63
5	Continuous-Gradient Parameters for Example 1 . . . .	64
6	Partial Ray Printout for Example 1 . . . . .	65
7	Input Deck for Computing Propagation Loss versus Range, Example 2 . . . . .	69-70
8	Conversion of Temperature-Salinity-Depth to Velocities for Example 2 . . . . .	71
9	Continuous-Gradient Parameters for Example 2 . . . .	72
10	Partial Eigenray Printout for Example 2 . . . . .	73
11	Input Deck for Constructing Reverberation Plot, Example 3 . . . . .	79-80
12	Continuous-Gradient Parameters for Example 3 . . . .	81
13	Input Deck for Computing Probability of Detection, Example 4 . . . . .	86-87
14	Continuous-Gradient Parameters for Example 4 . . . .	88

## NAVY INTERIM SURFACE SHIP MODEL (NISSM) II

## INTRODUCTION

The Navy Interim Surface Ship Model (NISSM) II is a FORTRAN V computer program designed to predict the performance of existing and proposed active sonar systems using ray-tracing techniques. The measure of performance is expressed in terms of probability of detection versus target range for a given false-alarm rate. Several intermediate computations, including ray trajectories, propagation losses, and boundary and volume reverberation, are also displayed.

Among the noteworthy features of NISSM II is the manner in which the velocity of sound in the ocean is represented. Whereas most ray-tracing techniques use a piecewise constant gradient fit, NISSM II approximates the sound velocity with a continuous function of depth having a continuous gradient. This reduces the problem of false caustics, a computational difficulty that may be encountered in the prediction of geometrical spreading loss. Since classical ray tracing is a high-frequency solution of the wave equation and does not accurately describe low-frequency diffraction phenomena, the ray theory is modified to improve results (pp. 21-26).

The most time consuming phase in executing NISSM II is the volume-reverberation computation. The volume-scattering strength, a function of depth, is expressed in terms of scattering strength per unit volume—not as scattering strength per unit area of water column. A careful integration of the volume-reverberation integral is performed, whereby the complicated multipath structures that may be encountered in practice are considered. Typical volume-reverberation computations by the Univac 1108 Multiprocessor System require 3 min. A plot of probability of detection versus target range requires approximately 3.5 min. On the other hand, NISSM II can produce a ray diagram or a propagation-loss curve in 10 to 20 s.

The major limitations of the NISSM II model are that (1) the ocean bottom must be horizontal, (2) the velocity of sound must not vary with range, and (3) the usual constraints on ray-tracing techniques must be satisfied.

Part I of this report discusses the theoretical aspects of the NISSM II computer program. Part II, a user's manual, contains several applications of that program.

# Part I

## THEORY\*

### NUMERICAL INTEGRATION OF RAY-TRACING INTEGRALS

In numerous areas of operational interest, the velocity of sound in the ocean may be approximated by a function of depth only. Then, if interactions with non-horizontal boundaries are neglected, a ray will remain in a vertical plane. Without loss in generality, let this be denoted by the (x-z) plane. It is shown in reference 1 that the velocity,  $c(z)$ , and the inclination angle,  $\theta$ , at a point on the ray are related by Snell's law:

$$\frac{c(z)}{\cos \theta} = c_v \quad (1)$$

The vertex velocity,  $c_v$ , is a constant that depends on the initial inclination angle;  $\theta$  is measured clockwise from the positive x-axis, as shown in figure 1.

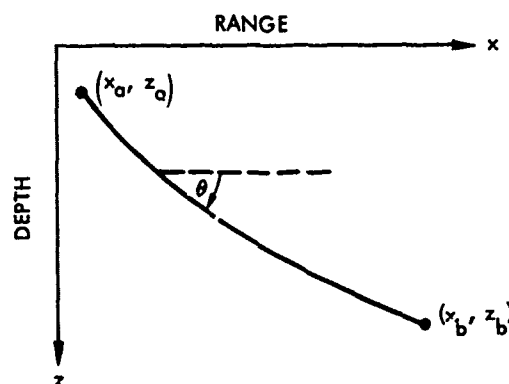


Figure 1. Inclination Angle Along a Ray

\*To prevent an excessive amount of material in the main text, the reader is referred to the appendixes and to the references for detailed analyses.



Snell's law implies that the range,  $x$ , and travel time,  $T$ , along the ray are, respectively,

$$x = x_a + \int_{z_a}^z \frac{c(z) |dz|}{\sqrt{c_v^2 - c^2(z)}} \quad (2)$$

and

$$T = T_a + \int_{z_a}^z \frac{c_v |dz|}{c(z) \sqrt{c_v^2 - c^2(z)}} \quad (3)$$

The range derivative,  $\partial x / \partial c_v$ , given by

$$\left. \frac{\partial x}{\partial c_v} \right|_{z=\text{const}} = \left. \frac{\partial x_a}{\partial c_v} \right|_{z=z_a} - \int_{z_a}^z \frac{c(z) c_v |dz|}{\left( c_v^2 - c^2(z) \right)^{3/2}}, \quad (4)$$

is used in computing the geometrical spreading-loss factor:

$$\eta_{sp} = |p| = \left| c_v \tan \theta \tan \theta_o x \frac{\partial x}{\partial c_v} \right|^{-1/2} \quad (5)$$

In the above equation,  $\theta_o$  is the inclination angle of the ray at a point source of unit magnitude situated at  $(x_a = 0, z_a = z_o)$ . The relative geometrical acoustic pressure,  $p$ , at the field point  $(x, z)$  and time,  $t$ , is then

$$p = \eta_{sp} e^{-i\omega t + i\omega T}, \quad (6)$$

where

$$\omega = 2\pi f \quad (7)$$

is the radian frequency. Since the range, travel time, and range-derivative integrals are symmetric with respect to the initial and final depths, it follows that pressure satisfies the law of reciprocity.

To evaluate the ray-tracing integrals numerically, the velocity of sound must be expressed as a known function of depth. In practice, discrete data points are used to generate an interpolation function from which the velocity at an arbitrary depth may be computed. This creates two possible approaches: (1) the resulting ray-tracing equations can be integrated in closed form or (2) the interpolation function can be used in conjunction with a numerical-integration formula.

The best-known variation of the first approach is the piecewise constant-gradient technique, where the sound velocity is approximated by linear segments as illustrated in figure 2. The corresponding ray diagram, figure 3, consists of circular arcs. Note the ray that becomes horizontal at the velocity maximum. It is called a split-ray beam since it can be refracted upward as well as downward. When the boundary-reflected rays are neglected, the constant-gradient technique predicts that no energy will enter the shadow zone. This is pessimistic, to say the least.

On the other hand, examples can be constructed for which the constant-gradient technique is optimistic. Referring back to equation (5), one sees that the pressure amplitude,  $|p|$ , becomes infinite wherever  $\partial x / \partial c_v$  vanishes. Such singular points are called caustics. However, the constant-gradient technique may also predict false caustics<sup>2</sup> and, thereby, regions of infinite intensity.

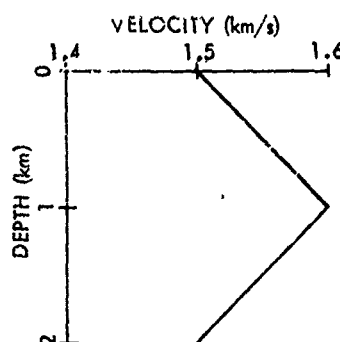


Figure 2. Piecewise Constant-Gradient Approximation of a Sound-Velocity Profile

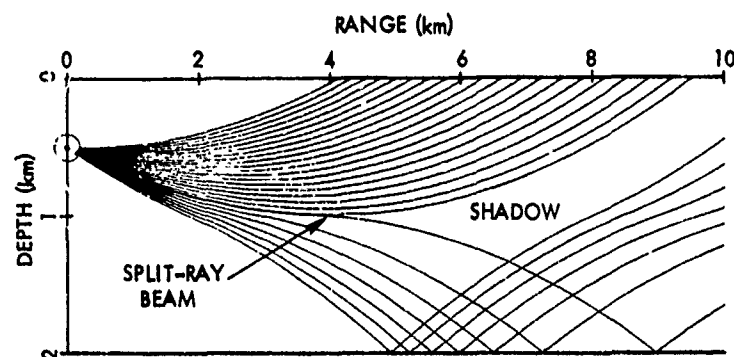


Figure 3. Ray Diagram Plotted Using Piecewise Constant-Gradient Techniques

Another variation of the first approach has been implemented in NISSM II; that is, the sound velocity is approximated by a continuous function of depth, which has a continuous gradient and allows one to integrate equations (2), (3), and (4) in terms of elementary transcendental functions. Thus false caustics associated with the constant-gradient technique have been eliminated, and further analytical investigation is possible.

The velocity interpolation function used in NISSM II is given by

$$c(z) = \left\{ v_0^{(i)} + \Delta z \frac{g_0^{(i)} + \Delta z g_1^{(i)}}{(1 + \Delta z g_2^{(i)})^2} \right\}^{-1/2} \quad (8)$$

where

$$\Delta z = z - z_0^{(i)} \quad (9)$$

in the interval

$$z_0^{(i)} \leq z < z_0^{(i+1)} \quad (10)$$

Parameters  $v_0^{(i)}$ ,  $g_0^{(i)}$ ,  $g_1^{(i)}$ , and  $g_2^{(i)}$  are chosen so that

- $c(z)$  is continuous at the velocity breakpoints,
- $\frac{dc}{dz}(z)$  is continuous at the velocity breakpoints, and
- the maximum deviation between  $c(z)$  and the input data is not to exceed 0.2 m/s.

The continuous-gradient curve-fitting technique is derived in detail in reference 3 and is summarized in appendix A. Similarly, the range, time, and range-derivative integrals are evaluated in detail in reference 4 and the results are summarized in appendix B.

#### TEMPERATURE-SALINITY-DEPTH TO VELOCITY CONVERSION

NISSM II allows the table of sound velocity to be entered directly, or indirectly, in terms of temperature, salinity, and depth. In the latter case, equation (7) in reference 5 is used to compute velocity from the temperature-salinity-depth data\*; that is,

$$c = c_o + c_a + c_b + c_c + c_d, \quad (11)$$

where

$$c_o = 1493.0 + 3(T-10) - 6 \times 10^{-3}(T-10)^2 - 4 \times 10^{-2}(T-18)^2 + 1.2(S-35) - 10^{-2}(T-18)(S-35) + Z/61; \quad (12)$$

$$c_a = + 10^{-1} \zeta^2 + 2 \times 10^{-4} \zeta^2 (T-18)^2 + 10^{-1} \zeta \phi / 90; \quad (13)$$

$$c_b = + 2.6 \times 10^{-4} T(T-5)(T-25); \quad (14)$$

$$c_c = - 10^{-3} \zeta^2 (\zeta - 4)(\zeta - 8); \quad (15)$$

$$c_d = 1.5 \times 10^{-3} (S-35)^2 (1-\zeta) + 3 \times 10^{-6} T^2 (T-30)(S-35); \quad (16)$$

---

\*Leroy<sup>5</sup> demonstrates that his equations fit Wilson's data<sup>6</sup> better than Wilson's second formula.

and

$c$  is the velocity in meters per second,

$Z$  is the depth in meters,

$\zeta$  is the depth in kilometers,

$S$  is the salinity in parts per thousand,

$T$  is the temperature in degrees centigrade, and

$\varphi$  is the latitude in degrees.

The last term in equation (11),  $c_d$ , is a corrective term for low salinities and should not be used if  $S$  is greater than 30‰.

#### CORRECTION FOR EARTH'S CURVATURE

The ray-tracing integrals (2), (3), and (4) were derived using a rectilinear coordinate system. Since it is customary to express results in terms of range along the ocean surface and depth below sea level, an appreciable error may occur in the ray trajectories unless the differences in coordinate systems are considered. For example, in the rectilinear coordinate system of figure 4, a ray in an isovelocity medium would be a straight line, and the ocean surface nearly circular. However, if one uses the range-depth coordinate system of figure 5, the ocean surface becomes horizontal and, to first order, the ray is an arc of a circle.

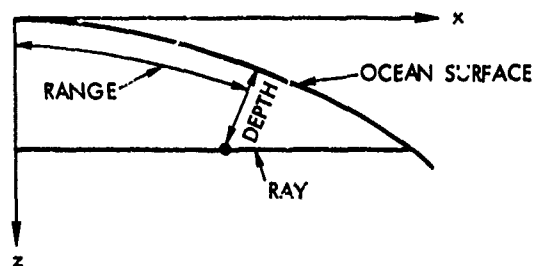


Figure 4. Ray in an IsovLOCITY Medium  
Plotted Using Rectilinear Coordinates

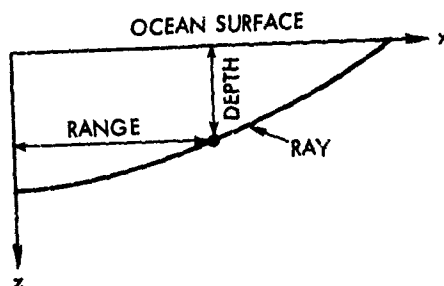


FIGURE 5. Ray in an IsovLOCITY Medium  
Plotted Using Range-Depth Coordinates

In NISSM II, correction for the earth's curvature is approximated by modifying the velocity of sound according to the equation

$$c_{\text{mod}} = c(1 + z/R) , \quad (17)$$

where

- $c_{\text{mod}}$  is the modified velocity of sound,
- $c$  is the unmodified velocity of sound,
- $z$  is the depth of the data point, and
- $R$  is the mean radius of the earth and equal to 6370 km.

Pekeris<sup>7</sup> in his discussion of velocity-modification techniques, shows that the errors introduced are small, providing that the horizontal range is less than half the earth's radius.

#### PROPAGATION LOSS ALONG A RAY

The relative acoustic pressure along a ray is obtained by multiplying the relative geometrical acoustic pressure in equation (6) by surface, bottom, and absorption-loss factors. Thus

$$p = \eta_{\text{sp}} (\eta_{\text{sur}})^{n_{\text{sur}}} (\eta_{\text{bot}})^{n_{\text{bot}}} e^{-i\omega t + i\omega T + i\Phi + \alpha s} , \quad (18)$$

where

$P = -20 \log |p|$  is the propagation loss in decibels,

$N_{sp} = -20 \log \eta_{sp}$  is the geometrical spreading loss in decibels,

$N_{sur} = -20 \log \eta_{sur}$  is the surface loss in decibels per bounce,

$N_{bot} = -20 \log \eta_{bot}$  is the bottom loss in decibels per bounce,

$A = -20 \alpha / \ln(10)$  is the absorption coefficient in decibels per kilometer,

$n_{sur}$  is the number of surface bounces,

$n_{bot}$  is the number of bottom bounces,

$t$  is the time in seconds,

$T$  is the travel time in seconds,

$\Phi$  is the accumulated phase shift in radians,

$s$  is the arc length in kilometers, and

$\omega$  is the frequency in radians per second.

## SURFACE LOSS

Surface loss may be entered as a table of surface loss per bounce,  $N_{sur}$ , versus the angle of incidence,  $\theta_{sur}$ . Here  $\theta_{sur}$  is the angle between the ray and the ocean surface at the point of intersection as shown in figure 6. The loss, entered in decibels per bounce, is converted to a pressure ratio according to

$$\eta_{sur} = 10^{-N_{sur}/20} = e^{-N_{sur} [\ln(10)/20]} \quad (19)$$

If the surface loss is not specified,  $\eta_{sur}$  is set equal to unity ( $N_{sur} = 0$ ) by default. The reader is referred to the user's manual (Part II) for additional details.

It must be pointed out that the surface loss discussed above only applies to the propagation-loss equation (18). A different surface loss, used in the Acoustic Meteorological and Oceanographic Survey (AMOS) surface-duct model, will be discussed shortly.

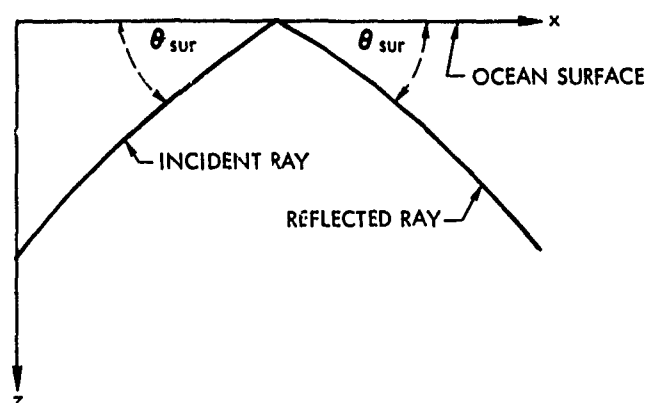


Figure 6. Intersection of a Ray with the Ocean Surface

#### BOTTOM LOSS

Bottom loss may be entered as a table of bottom loss per bounce,  $N_{bot}$ , versus angle of incidence,  $\theta_{bot}$ , or computed using either the Naval Undersea Center's (NUC) bottom-loss model in reference 8 or the one developed by Podeszwa (reference 9) at the Naval Underwater Systems Center (NUSC). All three models are functions of  $\theta_{bot}$ , as defined in figure 7; in each case, bottom loss is converted to a pressure ratio according to

$$\eta_{bot} = 10^{-N_{bot}/20} = e^{-N_{bot} [\ln(10)/20]} \quad (20)$$

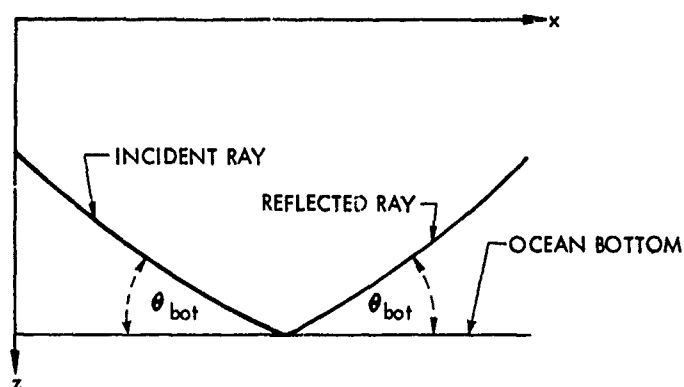


Figure 7. Intersection of a Ray with the Ocean Bottom



The NISSM II variation of the NUC bottom-loss model is

$$N_{\text{bot}} = [3.7 + 17.5(P - 0.27)] f^{1/3} \cdot \left\{ \tanh \left[ (\theta_{\text{bot}} P / 0.24)^{1.5/P} \right] + [(1 - P / 0.27) / 12.5] \cdot (\theta_{\text{bot}} / 90)^2 \right\}, \quad (21)$$

where

$\theta_{\text{bot}}$  is the angle of incidence in degrees,

$f$  is the frequency in kilohertz, and

$P$  is the porosity.

This model is evaluated at various frequencies and porosities in figures 8 through 11.

Podeszwa's bottom-loss model<sup>9</sup> is an approximation of the Marine Geophysical Survey (MGS) Acoustic Provinces 1 through 5. The losses for that model are given by

$$N_{\text{bot}} = 2.2435 \ln(0.1260 \theta_{\text{bot}} + 1.496) \quad \text{for Province 1,} \quad (22)$$

$$N_{\text{bot}} = 3.4315 \ln(0.1056 \theta_{\text{bot}} + 2.842) \quad \text{for Province 2,} \quad (23)$$

$$N_{\text{bot}} = 2.4910 \ln(0.8864 \theta_{\text{bot}} + 10.526) \quad \text{for Province 3,} \quad (24)$$

$$N_{\text{bot}} = 2.8377 \ln(1.8754 \theta_{\text{bot}} + 15.685) \quad \text{for Province 4, and} \quad (25)$$

$$N_{\text{bot}} = 2.4036 \ln(20.576 \theta_{\text{bot}} + 82.440) \quad \text{for Province 5} \quad (26)$$

and are displayed in figure 12. The user of NISSM II is allowed to input non-integral MGS provinces between 1 and 5. A linear interpolation is performed in determining coefficients  $c_1$ ,  $c_2$ , and  $c_3$  for the bottom-loss model,

$$N_{\text{bot}} = c_1 \ln(c_2 \theta_{\text{bot}} + c_3). \quad (27)$$

If the bottom loss is not specified,  $\theta_{\text{bot}}$  is set to unity ( $N_{\text{bot}} = 0$ ) by default.

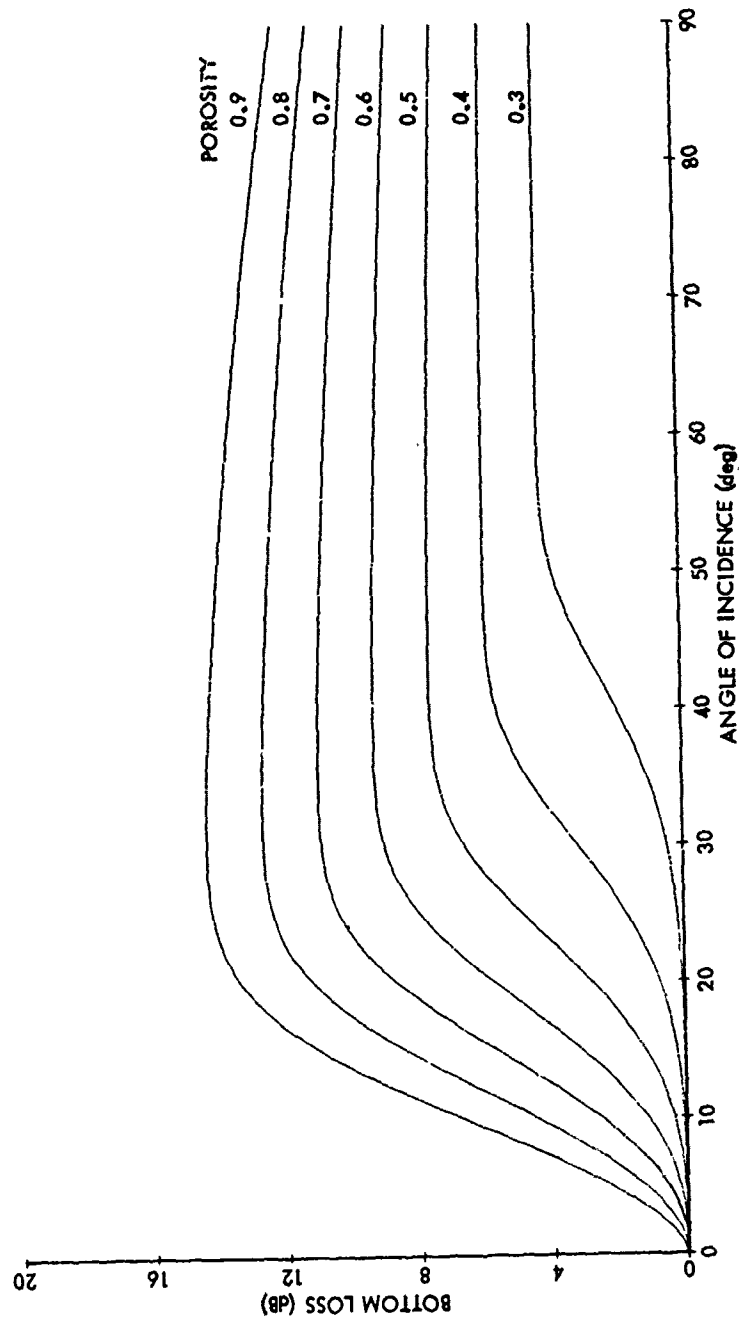


Figure 8. NUC Bottom-Loss Curves at 1.0 kHz

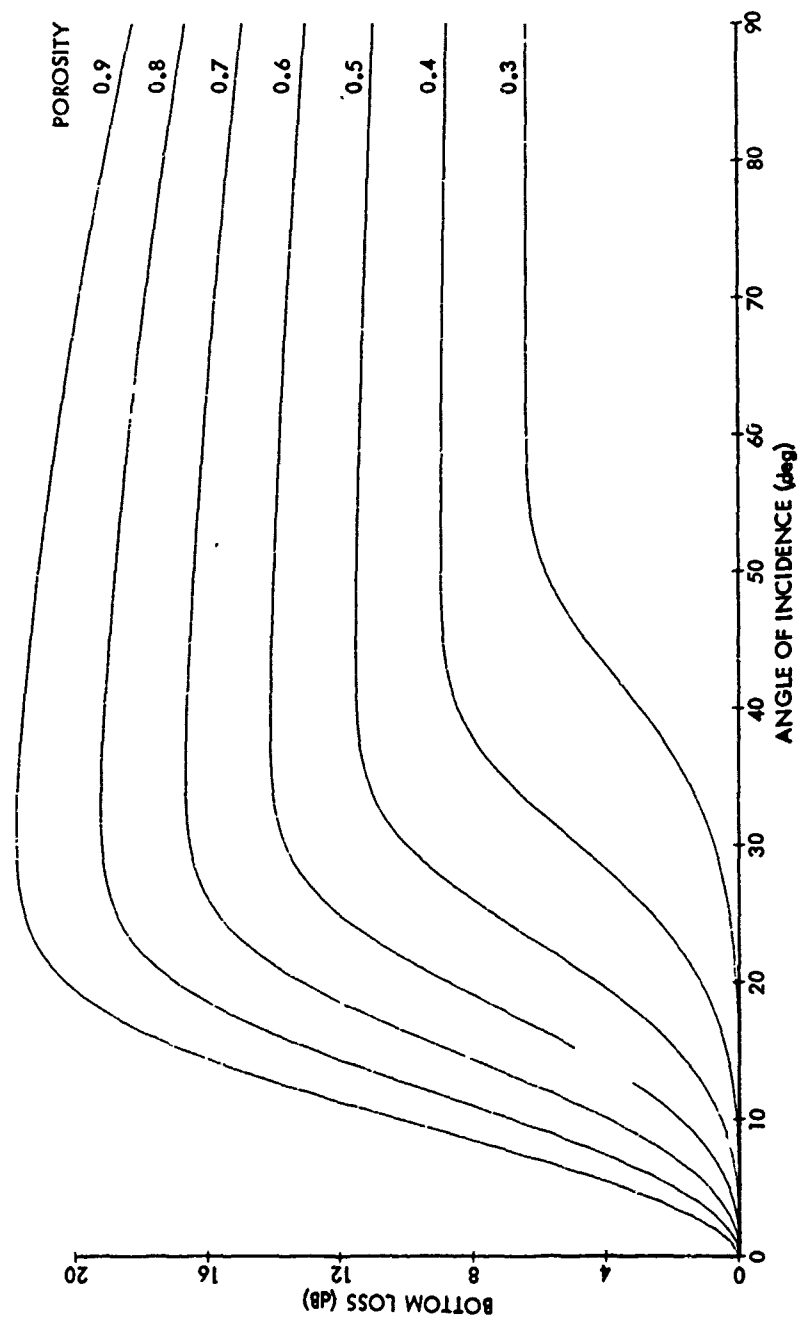


Figure 9. NUC Bottom-Loss Curves at 3.5 kHz

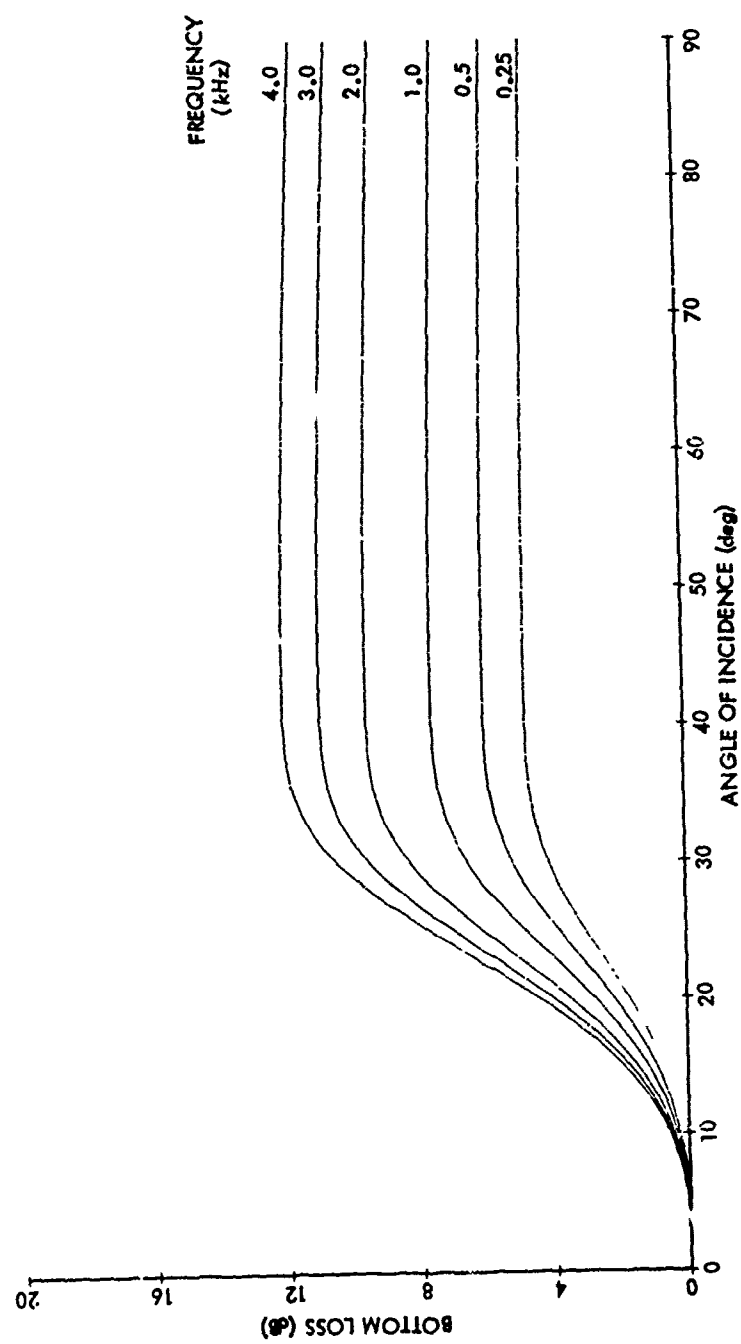


Figure 10. NUC Bottom-Loss Curves at 0.5 Porosity

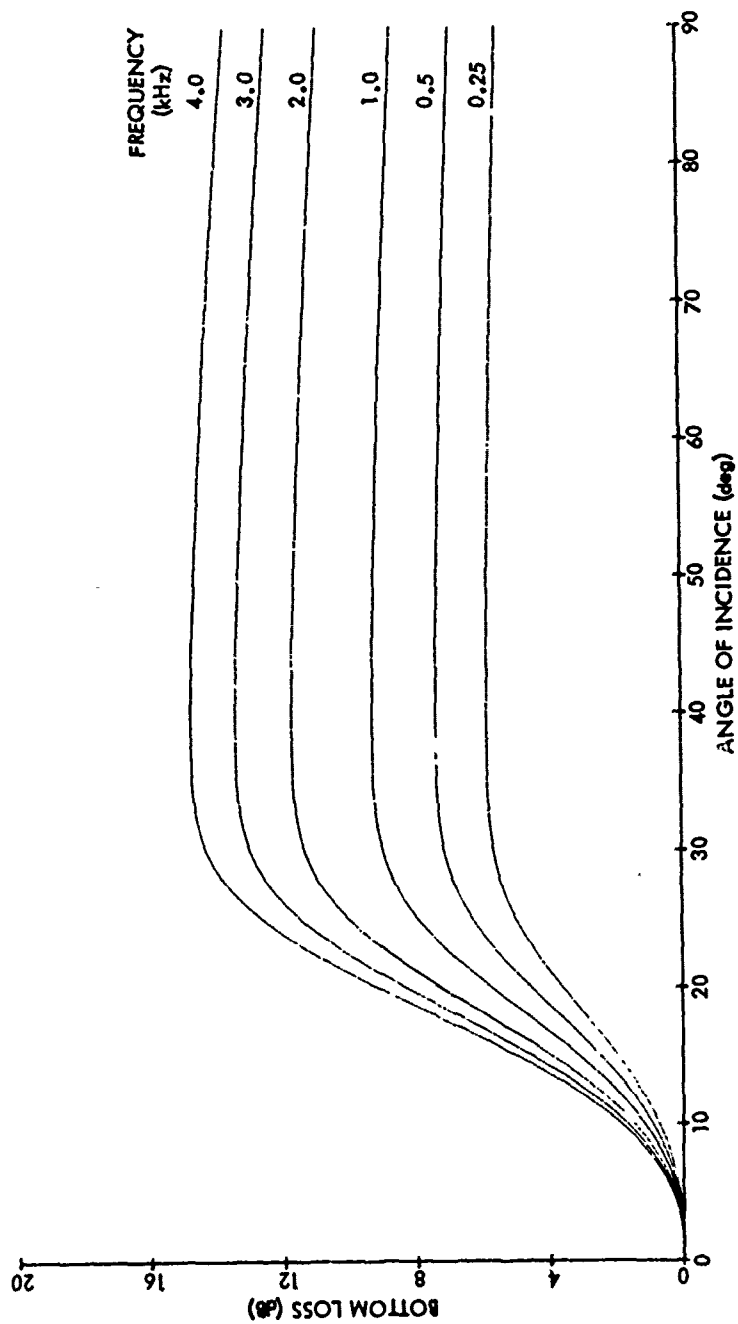


Figure 11. NUC Bottom-Loss Curves at 0.6 Porosity

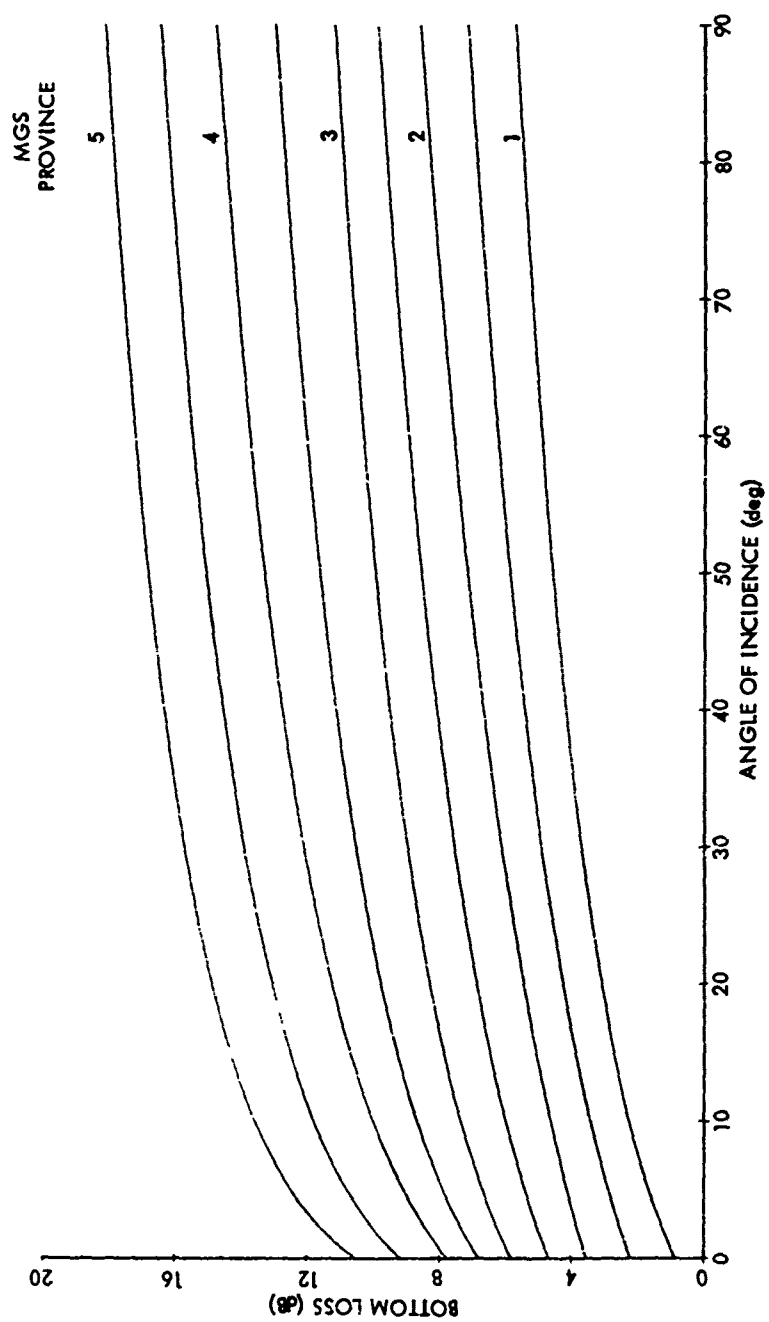


Figure 12. MGS Bottom-Loss Curves

## ABSORPTION COEFFICIENT

The absorption coefficient may be inputted as a table of absorption per unit distance,  $A$ , versus frequency,  $f$ , or computed using either Thorp's equation,<sup>10</sup>

$$A = f^2 \left[ \frac{0.1}{1 + f^2} + \frac{40}{4100 + f^2} \right] \quad (28)$$

or the Hall-Watson equation,<sup>11</sup>

$$A = \left\{ 1.776 f^{1.5} + f^5 \left[ \frac{0.65053 f_T}{f^2 + f_T^2} + \frac{0.026847}{f_T} \right] \right\} / [32.768 + f^3] \quad (29)$$

where

$$f_T = 21.9 \times 10^{\left[ \frac{30T + 102}{5T + 2297} \right]} \quad (30)$$

In equations (28), (29), and (30)

$A$  is the absorption coefficient in decibels per kiloyard,

$f$  is the frequency in kilohertz,

$f_T$  is the relaxation frequency in kilohertz, and

$T$  is the average ocean temperature in degrees Fahrenheit.

Since the units of  $\alpha$  in equation (18) are expressed in inverse kilometers, then, if either equation (28) or (29) is used to compute  $A$ ,

$$\alpha = - A [\ln(10)/20] / 0.9144 \quad (31)$$

When the absorption coefficient is not specified,  $A$  is computed according to Thorp's equation.<sup>10</sup> (See figure 13 for a comparison of the absorption coefficient for the two models.)

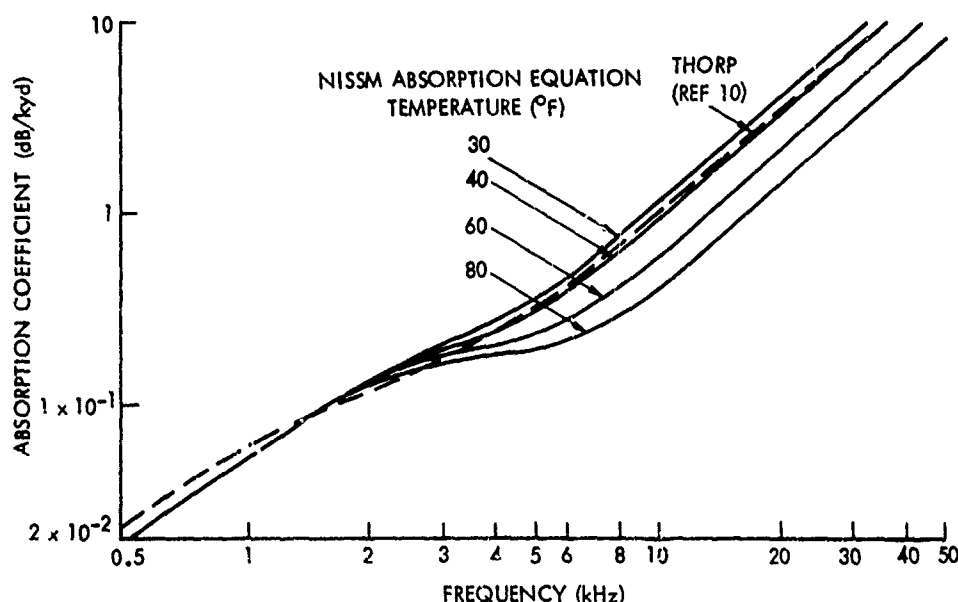


Figure 13. Absorption Coefficient versus Frequency for the Two Models

### EIGENRAYS

The propagation equation ((18)) describes the variation in pressure along a particular ray. Since a denumerable set of rays may pass through a single point, the total pressure is the result of the individual contributors. Rays that originate at one given point, henceforth called the sonar, and terminate at another given point, to be referred to as the target, are known as eigenrays. The problem is to determine the most important eigenrays as efficiently and as accurately as possible.

In NISSM II, eigenrays are found by tracing a preselected fan of test rays to the target depth. When two adjacent rays of the same type bracket a target range, a cubic interpolation is performed to determine the eigenray. The two steps for determining the most important eigenrays are as follows:

- a. A table of 128 vertex velocities (the  $c_v$  of equation (1)) should be constructed. The table, which begins with the sonar velocity, includes (1) velocities at breakpoints in the velocity-depth profile, at target depths, and at the ocean surface and bottom (providing they exceed the sonar velocity) and (2) approximately 32 entries that also correspond to vertexing rays. The remaining velocities correspond to nonvertexing rays, the steepest of which has an initial inclination angle slightly greater than 89.6 deg.



b. One ray segment from the sonar depth to the surface, another from the sonar depth to the bottom, and a third from the sonar depth to the target depth should be traced for each vertex velocity in the table. Shallow ray segments are terminated at their vertexing depths. Each range, travel time, and range-derivative increment is stored for future reference.

After initializing various index counters, two test rays having adjacent vertex velocities and the same ray type are generated by combining the previously computed ray increments. The first four ray types are shown in figure 14. Subsequent types are obtained by adding complete cycles to the basic four types. If the final ranges of the test rays bracket the target range, a cubic interpolation is performed to determine the eigenray. If they are not bracketed, another ray type is considered. Eventually, the end points of adjacent rays will extend well beyond the target range. Adding additional cycles will only move the end points farther to the right. Therefore, the ray-type counter is initialized and the vertex velocity index is incremented.

After eight eigenrays\* have been determined, they are sorted according to the sonar-inclination angle and entered into the propagation-loss, the reverberation, or the target-echo routine. Following the processing of the eigenrays, both the vertex-velocity and ray-type indexes are initialized and the target range is incremented.

Since the ray segments are computed only once, the method outlined above is extremely efficient. Usually, because shallower rays tend to sustain fewer losses, the most important eigenrays are determined.

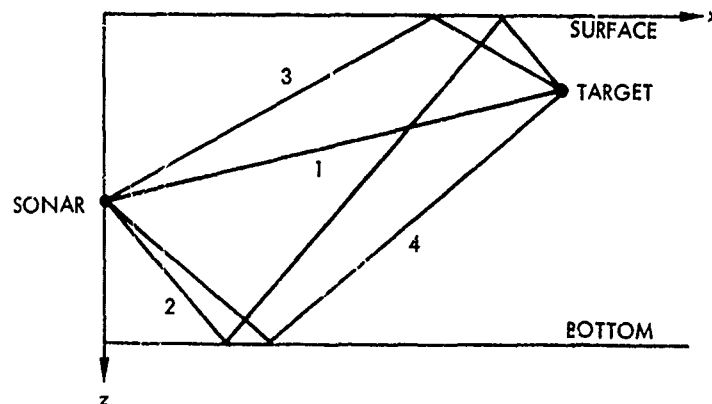


Figure 14. Principal Ray Types

\*If a sound channel exists, up to 32 eigenrays may be determined.

## SHADOW-ZONE PROPAGATION

When the sound velocity decreases monotonically from the ocean surface to the sonar depth, the ray that grazes the surface is a limiting ray and forms the boundary of a shadow zone. Figures 15, 16, and 17 illustrate such a situation.

Pekeris<sup>12</sup> shows that shadow-zone propagation is characterized by the equation

$$|p|^2 = |p_b|^2 \frac{x_b}{x} e^{-\alpha(x-x_b)}, \quad (32)$$

where

$$\alpha = \frac{5.93}{c_{\text{sur}}} g_{\text{sur}}^{2/3} f^{1/3} \quad (33)$$

and

$p$  is the pressure in the shadow zone at  $(x \text{ km}, z \text{ km})$ ,

$p_b$  is the pressure on the shadow boundary at  $(x_b \text{ km}, z \text{ km})$ ,

$c_{\text{sur}}$  is the surface velocity in kilometers per second,

$g_{\text{sur}}$  is the surface-velocity gradient in reciprocal seconds, and

$f$  is the frequency in hertz.

One may consider equation (32) to describe the pressure of an imaginary ray that travels upward along the limiting ray to the surface, horizontally along the surface a distance of  $x - x_b$  kilometers, and, finally, parallel to the downward portion of the limiting ray to  $(x, z)$ .

In NISSM II, limiting rays (if they exist) are traced for the first 32 ray types (see figure 14). If the target lies in the shadow of a particular type, the pressure of the corresponding imaginary ray is computed according to equations (32) and (33). \* The travel time of the imaginary ray is obtained by adding  $c_{\text{sur}}(x - x_b)$  to the travel time of the limiting ray. Only three imaginary rays are allowed for any particular target. Imaginary rays, once determined, are treated the same as the other rays.

\*For bottom shadows,  $c_{\text{sur}}$  and  $g_{\text{sur}}$  are replaced by the velocity and velocity gradient at the bottom.

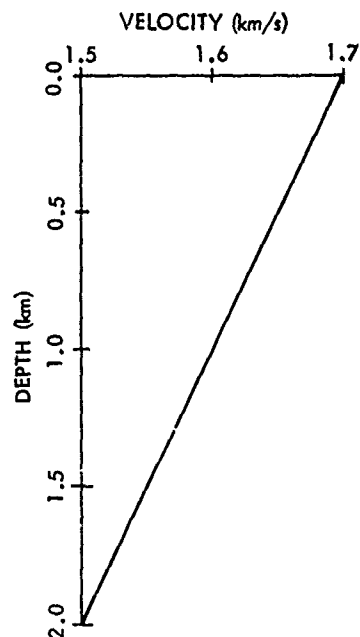


Figure 15. Half-Space in Which the Velocity Decreases with Depth

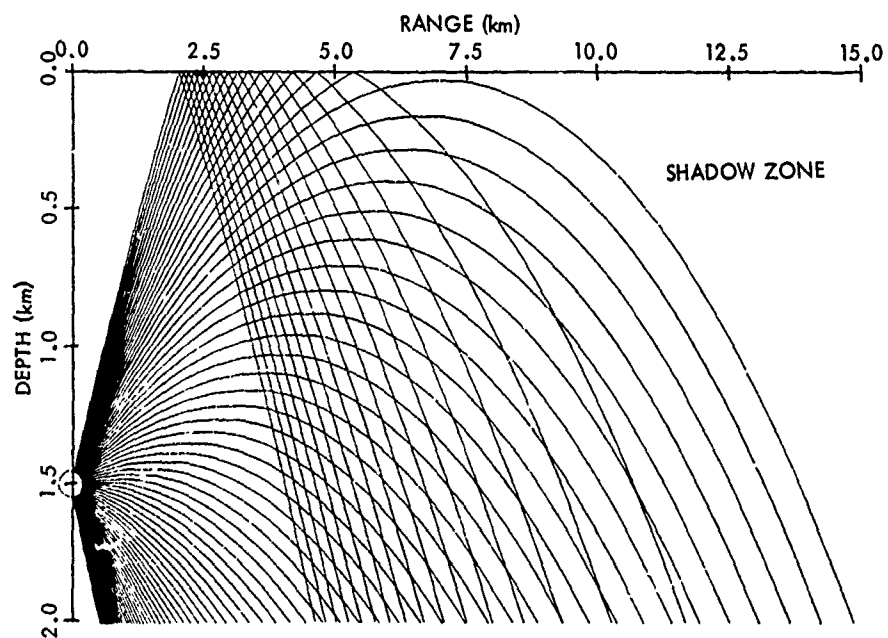


Figure 16. Formation of a Shadow Zone

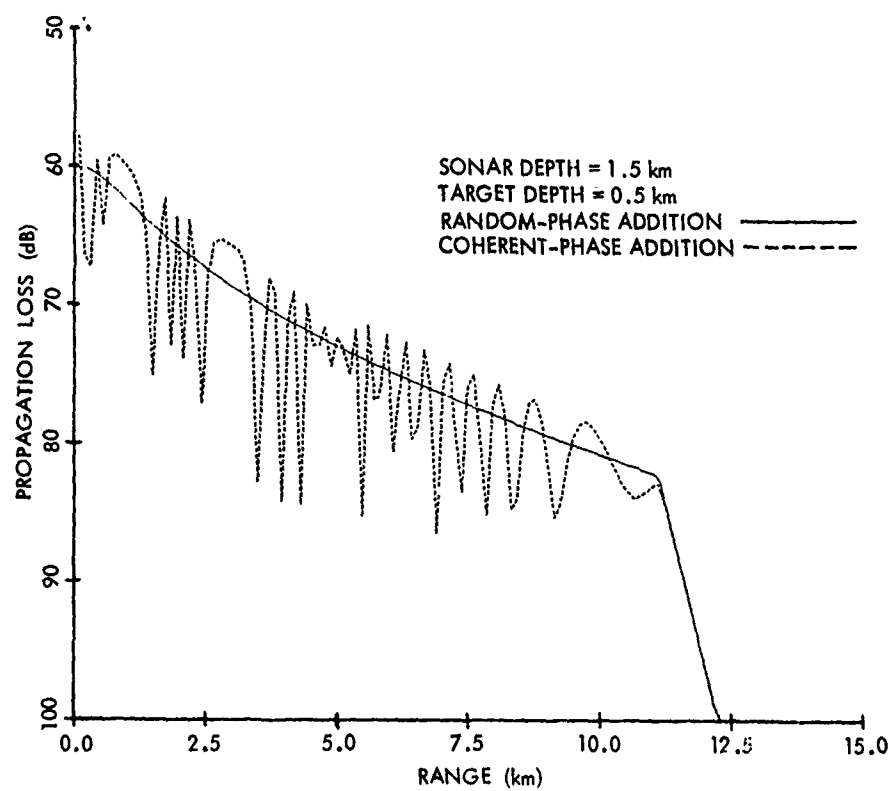


Figure 17. Propagation into a Shadow Zone

The procedure described above is not entirely correct. In particular, the value 5.93 in equation (33) was derived by solving a free-surface boundary-value problem that does not apply to the ocean bottom. However, it is hypothesized that the correct value should be in the neighborhood of 5.93; therefore, equation (32) is still meaningful. The correct value can easily be inserted when it becomes available.

#### UNIFORM ASYMPTOTIC EXPANSION AT A CAUSTIC

Shadow zones are not always caused by boundary surfaces. Under suitable conditions, rays of a particular type may be refracted away from an ocean region. The envelope of these rays, which is called a caustic, also forms the boundary of a shadow zone.

In practice, caustic curves assume many shapes; they may even reduce to a point in a perfectly focusing situation. However, we shall restrict this discussion to that of a smooth caustic. The velocity profile in figure 18 will produce the smooth caustic shown in the ray diagram in figure 19. Note that two rays pass through each point of the illuminated region in the vicinity of the caustic. As the caustic is approached,  $\partial x / \partial c_v$  vanishes for both rays and the geometrical spreading-loss factor, given by equation (5), increases without bound.

A more accurate description of the pressure in the vicinity of a caustic is given by Ludwig.<sup>13</sup> We have incorporated his equations into the following procedures: let  $T_+$ ,  $T_-$ ,  $|p_+|$ ,  $|p_-|$  be the travel times and pressure amplitudes of both the ray that has touched the caustic and the ray that has not touched the caustic, respectively. Next define  $\psi$  and  $\rho$  using, respectively, equations (34) and (35):

$$\psi = (2\pi f) (T_+ - T_-)/2 \quad (34)$$

and

$$\rho = \left( \frac{3}{2} \psi \right)^{2/3} \quad (35)$$

It can be shown that  $\psi$  vanishes on the caustic and is positive in the illuminated region. Then, if

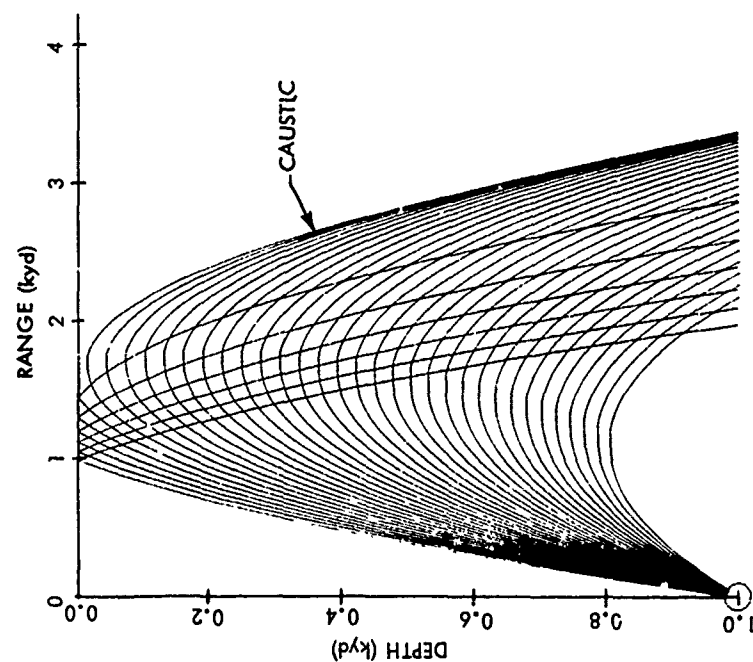


Figure 19. Formation of a Smooth Caustic

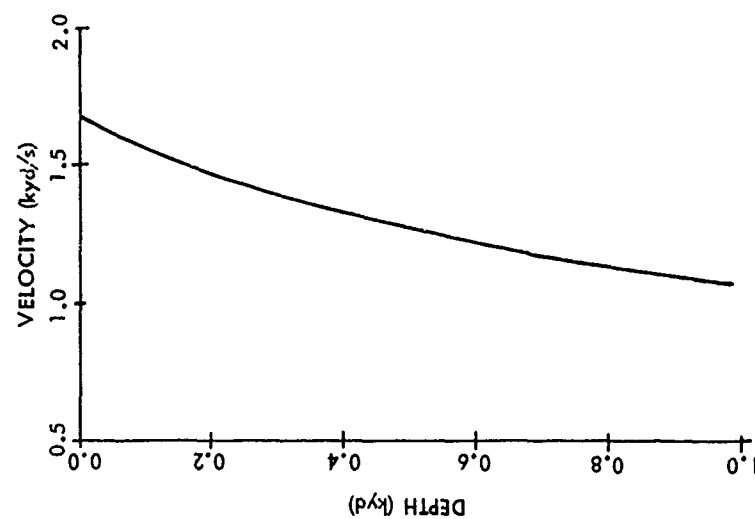


Figure 18. Half-Space Within Which  $(\text{Velocity})^{-2}$  Increases Linearly With Depth

a.  $2\pi \leq \psi$ , set

$$|p_{\text{-mod}}| = |p_-| \text{ and} \quad (36)$$

$$|p_{\text{+mod}}| = |p_+| ; \quad (37)$$

b.  $0.01 \leq \psi < 2\pi$ , set

$$|p_{\text{-mod}}| = \sqrt{\pi} \left[ \text{Ai}(-\rho) (|p_+| + |p_-|)^2 \sqrt{\rho} + \text{Ai}'(-\rho) (|p_+| - |p_-|)^2 / \sqrt{\rho} \right]^{1/2} \text{ and} \quad (38)$$

$$|p_{\text{+mod}}| = 0 ; \quad (39)$$

and

c.  $0 \leq \psi < 0.01$ , set

$$|p_{\text{-mod}}| = \sqrt{\pi} \left[ \text{Ai}(-\rho) (|p_+| + |p_-|)^2 \sqrt{\rho} \right]^{1/2} \text{ and} \quad (40)$$

$$|p_{\text{+mod}}| = 0 . \quad (41)$$

In equations (38) and (40),  $\text{Ai}(\zeta)$  is the Airy function of  $\zeta$ ,  $\text{Ai}'(\zeta)$  is its derivative and  $|p_{\text{+mod}}|$  and  $|p_{\text{-mod}}|$  are modified pressure amplitudes.

Since Ludwig's caustic expansion<sup>13</sup> is uniform, in theory, one can extend the bounds of the inequality  $0.01 \leq \psi < 2\pi$  indefinitely, thereby eliminating cases (a) and (c). However, equation (38) is a lengthier computation than (36) and becomes numerically ill-conditioned as  $\psi \rightarrow 0$ . Also, equation (38) can be continued analytically into the shadow zone. In that event,  $\rho$  is negative and  $|p_{\text{-mod}}|$  would decay exponentially with distance away from the caustic. Since the decay is extremely rapid at active frequencies, the logic to perform the analytic continuation does not appear in the present version of the computer program. This causes the erroneous discontinuity in pressure indicated in figure 20.

### PHASE SHIFTS

A ray that either reflects off a boundary surface or touches a caustic curve undergoes a corresponding change in phase. The accumulation of these abrupt phase shifts is signified by  $\Phi$  in equation (18). In NISSM II,  $\Phi$  is initially set to zero at the sonar and decreased by  $\pi$  radians at surface intersections and by  $\pi/2$  radians at caustics. Phase shifts at bottom intersections are set equal to zero for lack of data.

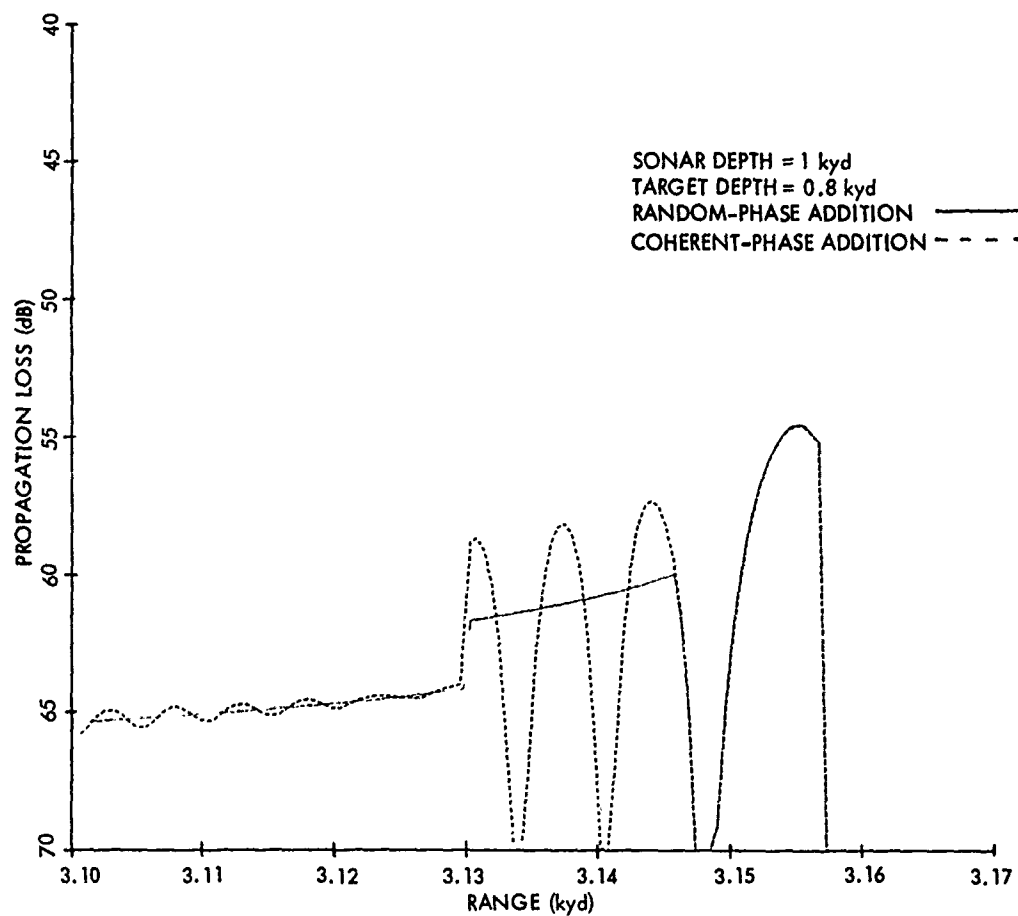


Figure 20. Propagation Loss versus Range in the Vicinity of a Smooth Caustic. (The discontinuity at 3.157 kyd would be removed if the solution were continued into the shadow zone.)



## SURFACE-DUCT PROPAGATION

When the sound velocity initially increases and then decreases with depth from the ocean surface, the region of increasing velocity is called a surface duct. Because ray theory does not make allowances for leakage from the layer into the underlying medium, and since the ray geometry is more complicated than that of a smooth caustic, the application of ray theory to surface-duct propagation is questionable.

In order to reduce the possibility of extremely erroneous predictions, propagation losses for surface-duct eigenrays are computed according to the modified AMOS model in reference 14 and ray theory. (The equations from that publication are repeated in appendix C for the reader's convenience.) Since the above paragraph implies that ray-tracing predictions are optimistic, the lower pressure (greater propagation loss) is taken to be the correct value. Only two surface-duct eigenrays per target are determined, and double the AMOS propagation loss factor (if used) is associated with each.

## PROPAGATION LOSS VERSUS RANGE AT A CONSTANT DEPTH

One of the most useful outputs provided by NISSM II is a plot of effective propagation loss versus range at constant depth. The value at a particular range is obtained by multiplying the relative acoustic pressure of each eigenray,  $p^{(i)}$ , by factors corresponding to the reference level,  $d_{\text{son}}$  or  $d_{\text{tar}}$ , and the respective array responses  $\eta_{\text{son}}$  and  $\eta_{\text{tar}}$ . The results are then combined using coherent- or random-phase addition. Both sonar and target responses are entered as tables of response in decibels versus inclination angle. The reference level is called the sonar or target level, depending on whether the system is active or passive, respectively. Thus for coherent-phase addition, \*

$$p_{\text{eff}} = \sum_{i=1}^{i_{\text{max}}} d_{\text{son}} \eta_{\text{son}}(\theta_{\text{son}}^{(i)}) p^{(i)} \eta_{\text{tar}}(\theta_{\text{tar}}^{(i)}) d_{\text{tar}}, \quad (42)$$

and for random-phase addition,

$$|p_{\text{eff}}|^2 = \sum_{i=1}^{i_{\text{max}}} |d_{\text{son}} \eta_{\text{son}}(\theta_{\text{son}}^{(i)}) p^{(i)} \eta_{\text{tar}}(\theta_{\text{tar}}^{(i)}) d_{\text{tar}}|^2, \quad (43)$$

---

\*In NISSM II, results for coherent-phase addition are indicated by broken lines and propagation losses computed using random-phase addition are indicated by solid lines.

where

$P_{\text{eff}} = -20 \log |p_{\text{eff}}|$  is the effective propagation loss in decibels,

$D_{\text{son}} = +20 \log d_{\text{son}}$  is the reference level in decibels for an active situation,

$D_{\text{tar}} = +20 \log d_{\text{tar}}$  is the reference level in decibels for a passive situation,

$P^{(i)} = -20 \log |p^{(i)}|$  is the propagation loss of the  $i$ -th eigenray,

$N_{\text{son}} = -20 \log \eta_{\text{son}}$  is the sonar response in decibels,

$N_{\text{tar}} = -20 \log \eta_{\text{tar}}$  is the target response in decibels,

$\theta_{\text{son}}^{(i)}$  is the inclination angle at the sonar of the  $i$ -th eigenray,

$\theta_{\text{tar}}^{(i)}$  is the inclination angle at the target of the  $i$ -th eigenray, and

$i_{\text{max}}$  is the number of eigenrays joining the sonar to the target.

The default value for  $d_{\text{son}}$ ,  $d_{\text{tar}}$ ,  $\eta_{\text{son}}$ , and  $\eta_{\text{tar}}$  is unity ( $D_{\text{son}}$ ,  $D_{\text{tar}}$ ,  $N_{\text{son}}$ , and  $N_{\text{tar}} = 0$ ).

#### REVERBERATION THEORY\*

Consider an acoustic signal that originates at a point source at a reference time equal to zero and is transmitted through the ocean. A portion of the signal is backscattered toward the source as the signal encounters scatterers on the ocean bottom or the surface or in the ocean volume. When the second order scattering of sound is neglected, a closed ray path from a source to a scatterer and back to the source (figure 21) can be constructed from an incident ray (a ray from the source at point "a" to the scatterer at point "b") and a backscattered ray (a ray from the scatterer back to the source). Let the incident ray enter the water at time  $t_0$  and have travel time  $t_1$ , and let the backscattered ray have travel time  $t_2$ . Then the closed ray path will have round-trip travel time,

$$t = t_1 + t_2, \quad (44)$$

and will return to the source at time

$$T = t_0 + t. \quad (45)$$

---

\*The text under this heading was excerpted from reference 1<sup>r</sup>

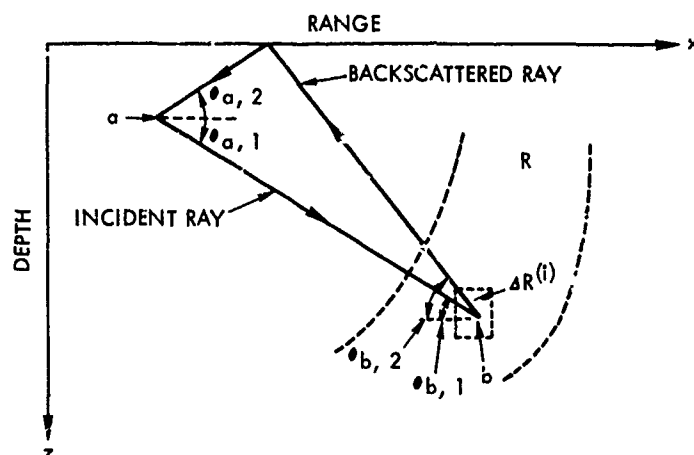


Figure 21. Closed Ray Path

The acoustic pressure at the end of the closed ray path is given by

$$p_{rev} = d_{tra} \eta_{tra}(\theta_{a,1}) p_1 p_2 \eta_{rec}(\theta_{a,2}) \nu, \quad (46)$$

where

$D_{tra} = +20 \log d_{tra}$  is the reference level in decibels of the transmitting array,

$P_1 = -20 \log |p_1|$  is the propagation loss in decibels of the incident ray,

$P_2 = -20 \log |p_2|$  is the propagation loss in decibels of the backscattered ray,

$N_{tra} = -20 \log \eta_{tra}$  is the transmitter response in decibels,

$N_{rec} = -20 \log \eta_{rec}$  is the receiver response in decibels, and

$\nu$  is a backscattering strength expressing the ratio of reflected pressure to incident pressure per scatterer.

If the acoustic signal has pulse length  $\tau$ , it follows that

$$0 \leq t_0 \leq \tau \quad (47)$$

and that the closed ray paths contributing to the reverberation pressure at time  $T$  are those with travel time

$$T - \tau \leq t \leq T. \quad (48)$$

The corresponding scatterers will be contained in region  $R$ . Let this region be partitioned into numerous subregions,  $\Delta R^{(i)}$ , in each of which  $p_1^{(i)}$ ,  $p_2^{(i)}$ ,  $\theta_{a,1}^{(i)}$ ,  $\theta_{a,2}^{(i)}$ , and  $\nu^{(i)}$  are representative values, and let there be  $n^{(i)}$  scatterers per unit region. Then, if the resultant reverberation pressure is the random-phase addition of the individual contributors,

$$|p_{\text{rev}}|^2 = \sum_i \left| d_{\text{tra}} \eta_{\text{tra}}(\theta_{a,1}^{(i)}) F_1^{(i)} p_2^{(i)} \eta_{\text{rec}}(\theta_{a,2}^{(i)}) \right|^2 \mu^{(i)} \Delta R^{(i)}, \quad (49)$$

where

$$\mu^{(i)} = (\nu^{(i)})^2 n^{(i)} \quad (50)$$

is the backscattering strength. In the limit as  $\Delta R^{(i)} \rightarrow 0$ ,

$$|p_{\text{rev}}|^2 = \int_R \left| d_{\text{tra}} \eta_{\text{tra}}(\theta_{a,1}) p_1 p_2 \eta_{\text{rec}}(\theta_{a,2}) \right|^2 \mu dR. \quad (51)$$

Thus the reverberation problem reduces to integrating equation (51). This is accomplished by approximating equation (51) with a summation similar to equation (49). Since NISSM II usually computes eight paths (see footnote on p. 20) to each representative scatterer, there may be as many as  $8^2 - 8 = 56$  differently oriented closed paths per scatterer.

## VOLUME REVERBERATION

For volume reverberation, equation (51) is replaced by the double summation,

$$|p_{vol}|^2 = \sum_{i,j} \left| d_{tra} \eta_{tra}(\theta_{a,1}^{(i,j)}) p_1^{(i,j)} p_2^{(i,j)} \eta_{rec}(\theta_{a,2}^{(i,j)}) \right|^2 \quad (52)$$

$$\cdot \mu_{vol}^{(j)} x^{(i)} \Delta x^{(i,j)} \Delta z^{(j)} \Delta \phi ,$$

where

$\Delta \phi$  is the horizontal beamwidth in radians,

$x^{(i)}$  is the range in kilometers of the  $(i,j)$ -th scatterer,

$z^{(j)}$  is the depth in kilometers of the  $(i,j)$ -th scatterer,

and

$U_{vol}^{(j)} = 10 \log \mu_{vol}^{(j)}$  is the volume-scattering strength per cubic kilometer in decibels,

The horizontal beamwidth,  $\Delta \phi$ , equidistant ranges,  $x^{(i)}$ , and a table of volume-scattering strengths,  $U^{(j)}$ , versus depth,  $z^{(j)}$ , are input data. They are converted by NISSM II to the appropriate units. Then  $z^{(j)}$ ,  $\mu_{vol}^{(j)}$ , and  $\Delta z^{(j)}$  are computed according to

$$z^{(j)} = 1/2 (z^{(j+1)} + z^{(j)}) , \quad (53)$$

$$\mu_{vol}^{(j)} = 1/2 (\mu_{vol}^{(j+1)} + \mu_{vol}^{(j)}) , \quad (54)$$

and

$$\Delta z^{(j)} = z^{(j+1)} - z^{(j)} , \quad (55)$$

respectively. At the ranges of interest, the quantity  $x^{(i)} \Delta x^{(i,j)} \Delta z^{(j)} \Delta \phi$  is a good approximation of the volume of the insonified region bounded by  $z^{(j)}$ ,  $z^{(j+1)}$  and surfaces of constant round-trip travel time (see figure 22).

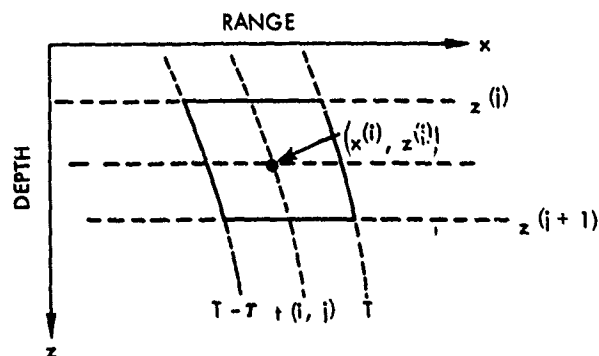


Figure 22. Insonified Region

Initially, the range increment  $\Delta x^{(i,j)}$  is set to

$$\Delta x^{(i,j)} = x^{(i+1)} - x^{(i)}, \quad (56)$$

and the round-trip travel times,  $t^{(i,j)\pm}$ , at  $(x^{(i)} \pm \Delta x/2^{(i,j)}, z^{(j)})$  are approximated by

$$t^{(i,j)\pm} = t^{(i,j)} \pm \left( \frac{1}{c_{v,1}^{(i,j)}} + \frac{1}{c_{v,2}^{(i,j)}} \right) \Delta x^{(i,j)}/2. \quad (57)$$

Here  $c_{v,1}^{(i,j)}$  and  $c_{v,2}^{(i,j)}$  are the vertex velocities of the incident and backscattered rays, respectively. Then, if

$$T - \tau \leq t^{(i,j)-} < t^{(i,j)} < t^{(i,j)+} \leq T, \quad (58)$$

the region whose sides are surfaces of constant  $t^{(i,j)\pm}$  is contained within the insonified region and  $\Delta x^{(i,j)}$  is left unchanged,

However, if the inequality (58) does not hold, modified values of  $t(i, j)_{\pm}$  and  $\Delta x(i, j)$  are determined according to

$$t_{\text{mod}}^{(i, j)-} = \left[ \max t^{(i, j)-}, T - \tau \right], \quad (59)$$

$$t_{\text{mod}}^{(i, j)+} = \left[ \min t^{(i, j)+}, \tau \right], \quad (60)$$

and

$$\Delta x_{\text{mod}}^{(i, j)} = \left( \frac{1}{c_{v, 1}^{(i, j)}} + \frac{1}{c_{v, 2}^{(i, j)}} \right)^{-1} \max \left[ \tau_{\text{mod}}^{(i, j)+} - \tau_{\text{mod}}^{(i, j)-}, 0 \right]. \quad (61)$$

Each term in the volume-reverberation summation ((52)) has now been found.

If the volume-scattering strength table is omitted, then the volume-reverberation computation is also omitted.

#### SURFACE REVERBERATION

Surface reverberation is computed according to summation (49), with

$$\Delta R^{(i)} = \mu_{\text{sur}}^{(i)} x^{(i)} \Delta x^{(i)} \Delta \phi \quad (62)$$

and

$$10 \log \mu_{\text{sur}}^{(i)} = 3.3 \beta \log \left( \frac{\theta_{\text{sur}, 1}^{(i)}}{30} \frac{\theta_{\text{sur}, 2}^{(i)}}{30} \right)^{1/2} - 42.4 \log \beta + 10 \log \underline{\mu}_{\text{sur}}, \quad (63)$$

where

$\theta_{\text{sur}, 1}^{(i)}$  is the surface-grazing angle, in degrees, of the incident ray to the  $i$ -th surface scatterer,

$\theta_{\text{sur}, 2}^{(i)}$  is the surface-grazing angle, in degrees, of the backscattered ray from the  $i$ -th surface scatterer, and

$\underline{\mu}_{\text{sur}} = 10 \log \underline{\mu}_{\text{sur}}$  is a surface-scattering constant per square kilometer, in decibels, and  $\beta = 158 (v f^{1/3}) - 0.58$ ,

where

$v$  is the wind speed in knots and

$f$  is the frequency in hertz.

Equation (63) reduces to the Chapman-Harris surface-scattering strength<sup>16</sup> when  $\theta_{\text{sur},1}^{(i)}$  equals  $\theta_{\text{sur},2}^{(i)}$  and  $\underline{U}_{\text{sur}}$  is set equal to 2.6 dB. If  $\underline{U}_{\text{sur}}$  is omitted from the input data, then the surface reverberation is also omitted.

#### BOTTOM REVERBERATION

Bottom and surface reverberations are computed similarly, except that for bottom reverberation

$$10 \log \mu_{\text{bot}}^{(i)} = 10 \log \left( \sin \theta_{\text{bot},1}^{(i)} \sin \theta_{\text{bot},2}^{(i)} \right) + 10 \log \underline{\mu}_{\text{bot}}, \quad (64)$$

where

$\underline{U}_{\text{bot}} = 10 \log \underline{\mu}_{\text{bot}}$  is a bottom-scattering constant per square kilometer in decibels.

When  $\underline{U}_{\text{bot}}$  equals -27 dB, equation (64) reduces to MacKenzie's bottom-scattering strength.<sup>17</sup> If  $\underline{U}_{\text{bot}}$  is omitted, then the bottom reverberation is not computed.

#### TOTAL REVERBERATION

A ray leaving the transmitter with an initial inclination angle of  $\pm 90$  deg will be reflected from the ocean's surface and bottom and will return energy to the receiver. This phenomenon is observed in actual measurements. The pressure associated with such eigenrays is computed using the propagation-loss equation ((43)) with subscripts "son" (sonar) and "tar" (target) replaced by "tra" (transmitter) and "rec" (receiver), respectively. The total reverberation is assumed to be the random-phase addition of surface and bottom echoes and volume, surface, and bottom reverberations.



### TARGET ECHO

The target echo at a particular time is determined using the summation

$$|p_{\text{echo}}|^2 = \sum_i \left| d_{\text{tra}} \eta_{\text{tra}}(\theta_{a,1}^{(i)}) p_1^{(i)} p_2^{(i)} \eta_{\text{rec}}(\theta_{a,2}^{(i)}) \right|^2 \mu_{\text{tar}}^{(i)}, \quad (65)$$

where  $\underline{U}_{\text{tar}} = 10 \log \underline{\mu}_{\text{tar}}$  is the target strength in decibels.

As for reverberation, the summation above is taken over all closed paths, with round-trip travel times between  $T - \tau$  and  $T$ . If  $\underline{U}_{\text{tar}}$  is omitted, then the target echo is not computed.

### NOISE

It is convenient to separate noise into the two components:

- $P_{\text{self}} = 20 \log p_{\text{self}}$  is the self-noise spectrum density in decibels, and
- $P_{\text{amb}} = 20 \log p_{\text{amb}}$  is the ambient-noise spectrum density in decibels.

A single value for self-noise,  $P_{\text{self}}$ , may be included in the input data. If not specified,  $p_{\text{self}}$  is assumed to be zero.

Ambient noise may be entered as a table of  $P_{\text{amb}}$  versus frequency or taken from an ambient-noise curve, which is obtained by adding the contributions from the moderate shipping and wind speed shown in figure 23. This graph, obtained by approximating figure 7.5 in reference 18, contains the Knudsen spectra in the 500- to 50,000-Hz band. The default value for ambient noise is determined by evaluating the stored curve at the particular frequency of interest.

Since self-noise and ambient noise are assumed to be isotropic, the total noise-spectrum density at the beamformer output is

$$P_{\text{noise}} = 10 \log \left[ \eta_{\text{DI}} (p_{\text{self}}^2 + p_{\text{amb}}^2) \right] \text{ (dB)}, \quad (66)$$

where  $\text{DI} = -10 \log \eta_{\text{DI}}$  is the directivity index in decibels. The default value for  $\eta_{\text{DI}}$  is unity ( $\text{DI} = 0$ ).

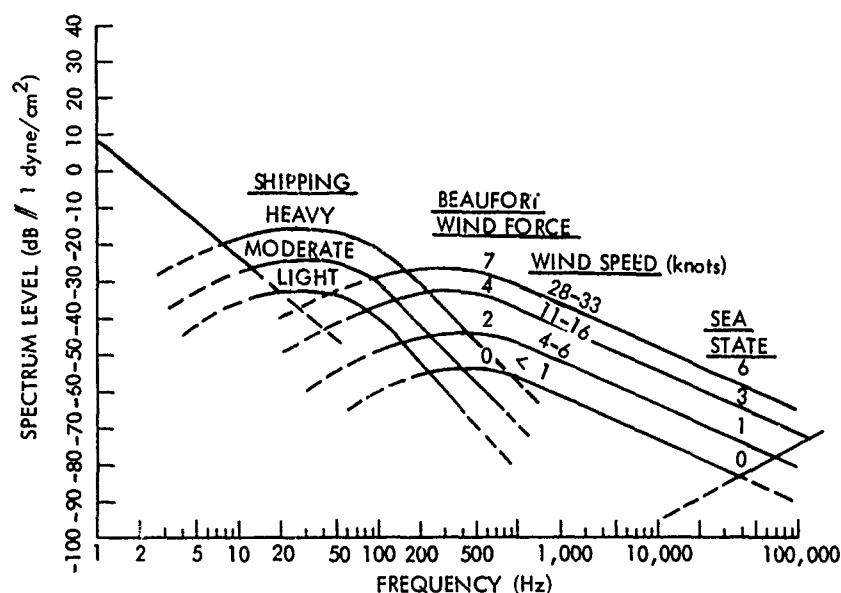


Figure 23. Ambient Noise versus Frequency  
(reference 18)

#### TARGET ECHO TO MASKING BACKGROUND

For a narrowband process, the signal-to-noise ratio ( $s/n$ ), that is, the target echo to masking background, at a particular time  $T$  may be approximated by

$$s/n = \frac{\Delta f_{\text{echo}} p_{\text{echo}}^2}{\Delta f_{\text{noise}} p_{\text{noise}}^2 + \Delta f_{\text{rev}} p_{\text{rev}}^2}, \quad (67)$$

where

$P_{\text{echo}} = 20 \log p_{\text{echo}}$  is the target echo spectrum density in decibels at time  $T$ ,

$P_{\text{rev}} = 20 \log p_{\text{rev}}$  is the reverberation spectrum density in decibels at time  $T$ ,

$P_{\text{noise}} = 20 \log p_{\text{noise}}$  is the noise-spectrum density in decibels at the beamformer output,

$\Delta f_{\text{echo}}$  is an equivalent bandwidth in hertz for the received echo,

$\Delta f_{\text{rev}}$  is an equivalent bandwidth in hertz for the received reverberation, and

$\Delta f_{\text{noise}}$  is an equivalent bandwidth in hertz for the received noise.

Assuming that the target echo is Gaussian distributed and centered about the receiving (Doppler shifted) frequency, with a standard deviation of  $1/2\tau$ ,

$$\Delta f_{\text{echo}} = \phi(\tau\Delta f) - \phi(-\tau\Delta f) , \quad (68)$$

where

$\Delta f$  is the receiving bandwidth in hertz,

$\tau$  is the pulse length in seconds, and

$$\phi(x) = \frac{1}{\sqrt{2\pi}} \int_{-\infty}^x e^{-y^2/2} dy \quad (69)$$

is the normal probability function.

Reverberation is also assumed to be Gaussian with a standard deviation of  $1/2\tau$ , but is centered about the transmitting frequency. Therefore, reverberation energy falling within the echo band is  $\Delta f_{\text{rev}} p_{\text{rev}}^2$ , where

$$\Delta f_{\text{rev}} = \phi(2\tau\Delta f_{\text{Dop}} + \tau\Delta f) - \phi(2\tau\Delta f_{\text{Dop}} - \tau\Delta f) . \quad (70)$$

In this equation

$\Delta f_{\text{Dop}} = 2fV_{\text{cl}}/c_s$  is the Doppler shift in hertz,

$f$  is the frequency in hertz,

$V_{\text{cl}}$  is the closing speed in kilometers per second, and

$c_s$  is the source velocity in kilometers per second.

If the noise-spectrum density can be considered constant over the receiving band, we have

$$\Delta f_{\text{noise}} = \Delta f . \quad (71)$$

# PROBABILITY OF DETECTION

Probability of detection is a useful concept in evaluating the performance of sonar systems. The particular narrowband detector modeled in NISSM II and depicted in figure 24 was developed by Nuttall and Magaraci.<sup>19</sup>

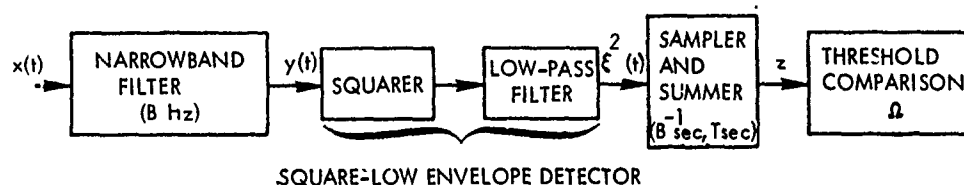


Figure 24. Narrowband Detector

The input  $x(t)$  is assumed to be either a stationary zero-mean Gaussian signal,  $s(t)$ , and noise,  $n(t)$ , or noise alone. It is assumed that the signal spectrum has the same  $B$  hertz bandwidth as the narrowband filter and is centered on it, and that the noise is flat over the frequency interval. Samples of the squared-envelope, which are taken every  $B^{-1}$  seconds, are accumulated for an observation time of  $T$  seconds. The threshold,  $\Omega$ , is fixed.

Then, if  $P_F$  is a given probability of a false alarm, a quantity  $A$  is determined by inverting the expression

$$P_F = e^{-A} \sum_{m=0}^{M-1} \frac{1}{m!} A^m, \quad (72)$$

where

$$M = BT + 1. \quad (73)$$

Once  $A$  is known, the probability of detection,  $P_D$ , is given by

$$P_D = e^{-A/(1+S/N)} \sum_{m=0}^{M-1} \frac{1}{m!} \left( \frac{A}{1+S/N} \right)^m, \quad (74)$$

where  $S/N$  is the maximum value with respect to time of  $s/n$  (equation (67)) at a particular target. If the probability of a false alarm is omitted from the input data, then the probability of detection is not computed.

# REMARKS

NISSM II is a combination of numerous theoretical and empirical models joined into one highly sophisticated computer program. It is unfortunate that the developers of these models chose to express their results in so many different sets of units. Although the computer execution time required to convert data to a consistent set of units is inconsequential, a great deal of otherwise unnecessary logic must be added to the program.

We chose to express our equations in a form that would approximate the original model as closely as possible so that the programmer and user could easily compare the original model with the one presented here.

Many of the environmental routines, such as bottom loss and attenuation, can easily be replaced as more accurate formulas are developed. Similarly, one may wish to use a more applicable detection model. We have tried to anticipate these as well as other possible modifications and have designed NISSM II accordingly.

## Part II

### USER'S MANUAL

This manual describes the input requirements of NISSM II. It is assumed that the reader has read Part I and is familiar with the terminology defined therein.

#### HARDWARE AND SOFTWARE REQUIREMENTS

At present, NISSM II is operational on both the NUSC and NUC Univac 1108, but there are minor differences in the NUSC and NUC models:

- The FORTRAN V compilers are not compatible with respect to ENCODE-DECODE statements. The arguments for these statements are in reverse order.
- The NUSC CalComp plot routines AXIS and SCALE have one more argument than those of NUC.

For both models the input is read from 80-column punched cards, and no peripheral equipment, save the Calcomp batch plot tape drive, is needed to store intermediate results.

Table 1 lists the various subroutines that constitute the computer program, but does not include the standard library software — it was decided to simplify the logic or use similar logic whenever feasible, even at the expense of computational efficiency. The programmer, once he has mastered a particular environmental subroutine, should be able to modify the remaining subroutines without much difficulty. Approximately 100,000 words of core are required. This number, which includes standard library software, could be reduced by decreasing the dimensions of several large arrays.

Table 1. Subroutines

Name	Entry Point	Description
AIRY		Computes both kinds of Airy functions and their derivatives for small, real arguments.
AMBENT		Computes ambient noise by interpolating in a table of noise versus frequency or by using Knudsen curves.
	INAMBN	Reads a table of ambient noise versus frequency and sets options.
AMOS		Computes propagation loss in surface ducts according to the modified AMOS equations.
AMRA		Determines the maximum-response axis of the various arrays.
ATTEN		Computes attenuation by interpolating in a table of attenuation versus frequency or by using either the Thorp <sup>10</sup> or the Watson-Hall <sup>11</sup> equation.
	INATTN	Reads a table of attenuation versus frequency and sets options.
BOTLOS		Computes bottom loss by interpolating in a table of bottom loss versus bottom angle or by using either MGS bottom-loss curves or the NUC bottom-loss model.
	INBTLS	Reads a table of bottom loss versus bottom angle, the MGS province, or the bottom porosity and sets options.
DERF		Evaluates the error function in double precision.
DINERF		Evaluates the inverse error function in double precision.
FACTR		Converts input units to NISSM II units according to table 2.

Table 1 (Cont'd). Subroutines

Name	Entry Point	Description
FITVEL		Reads the velocity or temperature-salinity profile and returns the corresponding continuous-gradient velocity parameters.
GRADE		Evaluates the gradient of the continuous-gradient velocity profile at a particular depth.
INPUT		Reads input data directly or transfers to an entry point in a subroutine that reads input data.
INTERP		Interpolates linearly in tables.
LAYER		Locates the continuous-gradient velocity-profile layer in which a depth is situated.
NISSM2		Oversees subroutines of the NISSM II program.
PRBDET		Determines the probability of detection as a function of signal-to-noise ratio for a given probability of false alarm and sample rate.
PRNTIG		Prints acoustic eigenray data.
	INPRIG	Initializes subroutine PRNTIG.
PRNTRY		Prints coordinates along rays.
	INPRRY	Initializes PRNTRY.
PROBF		Evaluates the Gaussian probability function.
RAY		Integrates the ray-tracing equations over one continuous-gradient velocity-profile layer.
RAYPLT		Constructs ray diagrams.
RECVR		Computes the response of the receiver array by interpolating in a table of response versus receiver angle.



Table 1 (Cont'd). Subroutines

Name	Entry Point	Description
REVERB  RTNSCL  SHAPE  SONAR  SURLOS  TABLE  TARGET	INRCVR	Reads a table of receiver response versus receiver angle and sets options.
		Computes the contribution of a scatterer to bottom, surface, and volume reverberation.
		Returns CalComp scale factors.
	INAXIS	Reads CalComp axis information.
		Computes the pulse shape of the signal at a target.
		Computes the response of the sonar array by interpolating in a table of response versus sonar angle.
	INSONR	Reads a table of sonar response versus sonar angle and sets options.
		Computes the surface loss by interpolating in a table of loss versus surface angle.
	INSRLS	Reads a table of surface loss versus surface angle and sets options.
		Reads tables.
		Computes the response of the target array by interpolating in a table of response versus target angle.
	INTARG	Reads a table of target response versus target angle and sets options.

Table 1 (Cont'd). Subroutines

Name	Entry Point	Description
TRANS	INTRAN	Computes the response of the transmitter array by interpolating in a table of response versus transmitter angle.
		Reads a table of transmitter response versus transmitter angle and set options.
VELOC		Evaluates the velocity of the continuous-gradient velocity profile at a particular depth.
VELTMP	INVLSC	Converts temperature-salinity-depth to velocity.
VOLSCA		Computes the volume-scattering strength by interpolating in a table of scattering strength versus depth.
		Reads a table of volume-scattering strengths versus depth and sets options.

Table 2. Input Units and Conversion Factors

Dimension	Input Unit	Conversion Factor	Code	Results
Length	centimeters	$1.00000000 \times 10^{-5}$	CM	km ↓
	inches	$2.54000000 \times 10^{-5}$	IN	
	feet	$0.30480000 \times 10^{-3}$	FT	
	yards	$0.91440000 \times 10^{-3}$	YD	
	meters	$1.00000000 \times 10^{-3}$	M	
	fathoms	$1.82880000 \times 10^{-3}$	F	
	kilofeet	0.30480000	KFT	
	kiloyards	0.91440000	KYD	
	kilometers	1.00000000	KM	
	miles	1.60934400	MI	
	nautical miles	1.85200000	N MI	
	degrees latitude	$1.11200000 \times 10^{+2}$	DEG L	
Velocity	centimeters/second	$1.00000000 \times 10^{-5}$	CM/S	km/s ↓
	inches/second	$2.54000000 \times 10^{-5}$	IN/S	
	feet/second	$0.30480000 \times 10^{-3}$	FT/S	
	yards/second	$0.91440000 \times 10^{-3}$	YD/S	
	meters/second	$1.00000000 \times 10^{-3}$	M/S	
	fathoms/second	$1.82880000 \times 10^{-3}$	F/S	
	kilofeet/second	0.30480000	KFT/S	
	kiloyards/second	0.91440000	KYD/S	
	kilometers/second	1.00000000	KM/S	
	miles/second	1.60934400	MI/S	
	knots	$0.51444444 \times 10^{-3}$	KNOTS	
Angle	degrees	$1.74532925 \times 10^{-2}$	DEG	rad ↓
	radians	1.00000000	RAD	
Frequency	radians/second	$0.15915494 \times 10^{-3}$	RAD/S	kHz ↓
	hertz	$1.00000000 \times 10^{-3}$	HZ	
	cycles/second	$1.00000000 \times 10^{-3}$	CPS	
	kilohertz	1.00000000	KHZ	
	kilocycles/second	1.00000000	KCPS	
Time	milliseconds	$1.00000000 \times 10^{-3}$	MS	s ↓
	seconds	1.00000000	SEC	
Temperature	degrees centigrade	1.00000000	DEG C	°C ↓
	degrees Fahrenheit	$5/9(T-32)$	DEG F	
Loss	decibels	1.00000000	DB	dB ↓
	MGS	1.00000000	MGS	

**Table 2 (Cont'd). Input Units and Conversion Factors**

Dimension	Input Unit	Conversion Factor	Code	Results
Attenuation	decibels/centimeter	$1.0000000 \times 10^5$	DB/CM	dB/km
	decibels/inch	$0.39370079 \times 10^5$	DB/IN	
	decibels/feet	$3.28083990 \times 10^3$	DB/FT	
	decibels/yard	$1.09361330 \times 10^3$	DB/YD	
	decibels/meter	$1.00000000 \times 10^3$	DE/M	
	decibels/fathom	$0.54680665 \times 10^3$	DB/F	
	decibels/kilofeet	3.28083990	DB/KFT	
	decibels/kiloyard	1.09361330	DB/KYD	
	decibels/kilometer	1.00000000	DB/KM	
	decibels/mile	0.62137119	DB/MI	
	decibels/nautical mile	0.53995680	DB/N M	↓
Dimensionless	thousand to 1	$1.00000000 \times 10^3$	1000/	1
	hundred to 1	$1.00000000 \times 10^2$	100/	
	ten to 1	$1.00000000 \times 10^1$	10/	
		1.00000000	1/	
		1.00000000	/1	
	parts per ten	$1.00000000 \times 10^{-1}$	/10	
	parts per hundred	$1.00000000 \times 10^{-2}$	/100	
	parts per thousand	$1.00000000 \times 10^{-3}$	/1000	↓

## PARAMETER CARDS

NISSM II input data cards are grouped according to format in table 3A, where we see that parameter cards specify a single number such as the sonar depth. The first 30 columns of the card contain the data-identification code, the next 10 list the value, and the following 10 indicate the units. For example, the following parameter card indicates that the sonar depth is 20 ft:

[illegible]

In the majority of cases, the unit may be any alphanumeric abbreviation taken from table 2, and the input parameter is simply multiplied by the corresponding conversion factor. Scattering strengths and intensity levels, on the

other hand, are converted to pressure ratios and must be entered in decibels. A large negative number less than -300 dB will be converted to zero.

If a parameter card is omitted from the input deck, the default value is assumed. If two or more parameter cards having the same identification code appear in the input deck, the most recently read value is used.

It is necessary to discuss several of the input parameters in somewhat more detail: The minimum and maximum ranges define the target-range coordinates by generating 128 equally spaced values. Similarly, the minimum and maximum times generate 256 equally spaced values for the reverberation and signal-to-noise computations.

We see from table 3A that one may input the sea state,  $ss$ , wave height,  $z_w$ , and wind speed,  $v$ , as three independent quantities. However, if, for example, the sea state is specified, but the wind speed and wave height are not, then  $v$  and  $z_w$  are computed according to

$$v = 5 \times ss \text{ knots}$$

and

$$z_w = 0.0026 \times v^{5/2} \text{ ft,}$$

respectively. The last equation may be found in reference 20. If not one of the three quantities is inputted, all are assumed to be zero by default.

Parameter cards must be punched as follows:

Columns 1-30	Data-identification code left justified.
Columns 31-40	Value in an F10.0 format.
Columns 41-50	Unit left justified.

Table 3A. Input Parameter Cards

Data-Identification Code	Default Value
Averaging Time	Pulse length
Bandwidth	1 Hz if the pulse length has not been read; (pulse length) <sup>-1</sup> if the pulse length has been read.
Bottom Depth	Maximum depth in the velocity-depth profile.
Bottom-Scattering Constant	0 ( $-\infty$ dB)
Closing Speed	0 km/s
Directivity Index	1 (0 dB)
Frequency	0 Hz
Horizontal Beamwidth	$2\pi$ rad (360 deg)
Maximum Range	0 km
Maximum Time	0 s
Minimum Range	0.1 km
Minimum Time	0.1 s
Probability of False Alarm	0
Pulse Length	0 s
Receiver Level	1 (0 dB)
Receiver Tilt Angle	0 rad
Sea State	Function of wave height or wind speed, depending on which is read in last.
Self-Noise	0 ( $-\infty$ dB)
Sonar Depth	0 km
Sonar Level	1 (0 dB)
Sonar-Tilt Angle	0 rad
Surface-Scattering Constant	0 ( $-\infty$ dB)
Target Depth	0 km

Table 3A (Cont'd). Input Parameter Cards

Data-Identification Code	Default Value
Target Level	1 (0 dB)
Target Strength	0 ( $-\infty$ dB)
Target-Tilt Angle	0 rad
Transmitter Level	1 (0 dB)
Transmitter Tilt Angle	0 rad
Wave Height	Function of sea state or wind speed, depending on which is read in last.
Wind Speed	Function of sea state or wave height, depending on which is read in last.

The data in table 3B may be entered as a table of dependent variables versus independent variables according to the format below:

Card 1	Columns 1-30	Data-identification code left justified.
Card 2	Columns 1-10	Units of the independent variable left justified.
	Columns 11-20	Units of the dependent variable left justified.
Card i+2	Columns 1-10	i-th entry of the independent variable in an F10.0 format. (The entries must form a strictly increasing sequence.)
	Columns 11-20	i-th entry of the dependent variable in an F10.0 format.
Last card	Columns 1-5	7/8 EOF (end of file)

When indicated, a compact format is allowed. The independent variable entries are assumed to be spaced one degree apart, and only the dependent variable entries are read:

Card 1	Columns 1-30	Data-identification code left justified.
	Columns 31-40	Word COMPACT left justified.
Card i + 1	Columns 1-50	Dependent variable entries in a 10F5.0 format.

Table 3B. Input Tables

Data-Identification Code	Default Value	Options
Ambient Noise	Knudsen curves	Ambient noise may be entered as a table of noise versus frequency (91 entries maximum). KNUDSEN CURVES punched in columns 31-40, left justified, activates the Knudsen curve option.
Attenuation Coefficient	Thorp's equation <sup>10</sup>	Attenuation may be entered as a table of attenuation coefficient versus frequency (91 entries maximum). THORP punched in columns 31-40, left justified, activates the Thorp equation option.
Bottom Loss	1 (0 dB)	A temperature unit punched in columns 41-50, left justified, activates the Hall-Watson equation option. The surface temperature must be punched in columns 31-40 according to an F10.0 format. Bottom loss may be entered as a table of loss versus bottom angle (91 entries maximum). Bottom loss may be entered using the compact format by specifying the loss for every degree from 0 to 90. MGS punched in columns 41-50, left justified, activates the MGS equation option. The province must be punched in columns 31-40 according to an F10.0 format. If an acceptable unit other than MGS is punched in columns 41-50, the NUC bottom-loss model is activated and the bottom porosity must be punched in columns 31-40.



Table 3B (Cont'd). Input Tables

Data-Identification Code	Default Value	Options
Receiver Response	1 (0 dB)	Receiver response may be entered as a table of response versus receiver angle (181 entries maximum). Receiver response may be entered using the compact format by specifying the response for every degree from -90 to +90. SONAR, TARGET, or TRANSMITTER punched in columns 31-40, left justified, sets the receiver response equal to the sonar, target, or transmitter response, respectively.
Sonar Response	1 (0 dB)	Sonar response may be entered as a table of response versus sonar angle (181 entries maximum). Sonar response may be entered using the compact format by specifying the response for every degree from -90 to +90.
Surface Loss	1 (0 dB)	Surface loss may be entered as a table of loss versus surface angle (91 entries maximum). Surface loss may be entered using the compact format by specifying the loss for every degree from 0 to 90.
Target Response	1 (0 dB)	Target response may be inputted as a table of response versus target angle (181 entries maximum). Target response may be entered using the compact format by specifying the response for every degree from -90 to +90. SONAR punched in columns 31-40, left justified, sets the target response equal to the sonar response.

Transmitter Response	1 (0 dB)	<p>Transmitter response may be entered as a table of response versus transmitter angle (181 entries maximum).</p> <p>Transmitter response may be entered using the compact format by specifying the response for every degree from -90 to +90.</p> <p>SONAR or TARGET punched in columns 31-40, left justified, sets the transmitter response equal to the sonar or target response, respectively.</p>
Velocity Profile		<p>Velocity may be entered as a table of velocity versus depth (48 entries maximum).</p> <p>A temperature unit punched in card 2, columns 11-20, left justified, activates the temperature-salinity option. The units of salinity must then be punched in card 2, columns 21-30, left justified. The latitude, in degrees, must be punched in card 2, columns 31-40, according to an F10.0 format. A depth-temperature-salinity table, punched according to a 3F10.0 format, and a 7/8 EOF card must follow.</p>
Volume-Scattering Strength	0 (-∞ dB)	<p>Volume-scattering strengths may be entered as a table of the volume-scattering strength versus depth (128 entries maximum).</p>

Axis cards listed in table 3C must be punched as follows:

- Columns 1-30 Data-identification code left justified.
- Columns 31-40 Minimum value to be plotted in an F10.0 format.
- Columns 41-50 Maximum value to be plotted in an F10.0 format.
- Columns 51-60 Axis length, in inches, in an F10.0 format.
- Columns 61-70 Axis unit left justified.

The default values listed below pertain to the axis length only. Under a default condition, the minimum and maximum values are set by the CalComp subroutine SCALE.

Table 3C. Input Axis Cards

Data-Identification Code	Default Value (in. )	Direction
Depth Axis	10	Vertical
Propagation-Loss Axis	10	Vertical
Range Axis	20	Horizontal
Reverberation Axis	10	Vertical
Signal-to-Noise-Ratio Axis	10	Vertical
Time Axis	20	Horizontal
Velocity Axis	10	Horizontal

The comment card allows the user to print 80-column comments on the printed output and CalComp plots:

- Card 1 Columns 1-30 Word COMMENT left justified.
- Card i+1 Columns 1-80 80-column comments.
- Last card Columns 1-5 7/8 EOF.

The process card signifies that all environmental data have been read and that the main program should begin processing the information:

- Columns 1-30 Word PROCESS left justified.
- Columns 31-40 Word PRINT, left justified, will cause eigenray data to be printed.
- Columns 41-50 Word TOTAL, left justified, will prevent the reverberation computation from being repeated; word VOLUME, left justified, will prevent the volume-reverberation computation from being repeated.

The initial inclination angle card specifies which rays are to be traced by RAYPLT:

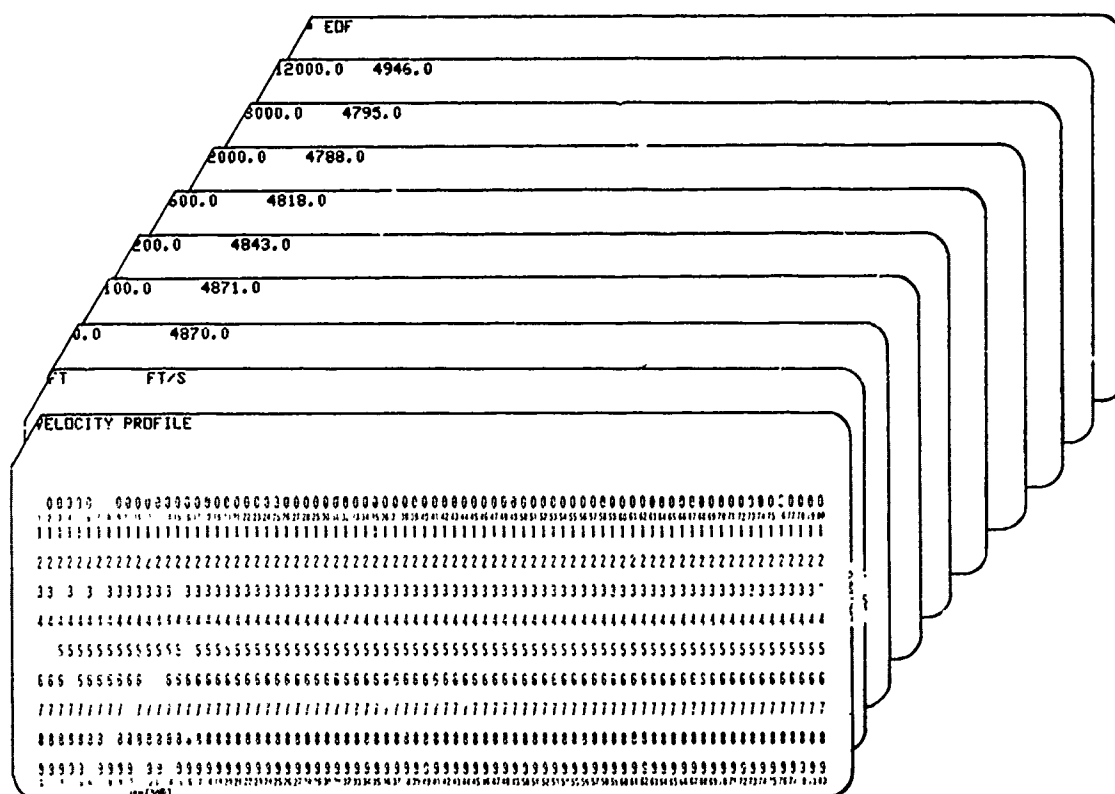
- Columns 1-10 Initial angle of the first ray in an F10.0 format.
- Columns 11-20 Initial angle of the final ray in an F10.0 format.
- Columns 21-30 Initial angle increment in an F10.0 format.
- Columns 31-36 Angle units, left justified.
- Columns 37-40 A print option in an I4 format. If blank or 0, the printing of ray coordinates will be suppressed. If i, the final coordinates of every i-th ray segment will be printed.
- Columns 41-50 Maximum number of surface intersections in an I10 format.
- Columns 51-60 Maximum number of bottom intersections in an I10 format.
- Columns 61-70 Maximum number of upper vertexes in an I10 format.
- Columns 71-80 Maximum number of lower vertexes in an I10 format.

The end card signifies that the execution should be terminated:

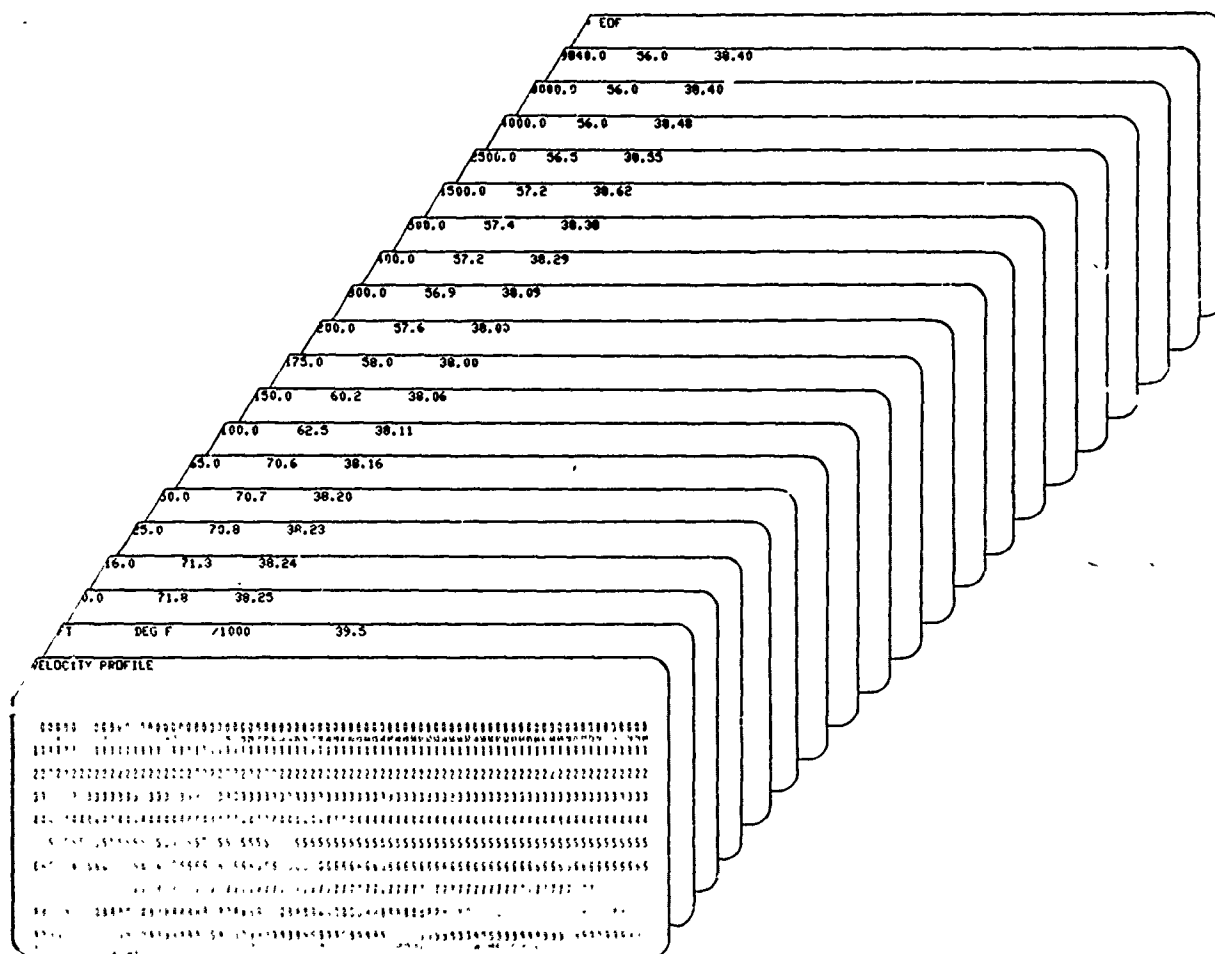
- Columns 1-30 Word END left justified.

## INPUT TABLES

Environmental and system characteristics that ordinarily can not be described by a single parameter may be entered as a table of independent versus dependent variable. The standard table format requires punching the data-identification code in columns 1-30 of the first card in the card set. Card 2 contains the independent and dependent units in columns 1-10 and 11-20, respectively. Then the table is inputted one data point per card according to a 2F10.0 format. An EOF follows the last data card of the set. For example, the following is a table of velocity-profile data.

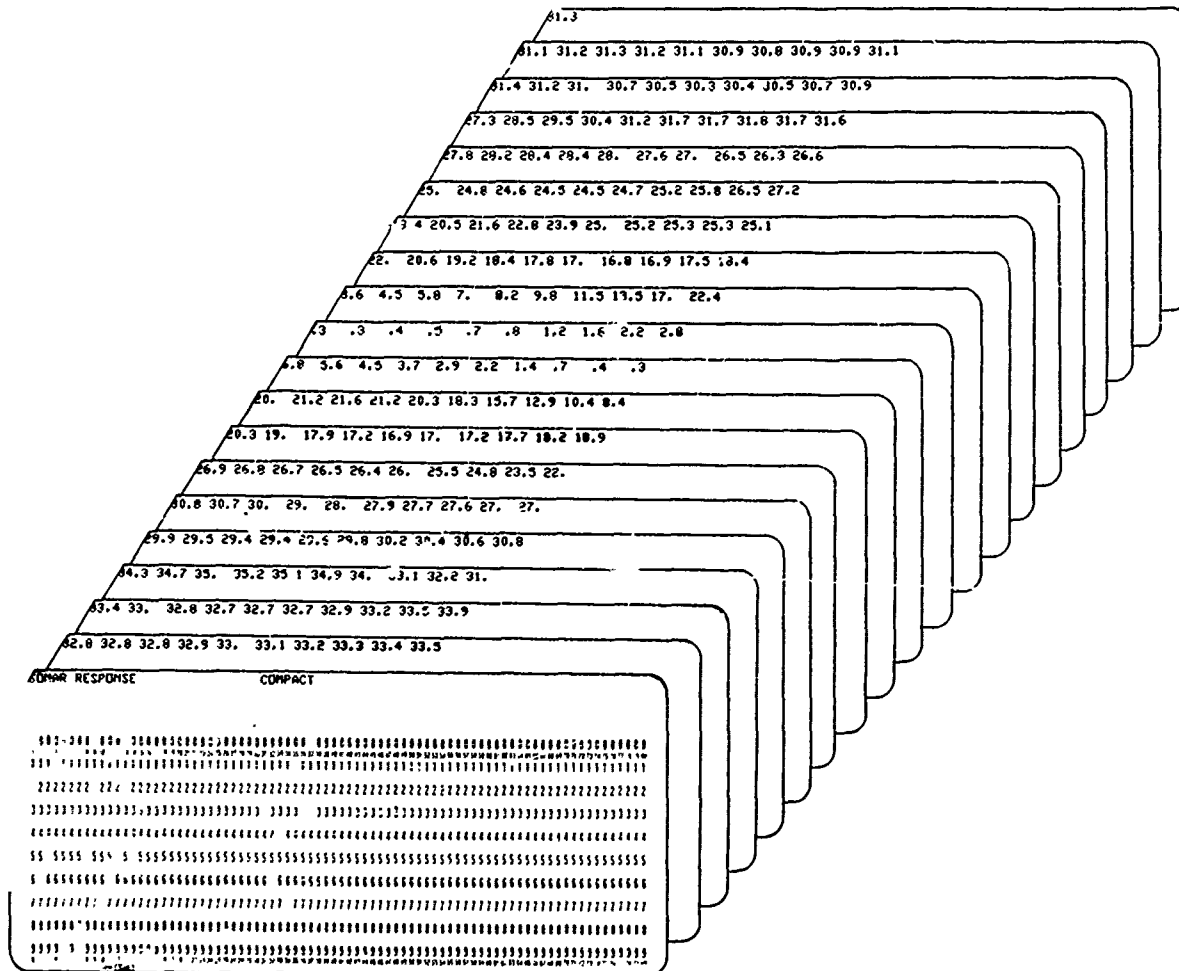


Velocity profiles may also be expressed in terms of depth, temperature, and salinity. Allowable temperature units can be in degrees Fahrenheit or centigrade, but salinity is usually in parts per thousand. The latitude, in degrees, appears in columns 31-40 of the units card. Depth, temperature, and salinity data punched in columns 1-10, 11-20, and 21-30, respectively, follow. For example,



The standard table format permits inserting, deleting, and correcting entries with minimum effort. Independent variables must form an increasing sequence, but are otherwise arbitrary. A possible disadvantage of the standard table format is that the input deck becomes difficult to manipulate when several large tables are present.

Thus we have given the option to enter certain environmental and system characteristics in a fixed compact format. The word COMPACT must be punched in columns 31-40 of the data-identification card, which is to be followed by the dependent variables, in decibels, according to a 10F5.0 format. If the compact option is used, 181 values of response must be entered for every degree from -90 to +90. Surface and bottom losses, however, must be entered for every degree from 0 to 90; for example,



Several environmental characteristics may be generated internally by the computer program. For example, the following card will activate the MGS 3 bottom-loss function:

[illegible]

See table 3B for a list of additional options.

## CALCOMP AXIS CARDS

The user may either (1) set CalComp axis values, lengths, and units or (2) use default values. If the first option is employed, the appropriate axis card must contain the data-identification code in columns 1-30, the minimum and maximum values, the axis length, and the output units in the four subsequent field of 10 columns each. The following axis card will allow reverberation values from -90 to 0 dB to be plotted on a graph whose vertical axis is 9 in.

[illegible]

Default values for axis lengths are listed in table 3C; minimum and maximum default values are set by the CalCom<sub>2</sub> subroutine SCALE, and the default units are determined by other input data cards.

### PROCESS CARD

The process card serves to separate cases and set certain options. If the word PRINT appears in columns 31-40, the acoustic eigenrays to each target will be listed. Since there are usually 8 eigenrays per target, and 128 targets per target depth, it follows that 1024 lines may be printed. This increases the running time of the program substantially.

A problem often encountered in sonar-system analysis is to determine the variation of the signal-to-noise ratio with target depth. Since reverberation is independent of the target depth, repetition of the rather lengthy reverberation



computation may be suppressed by punching TOTAL in columns 41-50. If, instead, VOLUME is punched in columns 41-50, surface and bottom reverberation will be computed, and only volume reverberation will be suppressed. An example of a valid process card follows:

[illegible]

### INITIAL INCLINATION ANGLES

Initial inclination angle cards specify those rays that are to be plotted.\* As indicated in table 3C, the first four fields on the card generate the angles and the last four limit the number of vertexes and boundary intersections. A positive integer punched in columns 37-40 will cause data to be printed as well. For example, the following card will plot rays having initial inclination angles of -5, -4, -3, -2, -1, -0, and +1 deg and print the coordinates of every fifth ray segment:

[illegible]

A ray will be terminated when it has undergone 2 surface intersections, 1 bottom intersection, 10 upper vertexes, or 10 lower vertexes.

END CARD

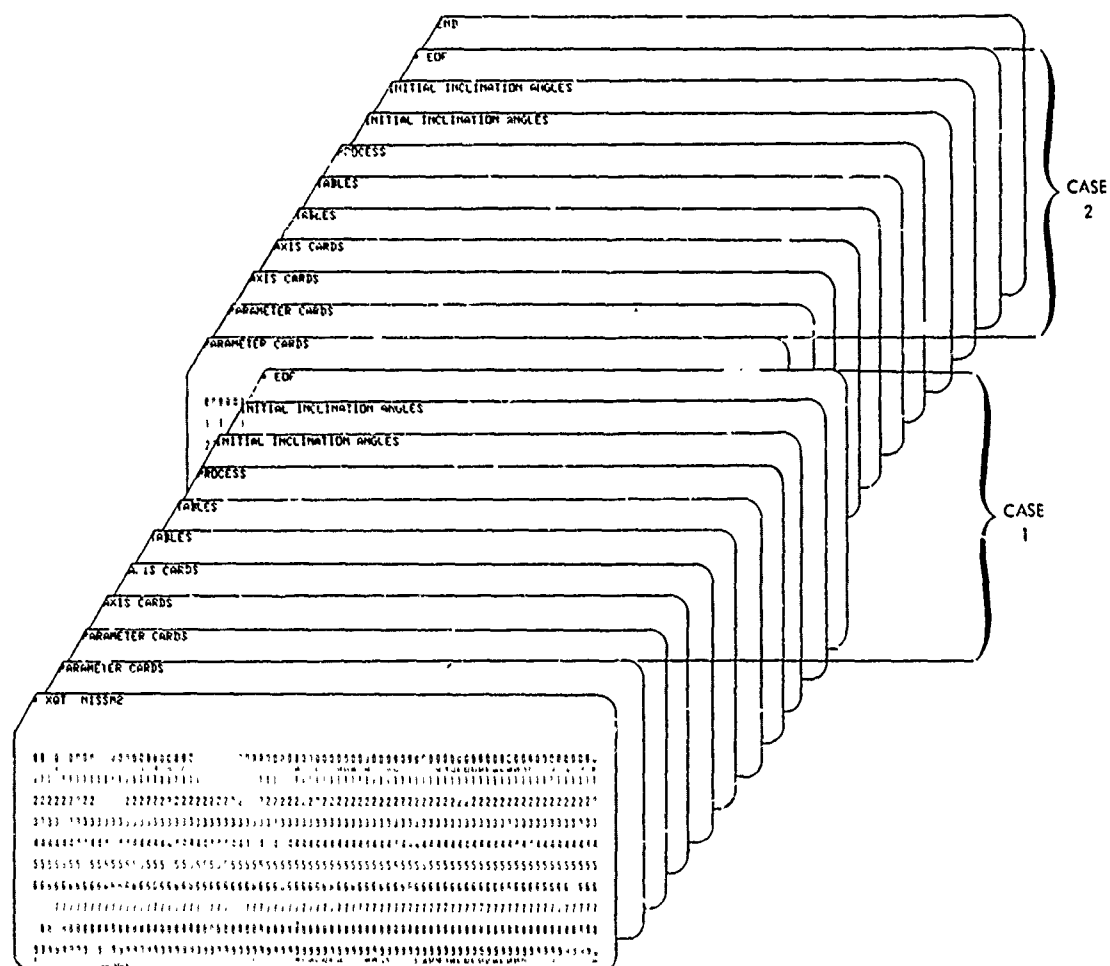
**The last card of the input deck should be the end card:**

[illegible]

\*These rays are not used in the acoustic eigenray computation.

## INPUT DECK

A NISSM II input deck, shown schematically below, begins with the execute (XQT) card and is followed by the table and parameter and axis cards comprising case 1 (see below).\* Then, after reading the process card, NISSM II



\*The order within a case is not important.

constructs a ray diagram using the indicated initial inclination angles. If the inclination angles are missing, the ray plot will be suppressed. The @ EOF card, which is necessary whether or not rays are plotted, returns control to the main program, where propagation loss, reverberation, signal-to-noise ratio, and probability-of-detection curves are constructed. Subsequent cases are similar to case 1, except that the data which do not change from one case to the next need not be repeated. The end card terminates the execution.

### RAY DIAGRAMS, EXAMPLE 1

As an example of a NISSM II run, let us consider the construction of ray diagrams (example 1), which required 24 s of Univac 1108 execution time. A typical input deck is listed in table 4. As stated earlier, axis cards are unnecessary if default values are satisfactory. The circles in figure 25 denote input-velocity data before curvature-of-the-earth corrections were performed. However, the continuous-gradient approximation to the velocity profile, indicated by the solid line in figure 25, does include curvature corrections. This difference becomes more apparent in deep ocean profiles. We see from table 5 that only four approximating functions (five breakpoints) were required to fit the data.

The ray diagram in figure 26 corresponds to a sonar placed on the sound-channel axis at 76 m. Rays were traced every 0.2 deg, from -7.0 to +7.0 deg, and were terminated upon intersecting a boundary surface or reaching the maximum range of 5 km. In this particular example, the maximum number of vertexes was not attained. A partial listing of printed output appears in table 6.

The ray diagram in figure 27 is similar to that in figure 26, except that the sonar was placed at 40 m, which is 36 m above the sound-channel axis.

Table 4. Input Deck for Constructing Ray Diagrams, Example 1

```

Δ XQT NISSM2
COMMENT
      EPSTEIN PROFILE
Δ EOF
RANGE AXIS      0.0      5.0      5.0      KM
DEPTH AXIS      0.0      200.0    4.0      M
VELOCITY AXIS   1495.0    1505.0    5.0      M/S
MAXIMUM RANGE   5.0      KM
SONAR DEPTH     76.0      M
VELOCITY PROFILE
M              M/S
  0.000 1502.19783
  4.000 1502.12858
 10.000 1501.99547
 14.000 1501.88285
 22.000 1501.58461
 30.000 1501.16430
 38.000 1500.59710
 46.000 1499.88046
 54.000 1499.00191
 62.000 1498.20630
 70.000 1497.69307
 74.000 1497.55792
 76.000 1497.53779
 78.000 1497.55156
 86.000 1497.94980
 94.000 1498.82055
102.000 1499.95718
110.000 1501.12684
118.000 1502.16418
126.000 1502.99650
134.000 1503.82023
142.000 1504.06651
150.000 1504.37602
158.000 1504.58627
166.000 1504.72716
174.000 1504.82071
180.000 1504.80935
Δ EOF
PROCESS
-7.0      +7.0      0.2      DEG      1      1      1      5      5
Δ EOF
SONAR DEPTH      40.0      M
PROCESS
-7.0      +7.0      0.2      DEG      1      1      5      5
Δ EOF
END
Δ FIN

```

Table 5. Continuous-Gradient Parameters for Example 1

LAYER	Z0	V0	G0	G1	G2	C0
1	.00000000	.44314400	.8859920-002	.46503297+000	-.63119712-001	.15021978+01
2	.54000000-001	.44499334+000	.59748715-001	-.17276681+001	-.12376590+002	.14990746+01
3	.75999999-001	.44589649+000	.00000000	-.43760503+001	.15868182+002	.14975557+01
4	.11000000+000	.44376212+000	-.81552398-001	.25443318+000	.59938219+001	.15011528+01
5	.10000000+000	.44154794+000	-.40951959-002	.00000000	.00000000	.15049119+01

Table 6. Partial Ray Printout for Example 1

RANGE KM	DEPTH M	ANGLE DEG	ARC LENGTH KM	TRAVEL TIME SEC	PROP LOSS DB	PHASE DEG	REMARKS
000000.0	759999990+02	-30000101+01	000000000	000000000	000000000	000000000	INITIAL POINT
522886.14+00	539999995+02	-13227673+01	348922748+00	348922748+00	546505418+02	000000000	ABSOLUTE UPPER VERTEX
9455536.7+00	484275222+02	000000000	631238297+00	631238297+00	598587070+02	000000000	CAUSTIC
9455536.7+00	484275222+02	000000000	631238297+00	631238297+00	598587070+02	000000000	ABSOLUTE LOWER VERTEX
13688186.2+01	539999995+02	13227673+01	913553841+00	913553841+00	636331015+02	000000000	CAUSTIC
1891107.3+01	759999990+02	300000098+01	126247659+01	126247659+01	662101030+02	000000000	ABSOLUTE UPPER VERTEX
2400464.1+01	917282495+02	923441142+00	160654777+01	160654777+01	299999996+03	000000000	CAUSTIC
2635965.7+01	987324171+02	000000000	175977091+01	175977091+01	625968646+02	-900000000+02	ABSOLUTE LOWER VERTEX
338082328+01	759999990+02	-300000098+01	225706524+01	225706524+01	701238956+02	-900000000+02	CAUSTIC
390311208+01	539999995+02	-13227673+01	260598800+01	260598800+01	658913231+02	-900000000+02	ABSOLUTE UPPER VERTEX
4100833.4+01	513969059+02	-816498145+00	273786721+01	273786721+01	299999996+03	-900000000+02	CAUSTIC
432637709+01	484275222+02	000000000	288630355+01	288630355+01	664630880+02	-180000000+03	ABSOLUTE UPPER VERTEX
474964207+01	539999995+02	13227673+01	288630355+01	288630355+01	664630880+02	-180000000+03	CAUSTIC
5271930.3+01	759999990+02	300000098+01	351954183+01	351954183+01	744237356+02	-180000000+03	ABSOLUTE UPPER VERTEX
5271930.3+01	759999990+02	300000098+01	351954183+01	351954183+01	744237356+02	-180000000+03	MAXIMUM RANGE
000000000	759999990+02	-20000103+01	000000000	000000000	000000000	000000000	INITIAL POINT
59784020.1+00	539999995+02	-10895340+01	399174906+00	399174906+00	556953425+02	000000000	ABSOLUTE UPPER VERTEX
889361105+00	512468243+02	000000000	593763560+00	593763560+00	590854740+02	000000000	CAUSTIC
118108207+01	539999995+02	10895340+01	788352214+00	788352214+00	618071318+02	000000000	ABSOLUTE LOWER VERTEX
177872233+01	759999990+02	20000103+01	118752712+01	118752712+01	648157387+02	000000000	CAUSTIC
224303833+01	893200636+02	100001704+01	149753217+01	149753217+01	299999996+03	000000000	ABSOLUTE UPPER VERTEX
250099802+01	967202988+02	000000000	166976185+01	166976185+01	622631307+02	-900000000+02	CAUSTIC
322527469+01	759999990+02	-20000103+01	215199655+01	215199655+01	689566956+02	-900000000+02	ABSOLUTE LOWER VERTEX
382091516+01	539999995+02	10895340+01	255117148+01	255117148+01	609773388+02	-900000000+02	CAUSTIC
3690004.8+01	533102002+02	-81655783+00	259992504+01	259992504+01	299999996+03	-900000000+02	ABSOLUTE UPPER VERTEX
411263603+01	512468243+02	000000000	274576011+01	274576011+01	657358852+02	-180000000+03	CAUSTIC
440435676+01	539999995+02	10895340+01	274576011+01	274576011+01	657358852+02	-180000000+03	ABSOLUTE UPPER VERTEX
5001997.3+01	759999990+02	20000103+01	339952370+01	339952370+01	731655121+02	-180000000+03	CAUSTIC
5001997.3+01	759999990+02	20000103+01	339952370+01	339952370+01	731655121+02	-180000000+03	MAXIMUM RANGE

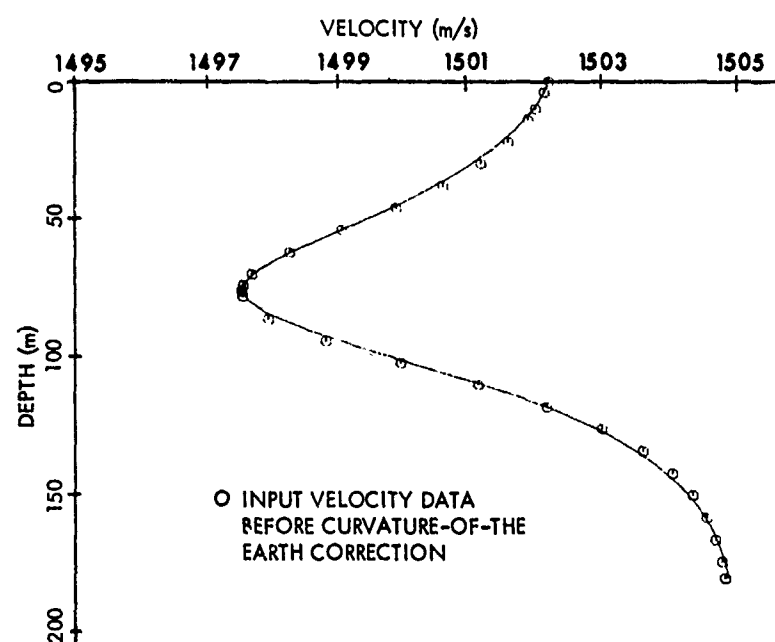


Figure 25. Velocity Profile for Example 1

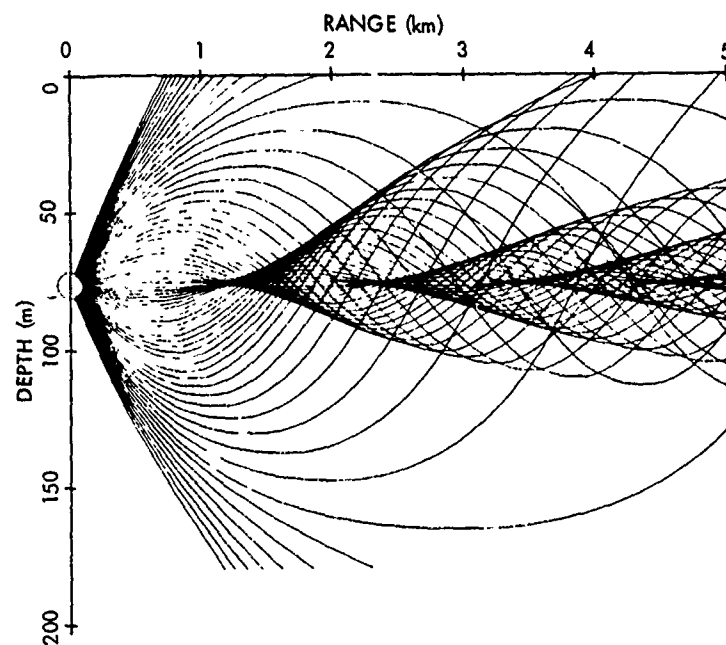


Figure 26. Ray Diagram Corresponding to a Sonar Placed on the Sound-Channel Axis, Example 1

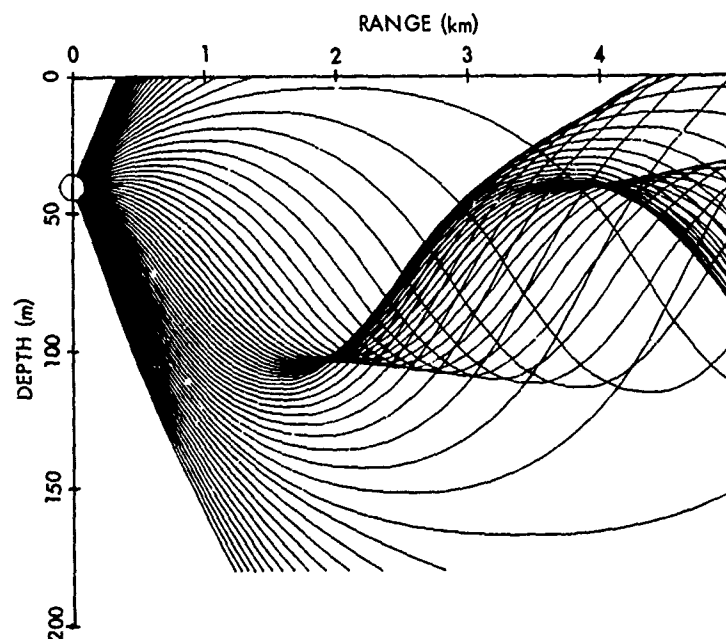


Figure 27. Ray Diagram Corresponding to a Sonar Placed Above the Sound-Channel Axis, Example 1



## PROPAGATION LOSS VERSUS RANGE, EXAMPLE 2

Propagation loss versus range is computed whenever a target-depth card appears in the input deck. For example, the cards listed in table 7 will generate the velocity profile in figure 28, the ray diagram in figure 29, and the propagation losses at the two target depths in figures 30 and 31.

Table 8 converts the temperature-salinity-depth data to velocities, which are then plotted in figure 28. See table 9 for the corresponding continuous-gradient parameters. By making use of the minimum-range card and inserting a new range axis, we are able to enlarge a particular region of interest, in this case, the first convergence zone.

Example 2 required 37 s of execution time.

If the word PRINT were punched in the process card, one would obtain the eigenray printout of table 10. The problem would then require 41 s to be processed.

Table 7. Input Deck for Computing Propagation  
Loss versus Range, Example 2

```

Δ XQT NISSM2
COMMLNT
      TYRRENIAN SEA-JUNE 1969

Δ EOF
RANGE AXIS          0.00      55.0      11.0      KYD
DEPTH AXIS          0.0      10000.0      5.0      FT
VELOCITY AXIS       1.50      1.56      6.0      KM/S
VELOCITY PROFILE
FT      DEG F      /1000      30.5
0.0      71.8      36.25
10.0      71.3      38.24
25.0      70.8      38.23
50.0      70.7      38.20
65.0      70.6      38.18
100.0      62.5      38.11
150.0      60.2      38.06
175.0      58.0      38.00
200.0      57.6      38.00
300.0      56.9      38.09
400.0      57.2      38.29
500.0      57.4      38.38
1500.0      57.2      38.62
2500.0      56.5      38.55
4000.0      56.0      38.48
6000.0      56.0      38.46
9840.0      56.0      38.40
Δ EOF
BOTTOM DEPTH        9840.0 FT
BOTTOM LOSS          3.0 MGS
FREQUENCY            3.55 KCPS
SONAR DEPTH          16.0 FT
MAXIMUM RANGE        55.0 KYD
SONAR TILT ANGLE     5.0 DEG
SONAR RESPONSE
LEG      DB
-90.0      18.0
-16.0      18.0
-15.0      17.6
-14.0      16.1
-13.0      17.4
-12.0      15.8
-11.0      13.2
-10.0      11.0
-9.0       8.8
-8.0       7.0
-7.0       5.2
-6.0       3.6
-5.0       2.3
-4.0       1.0
-3.0       0.5
-2.0       0.2
-1.0       0.1
0.0        0.0
2.0        0.2

```

Table 7 (Cont'd). Input Deck for Computing Propagation  
Loss versus Range, Example 2

3.0	0.4						
5.0	1.0						
7.0	2.4						
8.0	3.3						
9.0	4.7						
10.0	5.8						
11.0	6.8						
12.0	7.9						
13.0	9.0						
14.0	10.4						
15.0	12.2						
16.0	13.9						
17.0	15.8						
18.0	18.0						
90.0	18.0						
Δ EOF							
PROCLSS							
0.0	20.0	1.0	DEG	2	2	4	4
Δ EOF							
RANGE AXIS			35.0	55.0	4.0		KYD
PROPAGATION LOSS AXIS			40.0	140.0	5.0		DP
MINIMUM RANGE				35.0 KYD			
TARGET DEPTH				25.0 FT			
PROCESS							
Δ EOF							
TARGET DEPTH			150.0 FT				
PROCESS							
Δ EOF							
LND							
Δ FIN							

Table 8. Conversion of Temperature-Salinity-Depth  
to Velocities for Example 2

	DEPTH FT -----	TEMPERATURE DEG F -----	SALINITY /1000 -----	VELOCITY KM/S -----
1	0.0	71.8	38.25	1.53126
2	10.0	71.3	38.24	1.53061
3	25.0	70.8	38.23	1.52993
4	50.0	70.7	38.20	1.52987
5	65.0	70.6	38.16	1.52976
6	100.0	62.5	38.11	1.51734
7	150.0	60.2	38.06	1.51368
8	175.0	58.0	38.00	1.50992
9	200.0	57.6	38.00	1.50934
10	300.0	56.9	38.09	1.50870
11	400.0	57.2	38.29	1.50999
12	500.0	57.4	38.38	1.51096
13	1500.0	57.2	38.62	1.51592
14	2500.0	56.5	38.55	1.51963
15	4000.0	56.0	38.48	1.52623
16	8000.0	56.0	38.40	1.54661
17	9040.0	56.0	38.40	1.55616

Table 9. Continuous-Gradient Parameters for Example 2

LAYER	Z0	V0	G0	G1	G2	C0
1	.00000000	.42640370+000	.53556356-001	-.59936085+001	-.93899282+002	.15312594+01
2	.76200000-002	.42722609+000	.23192947-001	.28237036+002	.12661731+004	.15299284+01
3	.11430000-001	.42723078+000	.64019037-003	.42095717+000	-.40010830+002	.15299021+01
4	.19812000-001	.42731988+000	.26948293-001	.11632824+004	.31379257+003	.15297605+01
5	.30480000-001	.43433938+000	.30127238+000	.46450836+002	.15478423+003	.15173487+01
6	.36100000-001	.43539050+000	.63150388+001	.13659258+002	.13267219+002	.15155160+01
7	.45720000-001	.43644161+000	.19805973+000	-.20979784+002	-.82985634+002	.15136894+01
8	.53340000-001	.43861734+000	.84999463+001	.34303803+000	.34318253+002	.15099310+01
9	.91440000-001	.43931906+000	.00000000	-.54177586+001	.47703337+002	.15087246+01
10	.15240000+000	.43800081+000	-.11066962-001	.69366442-002	-.10579341+000	.15109933+01
11	.60560000+000	.43401469+000	-.61028012-002	-.71556015-002	.25609095+000	.15179161+01
12	.24384000+001	.41773804+000	-.92921991-002	-.98258041-004	.10574252-001	.15472054+01
13	.2999230+001	.41255740+000	-.91829593-002	.00000000	.00000000	.15568496+01

Table 10. Partial Eigenray Printout for Example 2

TARGET DPTH = .250000+02 FT											
RAYID	SURF ANGLE ULG	TARGET ANGLE DEG	ARC LENGTH KYU	TRAVEL TIME SEC	PROP LOSS DB	PHASE DEG	SURF REF	BOT REF	UPPER LOWFR VERTX	UPPER HIGHFR VERTX	
483500200+02	-.10582000+02	.107029000+02	.489171777+02	.290808594+02	.119270273+03	-.360000000+03	2	1	0	0	
483500200+02	-.105794421+02	-.107003367+02	.489153061+02	.290786363+02	.119085917+03	-.360000000+03	1	1	0	0	
483500200+02	-.105779231+01	-.907210611+01	.488538628+02	.290765276+02	.10807211+03	-.180000000+03	1	0	0	1	
483500200+02	-.105763079+01	.902855852+01	.488522840+02	.290761770+02	.106755525+03	-.360000000+03	2	0	0	1	
483500200+02	.105722397+01	.905670395+01	.488533278+02	.290771279+02	.10079102+03	-.180000000+03	1	0	0	1	
483500200+02	.105661400+01	.909990030+01	.488544803+02	.290754786+02	.100840099+03	.000000000	0	0	0	1	
483500200+02	.105771304+02	-.106906733+02	.489141226+02	.290776789+02	.11924888+03	.000000000	0	1	0	0	
483500200+02	.105803422+02	.107012559+02	.489159422+02	.290795000+02	.119004500+03	-.180000000+03	1	0	0	0	
483500200+02	-.105714200+02	.106903743+02	.490740633+02	.291731479+02	.110367295+03	-.360000000+03	2	1	0	0	
483500200+02	-.105751200+02	-.106901027+02	.490721922+02	.291713269+02	.119971712+03	-.180000000+03	1	1	0	0	
483500200+02	-.105073035+01	-.974061763+01	.490159879+02	.291693034+02	.10903671+03	-.180000000+03	1	0	0	1	
483500200+02	-.105630129+01	.909749284+01	.490144420+02	.291709530+02	.100853087+03	-.360000000+03	2	0	0	1	
483500200+02	.105918391+01	.972532300+01	.490154643+02	.291699042+02	.100886070+03	-.180000000+03	1	0	0	1	
483500200+02	.105352400+01	-.976812613+01	.490169849+02	.291682549+02	.100936192+03	.000000000	0	0	0	1	
483500200+02	.105738200+02	-.106940152+02	.490710082+02	.291701672+02	.120426621+03	.000000000	0	1	0	0	
483500200+02	.105759109+02	.106908759+02	.490728793+02	.291719882+02	.119732654+03	-.180000000+03	1	1	0	0	
487007000+02	-.105730067+02	.106940598+02	.492309484+02	.292606362+02	.120588678+03	-.360000000+03	2	1	0	0	
487007000+02	-.105713663+02	.106928062+02	.492290773+02	.292638152+02	.121247198+03	-.180000000+03	1	1	0	0	
487007000+02	-.105765153+01	-.908882514+01	.491781139+02	.292620800+02	.101000052+03	-.180000000+03	1	0	0	1	
487007000+02	-.105332362+01	.970661732+01	.491763995+02	.292637293+02	.100950142+03	-.360000000+03	2	0	0	1	
487007000+02	.106117394+01	.979369485+01	.491775013+02	.292626803+02	.100982552+03	-.180000000+03	1	0	0	1	
487007000+02	.107041027+01	.903603394+01	.491798895+02	.292610312+02	.101031826+03	.000000000	0	0	0	1	
487007000+02	.105700831+02	-.106919069+02	.492278943+02	.292626555+02	.121655800+03	.000000000	0	1	0	0	
487007000+02	.105724507+02	.106930619+02	.492297649+02	.292644765+02	.121007970+03	-.180000000+03	1	1	0	0	
488300000+02	-.105707309+02	.106917560+02	.49387.341+02	.293550124+02	.121709371+03	-.360000000+03	2	1	0	0	
488300000+02	-.105693640+02	-.106904040+02	.493859634+02	.293563035+02	.122344733+03	-.180000000+03	1	1	0	0	
488300000+02	-.105745421+01	.907679052+01	.493400846+02	.293554840+02	.101095736+03	-.180000000+03	1	0	0	1	
488300000+02	-.107020509+01	.903460212+01	.493387575+02	.293565056+02	.101046707+03	-.360000000+03	2	0	0	1	
488300000+02	.107302.570+01	.908182153+01	.493392739+02	.293554580+02	.101078564+03	-.180000000+03	1	0	0	1	
488300000+02	.107727067+01	-.903370504+01	.493406811+02	.293537545+02	.101126874+03	.000000000	0	0	0	1	
488300000+02	.105603862+02	-.106896361+02	.493847804+02	.293551440+02	.122671362+03	.000000000	0	1	0	0	
488300000+02	.105669143+02	.106901789+02	.493866506+02	.293569644+02	.122142617+03	-.180000000+03	1	1	0	0	

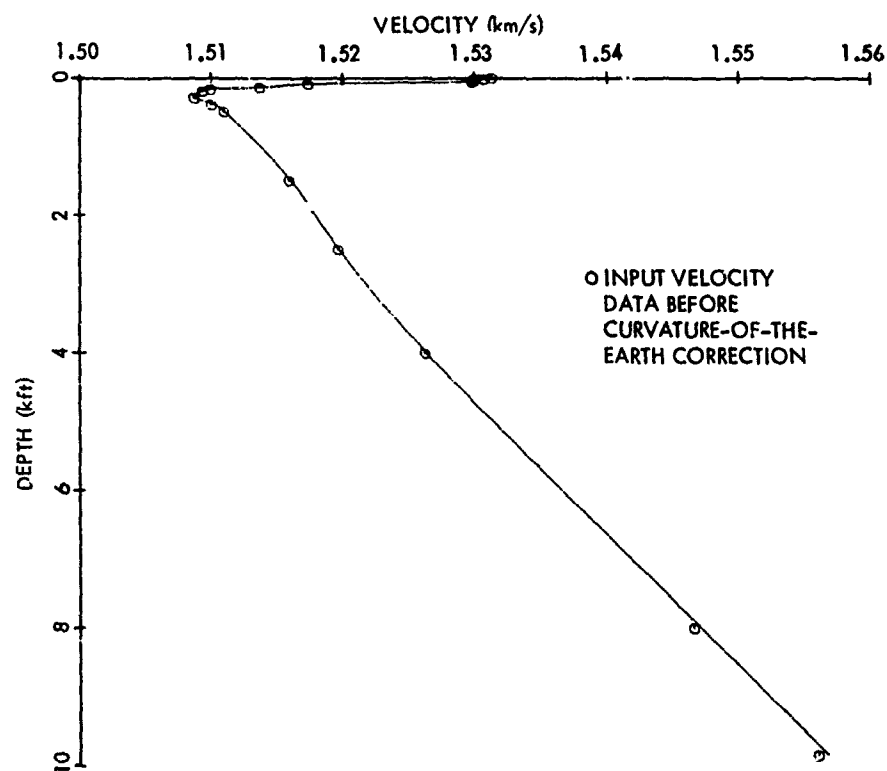


Figure 28. Velocity Profile for Example 2

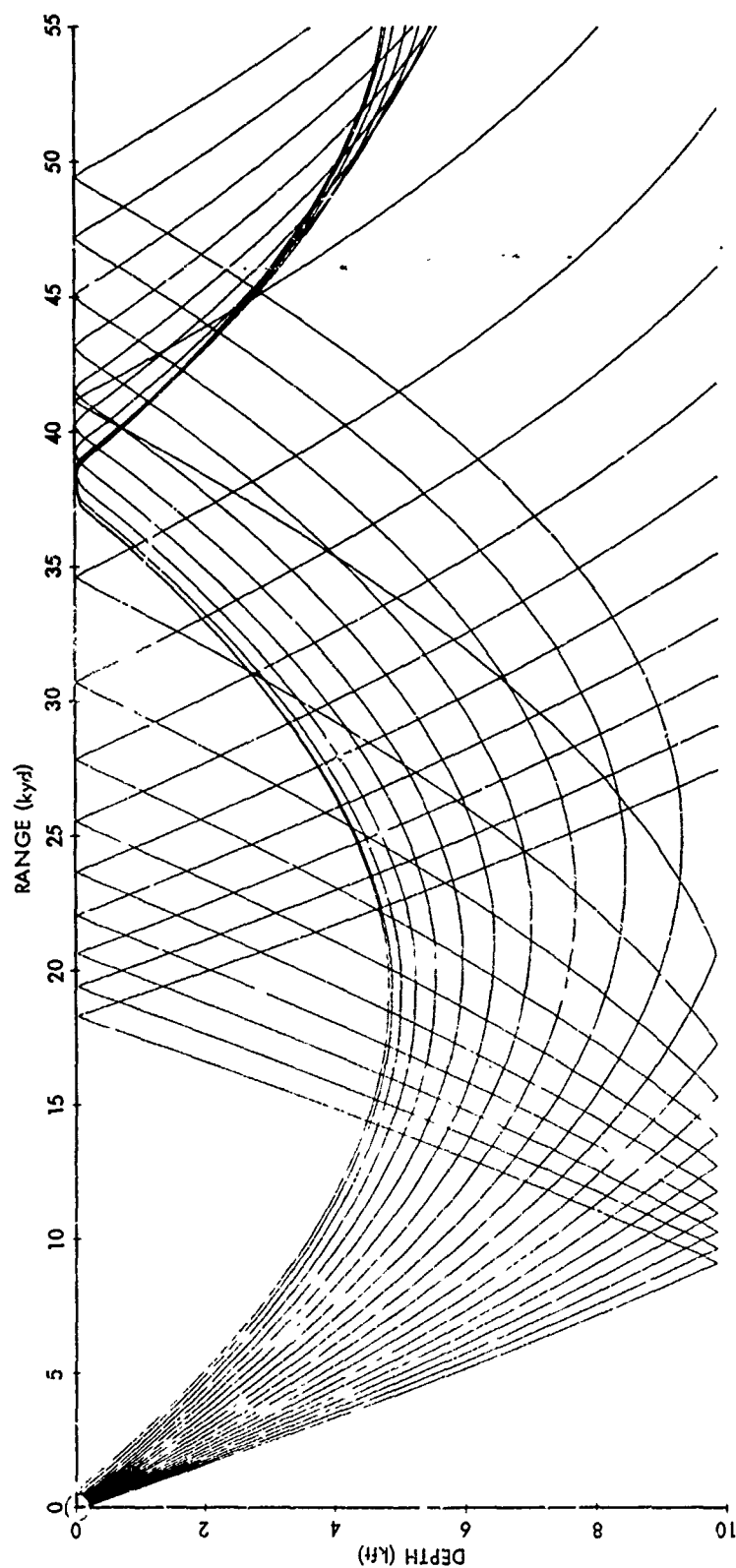


Figure 29. Ray Diagram for Example 2



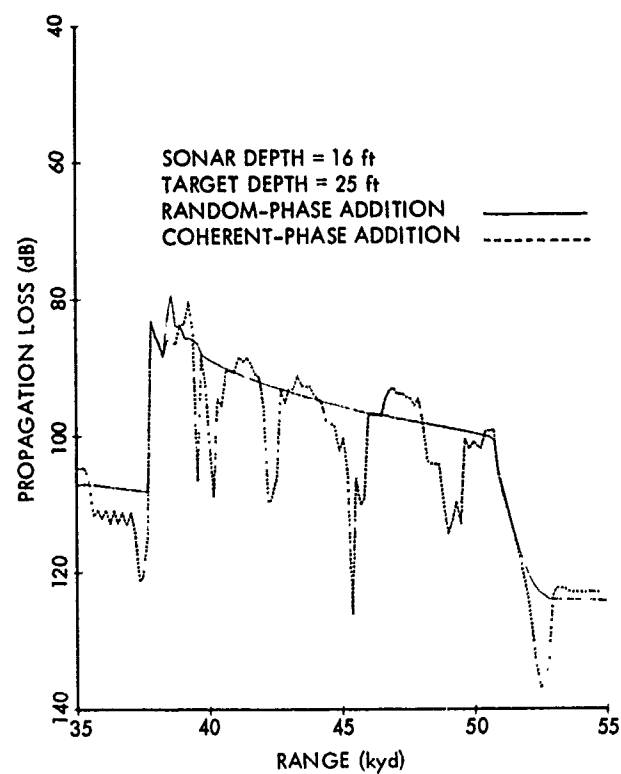


Figure 30. Propagation Loss for a 25-ft Target Depth, Example 2

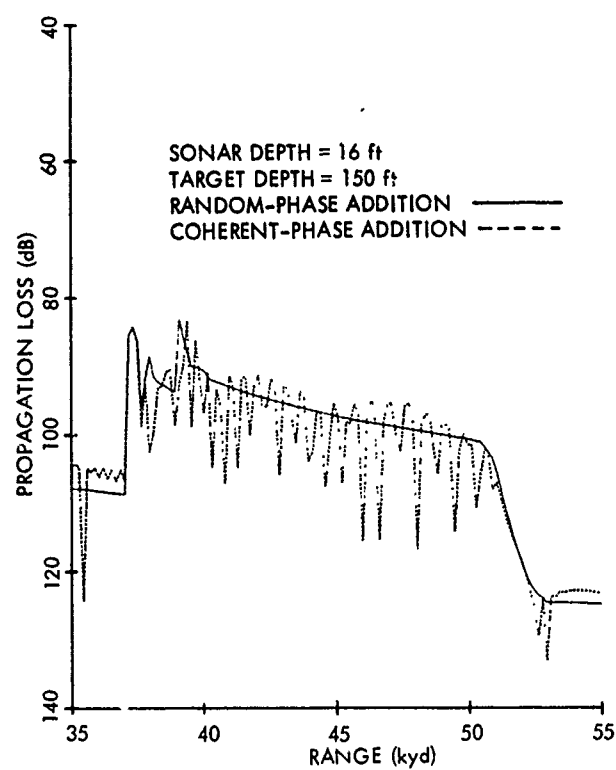


Figure 31. Propagation Loss for a 150-ft Target Depth, Example 2

### REVERBERATION, EXAMPLE 3

The input deck in table 11 will produce the velocity-profile curve, ray diagram, and reverberation plot in figures 32, 33, and 34, respectively, in 3 min, 11 s. Table 12 lists the corresponding continuous-gradient-velocity parameters.

Table 11. Input Deck for Constructing  
Reverberation Plot, Example 3

```

Δ XQT NISSM2
COMMENT
      REVERBERATION - RUN 6 - SACLANTCEN
Δ EOF
RANGE AXIS          0.0      50.0      10.0      KM
DEPTH AXIS          0.0      2.5      5.0      KM
VELOCITY AXIS       1.50     1.55     5.0      KM/S
TIME AXIS           0.0      50.0      10.0      SEC
REVERBERATION AXIS -100.0     0.0      5.0      DB
MAXIMUM RANGE       50.0 KM
MAXIMUM TIME        50.0 SEC
SONAR DEPTH         150.0 M
BOTTOM LOSS         3.0 MGS
WIND SPELD          11.0 KNOTS
FREQUENCY           3.5 KCPS
PULSE LENGTH        0.58 SEC
TRANSMITTER LEVL    110.0 DB
TRANSMITTER RESPONSE SONAR
RECEIVER RESPONSE   SONAR
HORIZONTAL BEAMWIDTH 0.2 RAD
BOTTOM SCATTERING CONSTANT -27.0 DB/YD
SURFACE SCATTERING CONSTANT +2.6 DB/YD
VOLUME SCATTERING STRNGTH
M DB/YD
0. -105.
150. -105.
270. -105.
490. -97.
510. -105.
595. -97.5
440. -96.
500. -102.
600. -95.
730. -90.
790. -84.
850. -75.
920. -75.
1050. -83.5
1100. -85.7
1315. -85.7
2000. -105.
2500. -105.
Δ EOF
VELOCITY PROFILE
M M/S
0.0 1516.0
14.0 1515.7
27.0 1514.0
50.0 1506.4
120.0 1507.0
250.0 1510.2
440.0 1513.0
2500.0 1547.5
Δ EOF

```

Table 11 (Cont'd). Input Deck for Constructing  
Reverberation Plot, Example 3

SONAR RESPONSE										COMPACT									
32.8	32.8	32.8	32.9	33.	33.1	33.2	33.3	33.4	33.5										
33.4	33.	32.8	32.7	32.7	32.7	32.9	33.2	33.5	33.9										
34.3	34.7	35.	35.2	35.1	34.9	34.	33.1	32.2	31.										
29.9	29.5	29.4	29.4	29.6	29.8	30.2	30.4	30.6	30.8										
30.8	30.7	30.	29.	28.	27.9	27.7	27.6	27.	27.										
26.9	26.8	26.7	26.5	26.4	26.	25.5	24.8	23.5	22.										
20.3	19.	17.9	17.2	16.9	17.	17.2	17.7	18.2	18.9										
20.	21.2	21.6	21.2	20.3	18.3	15.7	12.9	10.4	8.4										
0.8	5.6	4.5	3.7	2.9	2.2	1.4	.7	.4	.3										
.3	.3	.4	.5	.7	.8	1.2	1.6	2.2	2.8										
3.6	4.5	5.8	7.	8.2	9.8	11.5	13.5	17.	22.4										
22.	20.6	19.2	18.4	17.8	17.	16.8	16.9	17.5	18.4										
19.4	20.5	21.6	22.8	23.9	25.	25.2	25.3	25.3	25.1										
25.	24.6	24.6	24.5	24.5	24.7	25.2	25.8	26.5	27.2										
27.8	28.2	28.4	28.4	28.	27.6	27.	26.5	26.3	26.6										
27.5	28.5	29.5	30.4	31.2	31.7	31.7	31.8	31.7	31.6										
31.4	31.2	31.	30.7	30.5	30.3	30.4	30.5	30.7	30.9										
31.1	31.2	31.3	31.2	31.1	30.9	30.8	30.9	30.9	31.1										
31.3																			
PROCESS																			
0.0	20.0		0.5		DEG		2		3		3		3						
Δ EOF																			
END																			
Δ FIN																			

Table 12. Continuous-Gradient Parameters for Example 3

LAYER	Z0	V0	G0	G1	G2	CC
1	.0000000	.43511254+000	.48979907-002	.47192408+000	-.13166995+002	.15160000+01
2	.27000000-001	.43625918+000	.11989622+000	-.44009341+001	-.29872953+002	.15140064+01
3	.50000000-001	.44066908+000	.0000000	-.27518140+000	.60439175+001	.15064118+01
4	.34500000+000	.43760306+000	-.74377154-002	-.45287163-002	.16215089+000	.15116799+01
5	.25000000+001	.41725146+000	-.99123436-002	.00000000	.00000000	.15481073+01

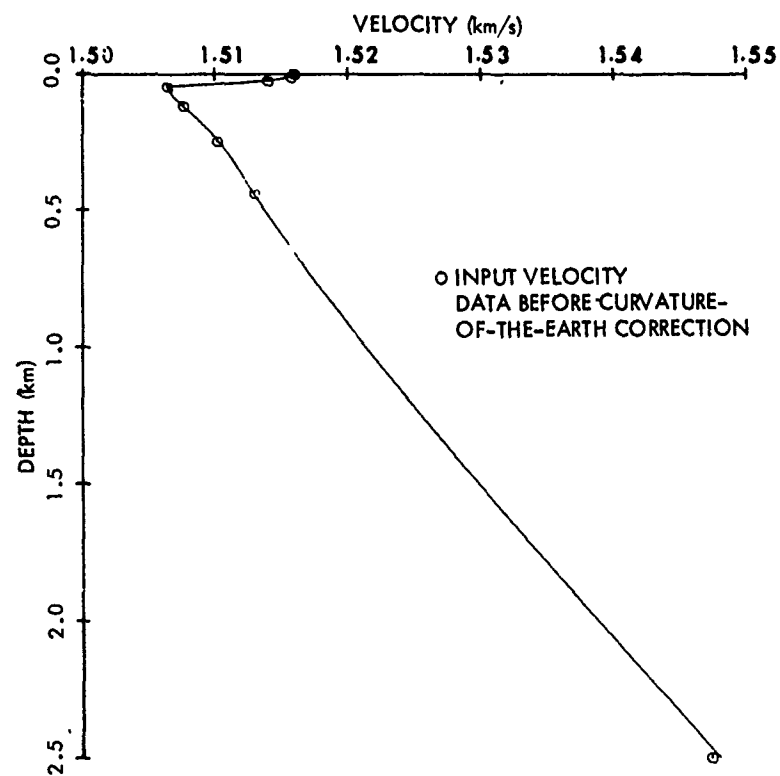


Figure 32. Velocity Profile for Example 3

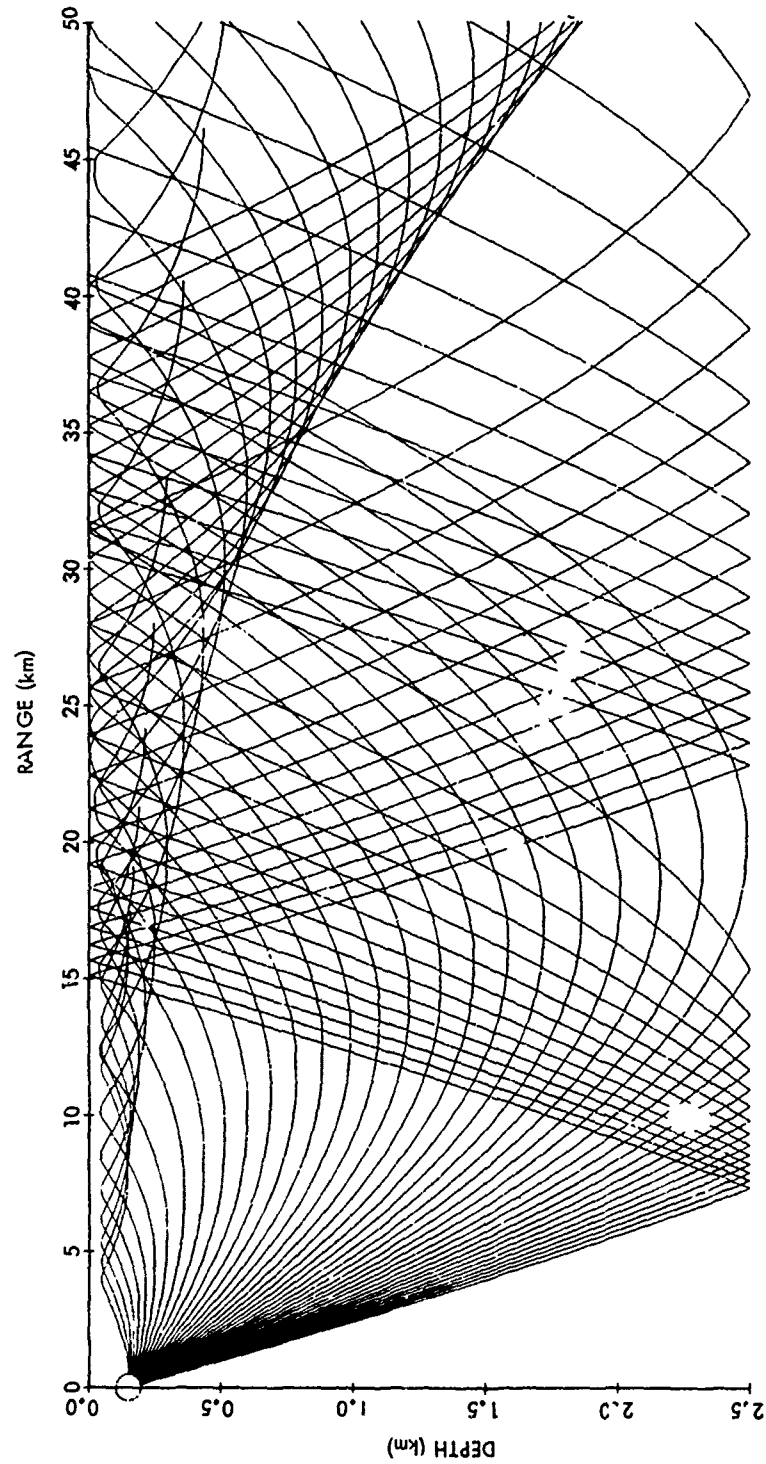


Figure 33. Ray Diagram for Example 3



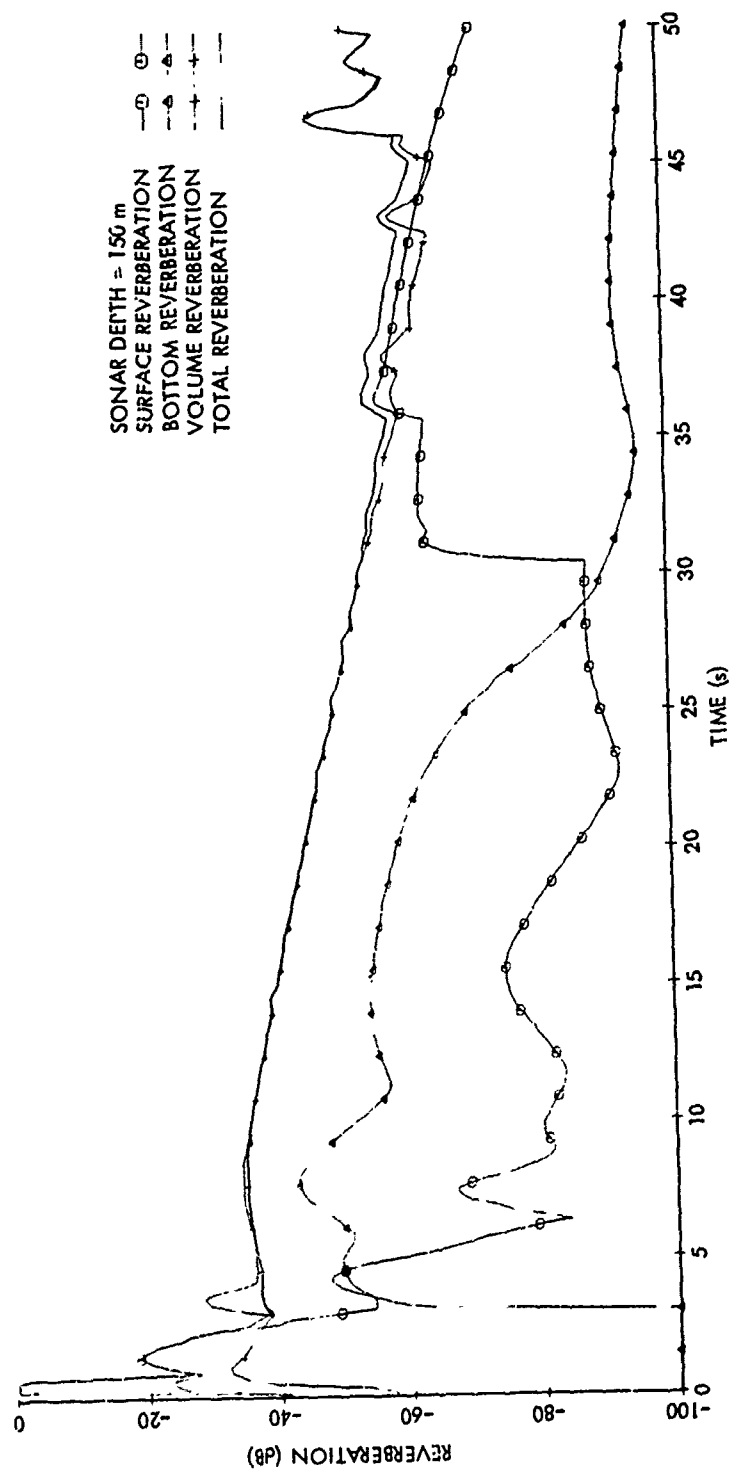


Figure 34. Reverberation versus Time for Example 3

## PROBABILITY OF DETECTION, EXAMPLE 4

In this final example, we consider the effect of varying array tilt angles on the probability of detection. Table 13 lists the input deck from which figures 35 through 44 are plotted; table 14 contains the continuous-gradient parameters. Example 4 required 5 min, 23 s of computer time.

Table 13. Input Deck for Computing Probability of Detection, Example 4

```

Δ XQT NISSM2
COMMENT
      COMPARE WITH FAST NISSM.
Δ EOF
RANGE AXIS          0.0      70.0      7.0      KYD
DEPTH AXIS          0.0      12.0      6.0      KFT
VELOCITY AXIS       4.75     4.95     5.0      KFT/S
TIME AXIS           0.0      70.0      7.0      SEC
PROPAGATION LOSS AXIS 60.0     120.0     6.0      DB
REVERBERATION AXIS  -80.0     +80.0     5.0      DB
SIGNAL TO NOISE RATIO AXIS -80.0     +80.0     5.0      DB
BOTTOM DEPTH        12000.0 FT
SONAR DEPTH         20.0 FT
TARGET DEPTH        300.0 FT
FREQUENCY           3.5 KCPS
WIND SPEED          12.0 KNOTS
ATTENUATION COEFFICIENT 30.0 DEG F
BOTTOM SCATTERING CONSTANT -27.0 DB/YD
SURFACE SCATTERING CONSTANT +2.6 DB/YD
VOLUME SCATTERING STRENGTH
FT DB/YD
  0.0 - 70.0
 25.0 - 69.1
 75.0 - 56.5
125.0 - 56.5
175.0 - 69.1
225.0 - 80.0
300.0 - 80.0
400.0 - 90.0
1790.0 - 90.0
1810.0 -120.0
12000.0 -120.0
Δ EOF
BOTTOM LOSS          4.0 MGS
VELOCITY PROFILE
FT FT/S
  0 0 4870.0
100.0 4871.0
200.0 4843.0
600.0 4818.0
2000.0 4788.0
3000.0 4795.0
12000.0 4946.0
Δ EOF
TRANSMITTER LEVEL 148.0 DB
HORIZONTAL BEAMWIDTH 10.0 DEG
DIRECTIVITY INDEX 26.0 DB
PULSE LENGTH       0.5 SEC
AVERAGING TIME     0.5 SEC
PROBABILITY OF FALSE ALARM 0.0001 /1
TARGET STRENGTH    15.0 DB
BANDWIDTH          100.0 HZ
CLOSING SPEED      10.0 KNOTS
MAXIMUM RANGE      60.0 KYD

```

Table 13 (Cont'd). Input Deck for Computing Probability of Detection, Example 4

MAXIMUM TIME	80.0	SEC						
RECEIVER RESPONSE	SONAR							
TRANSMITTER RESPONSE	SONAR							
SONAR RESPONSE	COMPACT							
32.8	32.0	32.8	32.9	33.1	33.2	33.3	33.4	33.5
33.4	33.1	32.8	32.7	32.7	32.9	33.2	33.5	33.9
34.3	34.7	35.1	35.2	35.1	34.9	34.1	32.2	31.1
29.9	29.5	29.4	29.6	29.8	30.2	30.4	30.6	30.8
30.8	30.7	30.1	29.1	28.1	27.9	27.7	27.6	27.1
26.9	26.8	26.7	26.5	26.4	26.1	25.5	24.8	23.5
20.3	19.1	17.9	17.2	16.9	17.1	17.2	17.7	18.2
20.1	21.2	21.6	21.2	20.3	18.3	15.7	12.9	10.4
0.8	5.6	4.5	3.7	2.9	2.2	1.4	.7	.3
.3	.3	.4	.5	.7	.8	1.2	1.6	2.2
3.6	4.5	5.8	7.1	8.2	9.8	11.5	13.5	17.1
22.1	20.0	19.2	18.4	17.8	17.1	16.8	16.9	17.5
19.4	20.5	21.6	22.8	23.9	25.1	25.2	25.3	25.3
25.1	24.8	24.6	24.5	24.5	24.7	25.2	25.8	26.5
27.8	28.2	28.4	28.4	28.1	27.6	27.1	26.5	26.3
27.3	28.5	29.5	30.4	31.2	31.7	31.7	31.8	31.7
31.4	31.2	31.1	30.7	30.5	30.3	30.4	30.5	30.7
31.1	31.2	31.3	31.2	31.1	30.9	30.8	30.9	30.9
31.3								
TRANSMITTER TILT ANGLE	20.0	DEG						
RECEIVER TILT ANGLE	20.0	DEG						
SONAR TILT ANGLE	20.0	DEG						
PROCESS								
-20.0	0.0	+0.5	DEG		2	3	2	3
Δ EOF								
TRANSMITTER TILT ANGLE	10.0	DEG						
RECEIVER TILT ANGLE	10.0	DEG						
SONAR TILT ANGLE	10.0	DEG						
PROCESS								
Δ EOF								
END								
Δ FIN								

Table 14. Continuous-Gradient Parameters for Example 4

LAYER	Z <sub>0</sub>	V <sub>0</sub>	G <sub>0</sub>	G <sub>1</sub>	G <sub>2</sub>	C <sub>0</sub>
1	.0000000	.45384961+000	-.12510243-001	.20522052+000	.00000000	.14843760+01
2	.30430000-001	.45365915+000	.00000000	.15310465+003	.13785773+003	.14846879+01
3	.64900000-001	.45891561+000	.66305023-001	.37847955+000	.57220370+001	.14761605+01
4	.13288000+000	.46367273+000	.22961002-001	-.30948608-001	-.35230229+000	.14685685+01
5	.94959999+000	.46943848+000	.00000000	-.27182101-001	.11029325+001	.14595220+01
6	.91440000+000	.46802466+000	-.69458315-002	.84039057-003	-.12099204+000	.14617258+01
7	.55576000+001	.43950444+000	-.15561390-001	.00000000	.00000000	.15084064+01

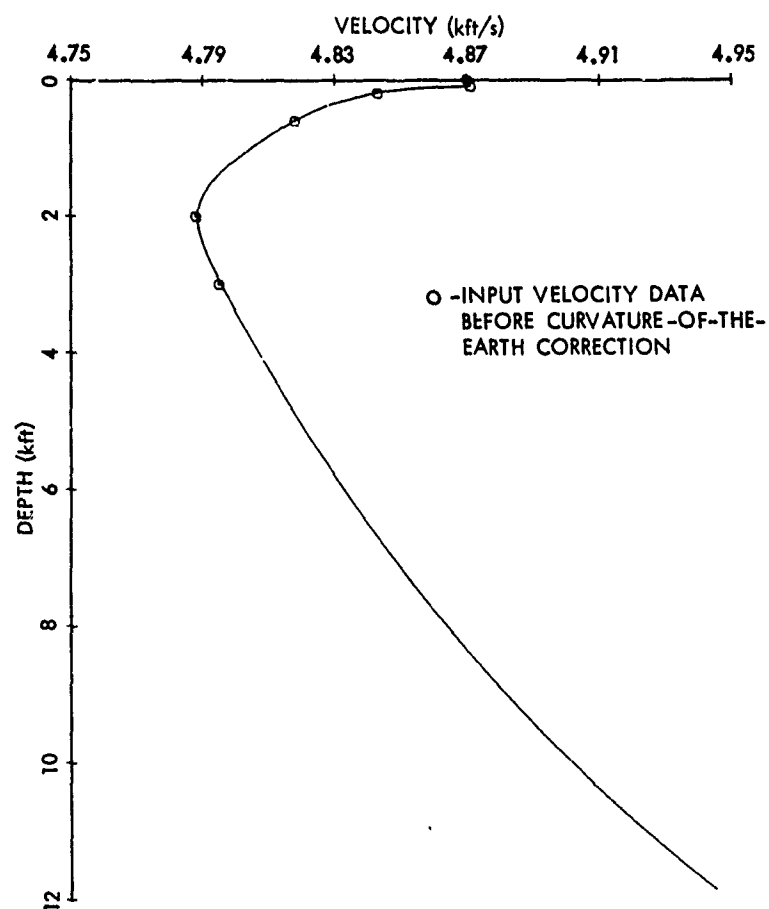


Figure 35. Velocity Profile for Example 4

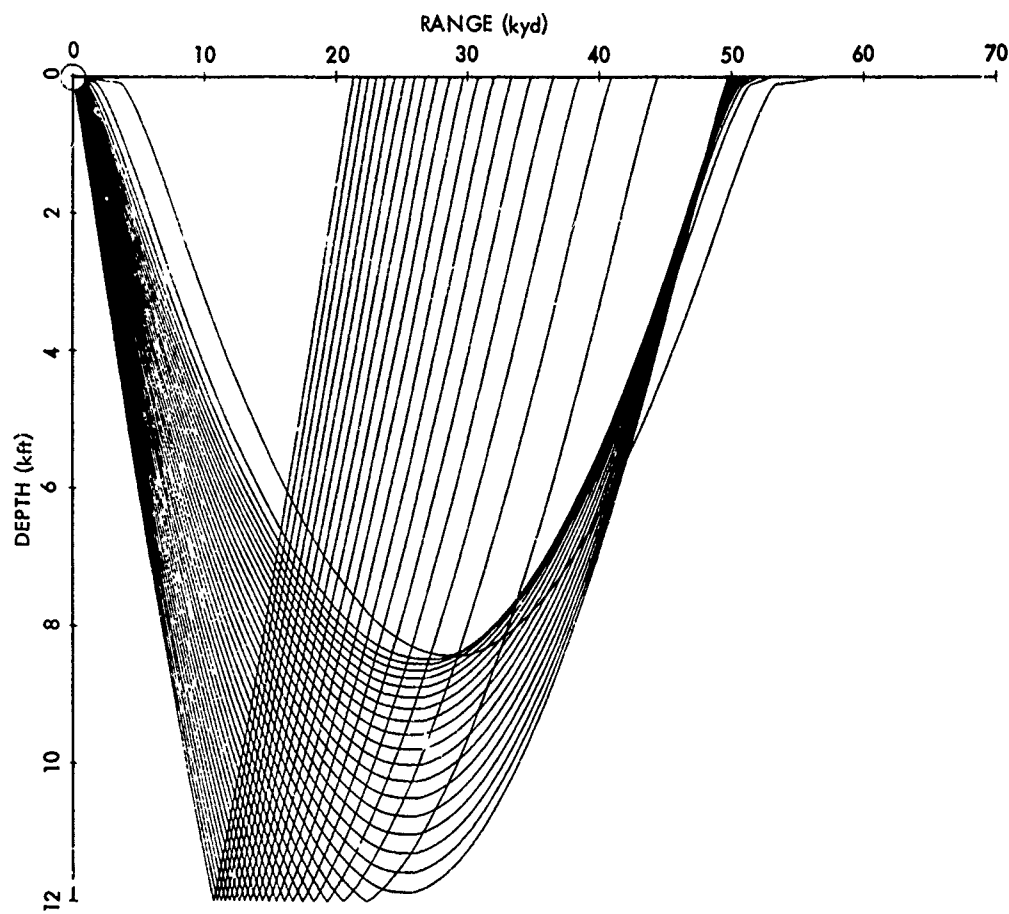


Figure 36. Ray Diagram for Example 4

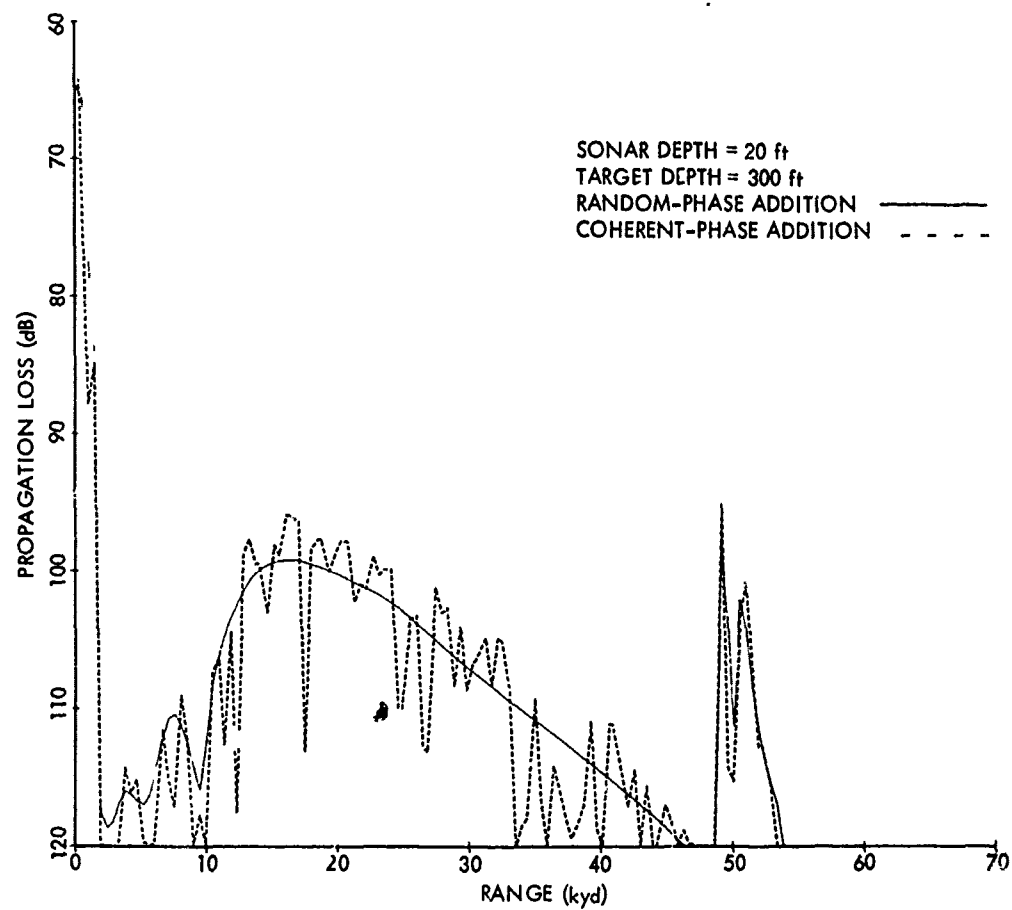


Figure 37. Propagation Loss for Case 1 of Example 4



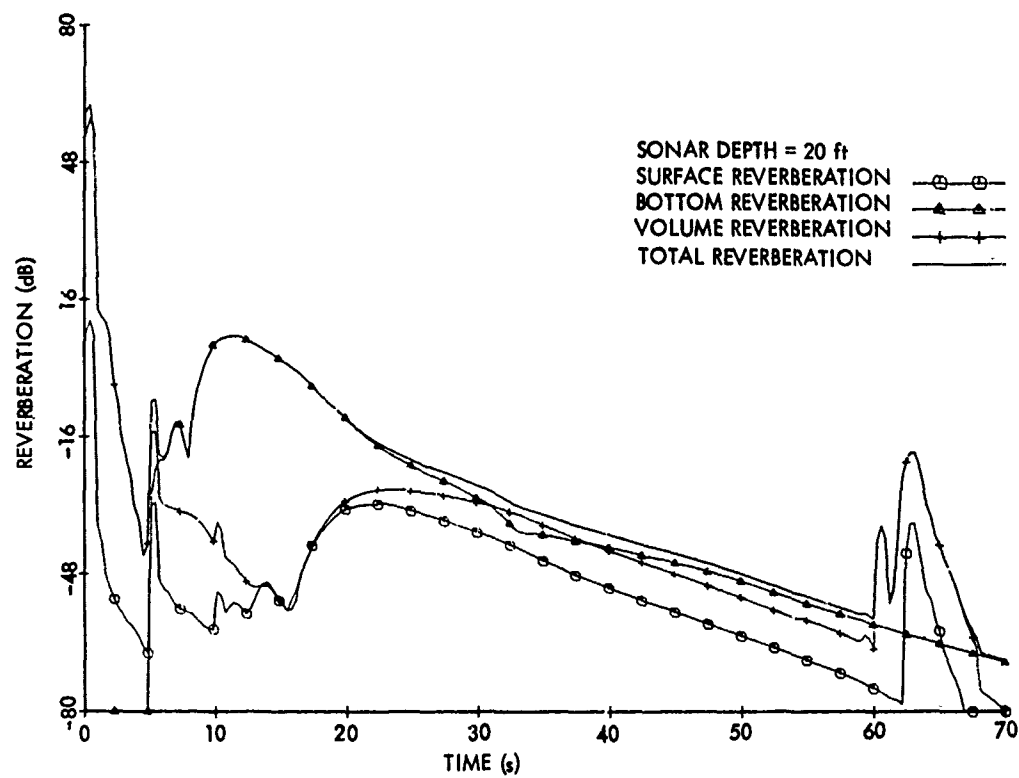


Figure 38. Reverberation versus Time for Case 1 of Example 4

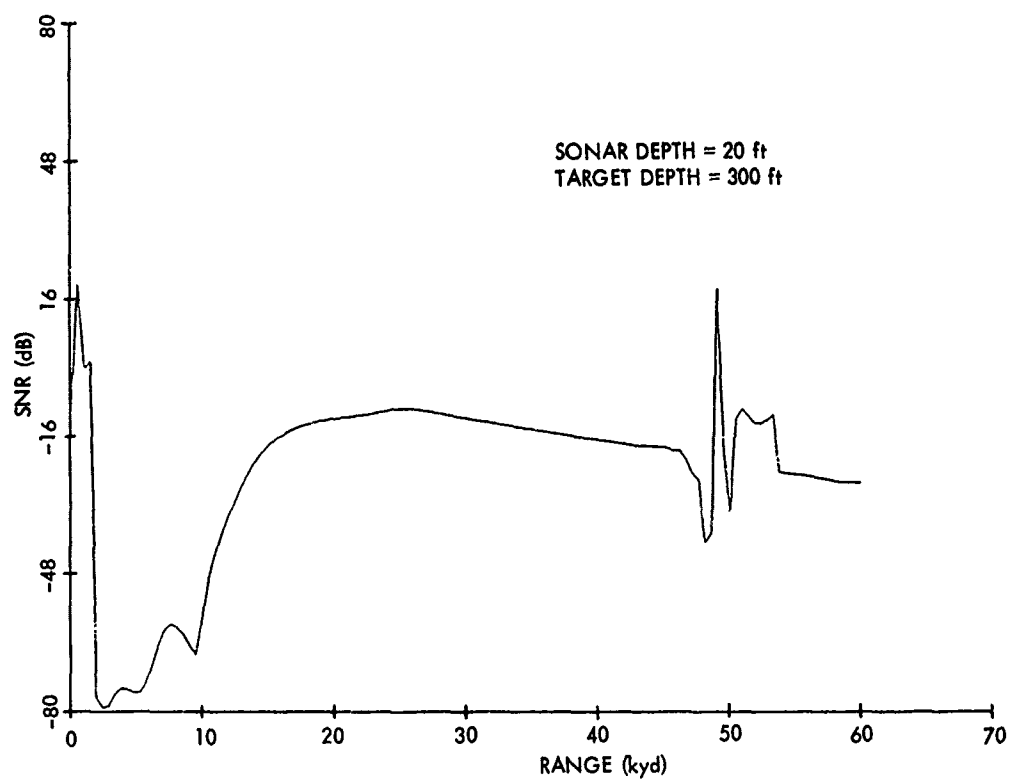


Figure 39. Signal-to-Noise Ratio for Case 1 of Example 4

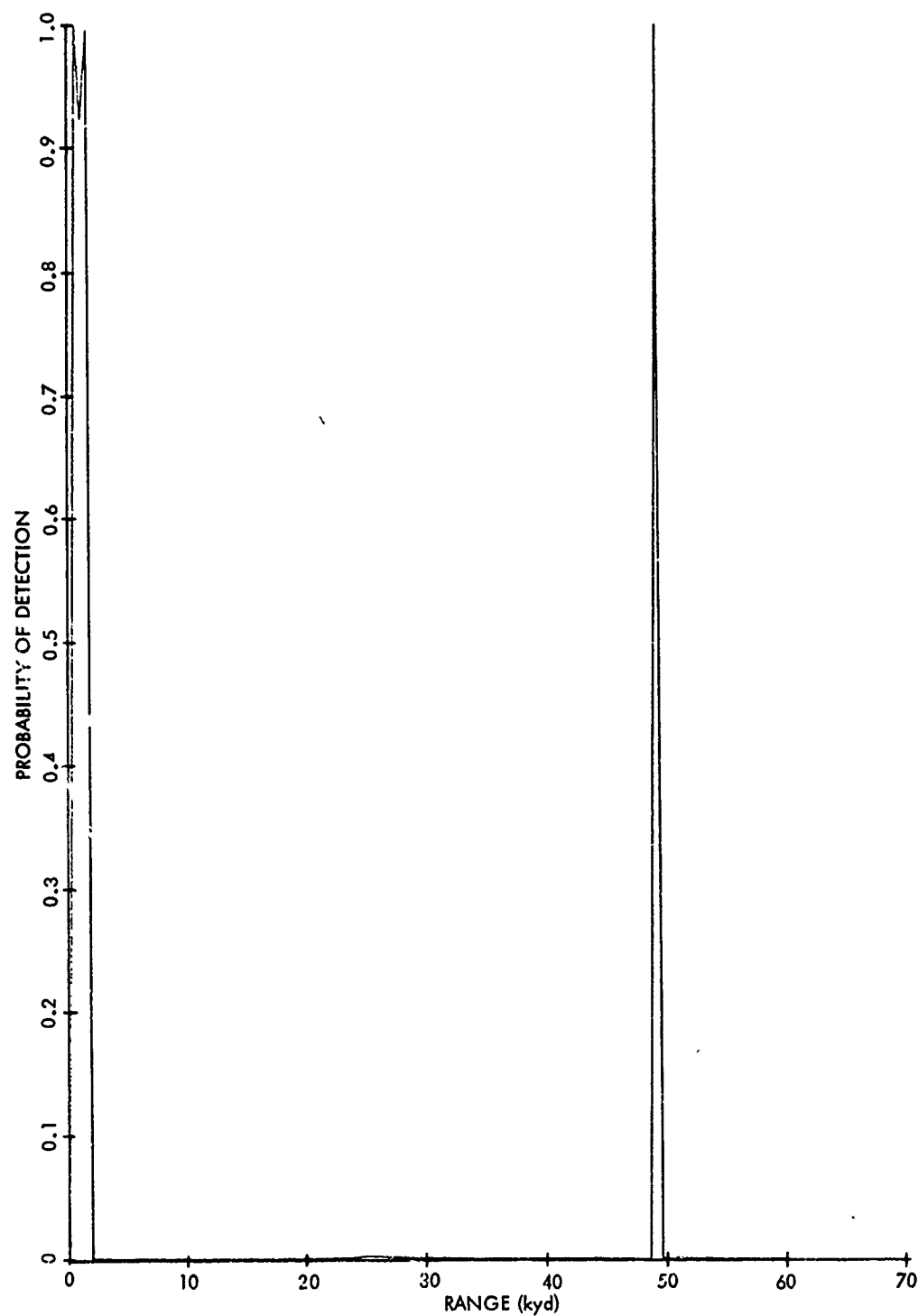


Figure 40. Probability of Detection for Case 1 of Example 4

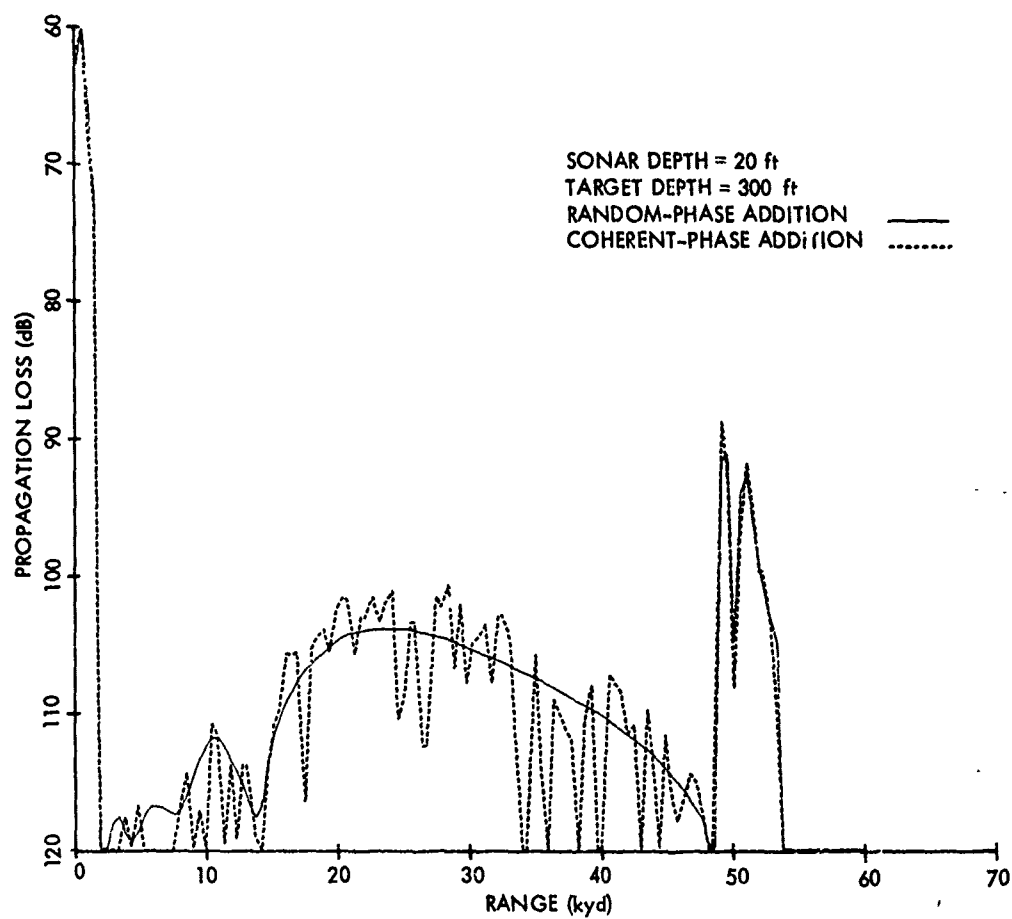


Figure 41. Propagation Loss for Case 2 of Example 4

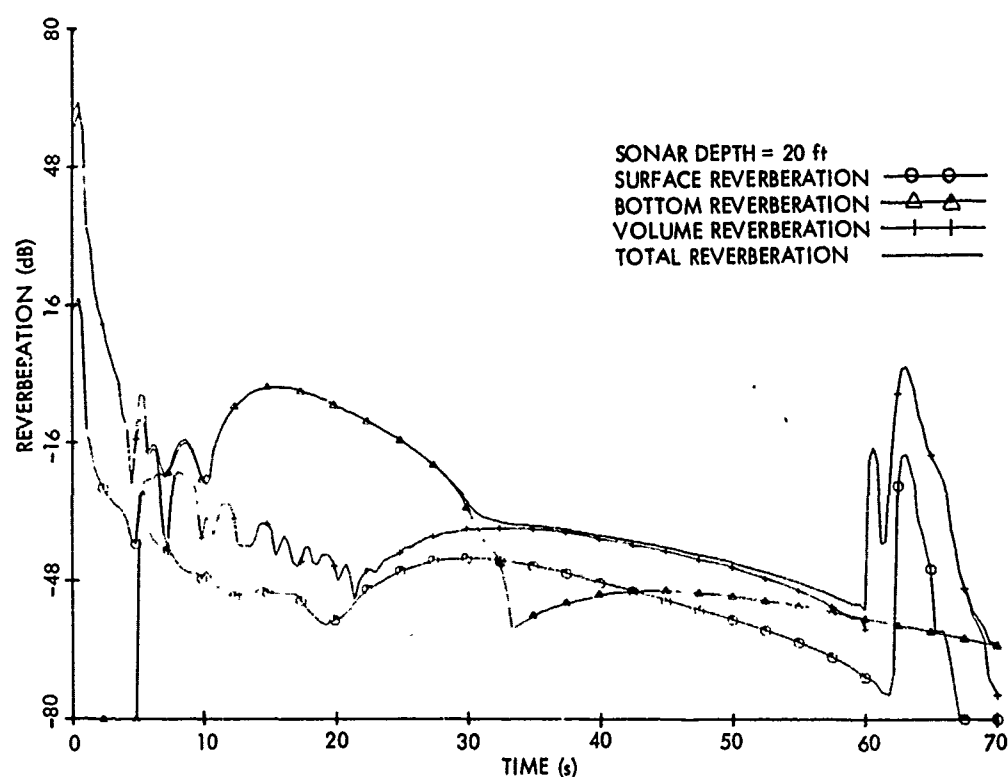


Figure 42. Reverberation versus Time for Case 2 of Example 4

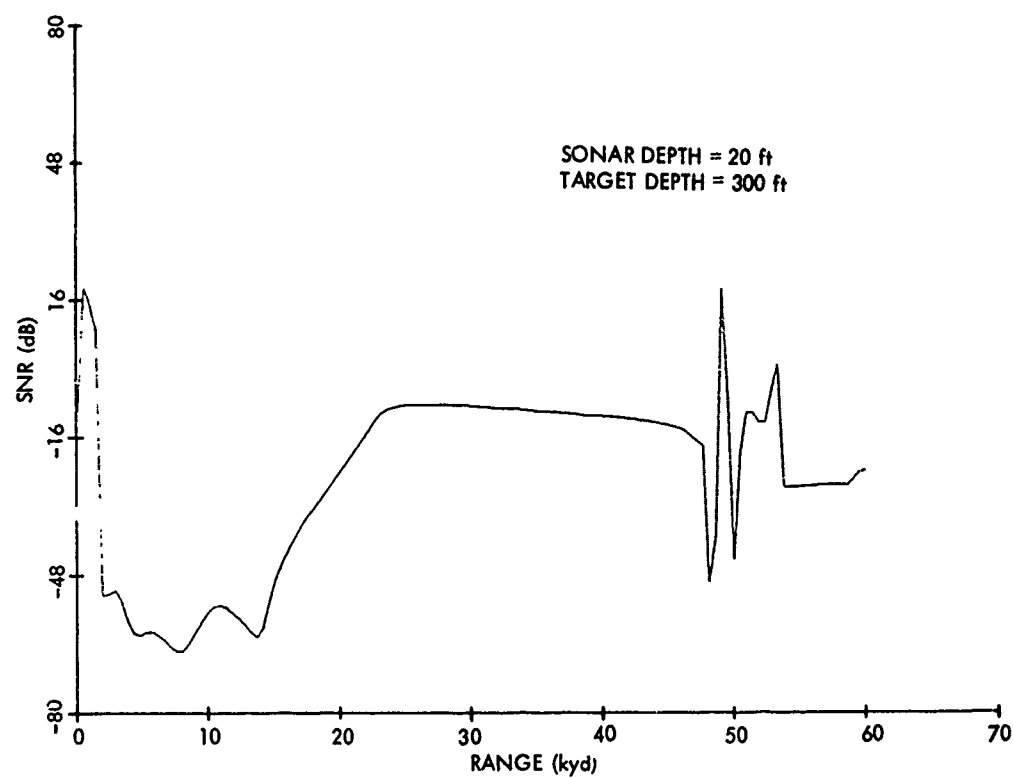


Figure 43. Signal-to-Noise Ratio for Case 2 of Example 4

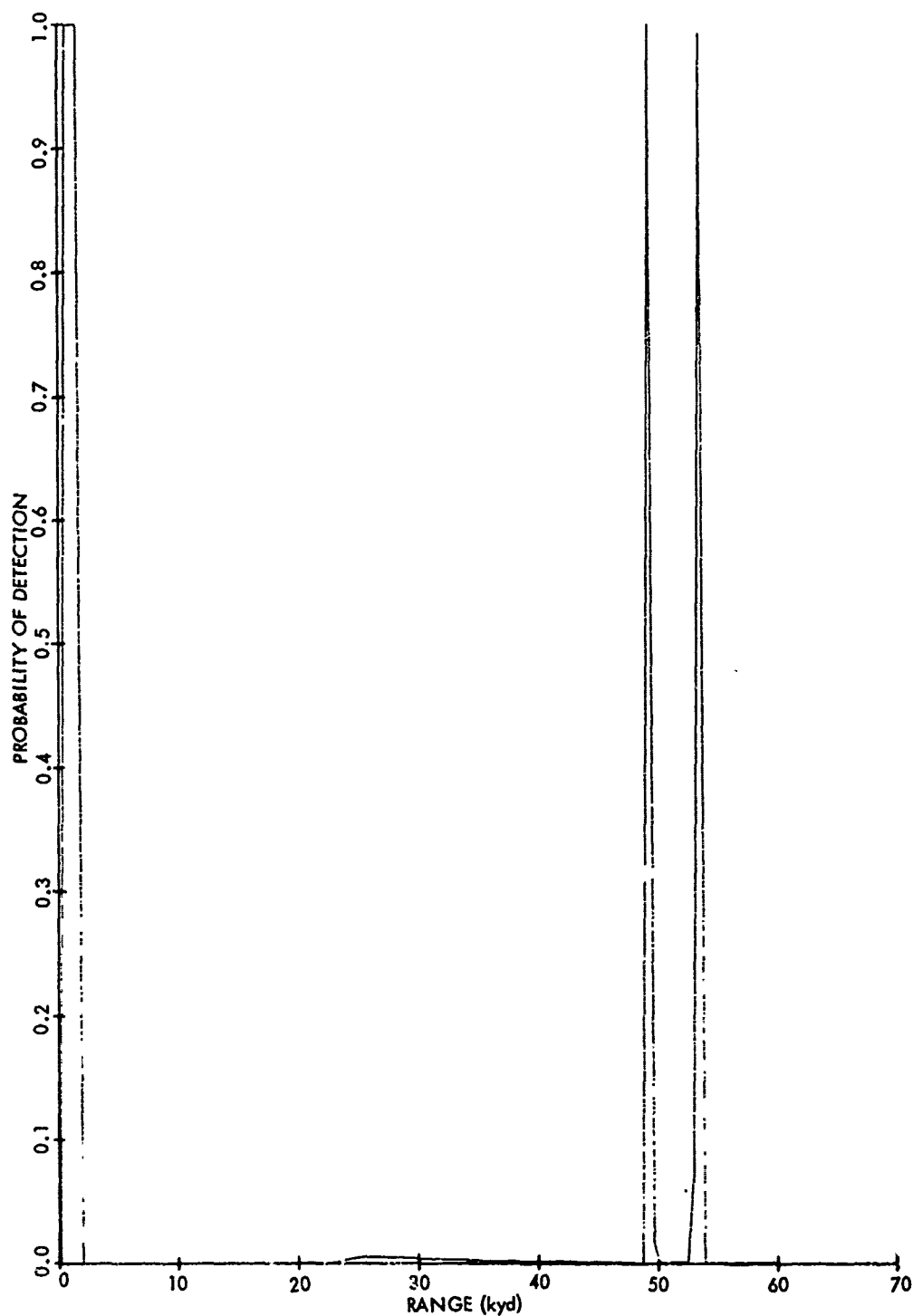


Figure 44. Probability of Detection for Case 2 of Example 4

## REMARKS

The last example illustrates that the NISSM II input deck is relatively complicated when compared with those of other ray-tracing programs. Although this will somewhat inconvenience the user, he will find compensations in the numerous input-output features of the computer program.

We have purposely omitted comparisons with actual data in order to keep this document unclassified. The interested reader should see references 21, 22, and 23, where the predictions for the Continuous Gradient Ray-Tracing System (CONGRATS)<sup>15</sup> are superimposed on the Mediterranean convergence-zone and reverberation measurements. NISSM II and CONGRATS differ basically with respect to program efficiency, but the predictions for both models are similar and the program results agree reasonably well with the measurements.

It is felt that NISSM II is a validated program and should be used in evaluating active sonar systems, providing the limitations of the model are understood. For example, several irregularities appearing in the volume-reverberation plot in figure 34 are a result of caustic curves intersecting a strong scattering layer. The treatment of caustics in this situation is questionable; therefore, the data represented by the irregularities may be erroneous or at least smaller. Hopefully, further analysis will result in improvements to NISSM II.



## LIST OF REFERENCES

1. C. B. Officer, Introduction to the Theory of Sound Transmission, McGraw-Hill Book Company, New York, 1958.
2. M. A. Pederson, "Acoustic Intensity Anomalies Introduced by Constant Gradients," Journal of the Acoustical Society of America, vol. 33, no. 4, April 1961, pp. 465-474.
3. H. Weinberg, A Curve Fitting Technique for Acoustic Ray Analysis, NUSL Report 805, 14 March 1967.
4. H. Weinberg, A Continuous Gradient Ray Tracing Technique, NUSC Report 829, 16 June 1967.
5. C. C. Leroy, "Development of Simple Equations for Accurate and More Realistic Calculation of the Speed of Sound in Seawater," Journal of the Acoustical Society of America, vol. 46, no. 1 (Part 2), July 1969, pp. 216-226.
6. W. D. Wilson, "Equation for the Speed of Sound in Sea Water," Journal of the Acoustical Society of America, vol. 32, no. 10, October 1960, p. 1357.
7. C. L. Pekeris, "Accuracy of the Earth Flattening Approximation in the Theory of Microwave Propagation," Physical Review, vol. 70, 1949, p. 518.
8. H. R. Hall and W. H. Watson, "An Empirical Bottom Reflection Loss Expression for Use in Sonar Range Prediction," July 1967, NUC Technical Note 10, San Diego, California.
9. J. S. Cohen and T. A. Garrett, "Continuous Gradient Ray Tracing System (CONGRATS) Bottom Loss Models," NUSL Technical Memorandum 2070-35-70, 5 February 1972.
10. W. H. Thorp, "Analytic Description of the Low-Frequency Attenuation Coefficient," Journal of the Acoustical Society of America, vol. 42, no. 1, July 1967, p. 270.
11. H. R. Hall and W. H. Watson, "A New Absorption Coefficient Expression for Use in Sonar Range Prediction" (U), U. S. Navy Journal of Underwater Acoustics, vol. 17, no. 4, October 1967, pp. 617-637 (CONFIDENTIAL).
12. C. L. Pekeris, "Theory of Propagation of Sound in a Half-Space of Variable Sound Velocity under Conditions of Formation of a Shadow Zone," Journal of the Acoustical Society of America, vol. 18, no. 2, October 1946, pp. 295-315.
13. D. Ludwig, "Uniform Asymptotic Expansions at a Caustic," Communications on Pure and Applied Mathematics, vol. XIX, no. 1, 1966, pp. 215-260.

14. W. H. Watson and R. W. McGirr, An Active Sonar Performance Prediction Model, NUC Technical Publication 286, April 1972.
15. J. S. Cohen and H. Weinberg, Continuous Gradient Ray-Tracing System (CONGRATS) III: Boundary and Volume Reverberation, NUSC Report 4071, 30 April 1971.
16. R. P. Chapman and J. H. Harris, "Surface Backscattering Strengths Measured with Explosive Sound Sources," Journal of the Acoustical Society of America, vol. 34, no. 10, October 1962, pp. 1592-1597.
17. K. V. MacKenzie, "Bottom Reverberation for 530- and 1030-cps Sound in Deep Water," Journal of the Acoustical Society of America, vol. 33, no. 11, November 1961, pp. 1498-1504.
18. R. J. Urick, Principles of Underwater Sound for Engineers, McGraw-Hill Book Company, New York, 1967.
19. A. H. Nuttall and A. F. Magaraci, "Signal-to-Noise Ratios Required for Short-Term Narrowband Detection of Gaussian Processes," NUSC Technical Memorandum TC-116-72, 31 May 1972.
20. M. Schulkin and R. Schaffer, "Backscattering of Sound from the Sea Surface," Journal of the Acoustical Society of America, vol. 36, no. 9, September 1964, pp. 1699-1703.
21. G. Vettori and E. Cernich, "Comparison of Propagation Measurements using MEDUSA System with Computer Modeled Data" (U), Unconfirmed Minutes -- 19th Meeting, 19-21 October 1971, SACLANT ASW Research Centre, Scientific Committee of National Representatives, pp. 60-70 (NATO CONFIDENTIAL).
22. W. Bachmann and B. de Raigniac, "Comparison of CONGRATS Ray Tracing Predictions with MEDUSA Reverberation Measurements" (U), Unconfirmed Minutes -- 19th Meeting, 19-21 October 1971, SACLANT ASW Research Centre, Scientific Committee of National Representatives, pp. 71-78 (NATO CONFIDENTIAL).
23. S. R. Santaniello, B. F. Cole, S. R. van der Veen, et al., personal communications.

## Appendix A

### CONTINUOUS-GRADIENT CURVE-FITTING TECHNIQUE

Let the velocities,  $c^{(i)}$ , be given at  $n$  distinct depths,  $z_0^{(i)}$ , where  $i = 1, 2, \dots, n$ . Then if  $4n$  parameters ( $v_0^{(i)}$ ,  $g_0^{(i)}$ ,  $g_1^{(i)}$ , and  $g_2^{(i)}$ ) can be determined such that the  $n-1$  functions

$$v_i(z) = v_0^{(i)} + \Delta z \frac{g_0^{(i)} + \Delta z g_1^{(i)}}{\left[1 + \Delta z g_2^{(i)}\right]^2} \quad (\text{A-1})$$

satisfy

$$v_i(z) \Big|_{z=z_0^{(i+1)}} = v_{i+1}(z) \Big|_{z=z_0^{(i+1)}} = \left[c^{(i+1)}\right]^{-2} \quad (\text{A-2})$$

and

$$\frac{dv_i(z)}{dz} \Big|_{z=z_0^{(i+1)}} = \frac{dv_{i+1}(z)}{dz} \Big|_{z=z_0^{(i+1)}}, \quad (\text{A-3})$$

where

$$\Delta z = z - z_0^{(i)}, \quad (\text{A-4})$$

it follows that the composite function,

$$c(z) = v_i(z)^{-1/2}, \quad (\text{A-5})$$

will fit the data and have a continuous gradient.

The parameters  $v_0^{(i)}$  can easily be found:

$$v_0^{(i)} = [c^{(i)}]^{-2}, \quad (A-6)$$

but the parameters,  $g_0^{(i)}$ , which are given by

$$g_0^{(i)} = \frac{dv_i(z)}{dz} \bigg|_{z=z_0^{(i)}}, \quad (A-7)$$

are not uniquely determined by the input data. However, they can be, and are, estimated by the following numerical differentiation formula: Define

$$g^{(i)} = \frac{v_0^{(i+1)} - v_0^{(i)}}{z_0^{(i+1)} - z_0^{(i)}}. \quad (A-8)$$

Then

$$g_0^{(i)} = \pm \sqrt{g^{(i)} g^{(i-1)}} \quad (A-9)$$

if  $1 < i < n$ , and the quantity under the square root is positive. The sign is positive or negative if the  $v_0^{(i)}$  are increasing or decreasing, respectively.

We set

$$g_0^{(i)} = 0 \quad (A-10)$$

if  $1 < i < n$  and the quantity under the square root is not positive;

$$g_0^{(1)} = \frac{[g^{(1)}]^2}{g_0^{(2)}} \quad (A-11)$$

if  $g_0^{(2)} \neq 0$ ;

$$g_0^{(1)} = 2g^{(1)} \quad (A-12)$$

if  $g_0^{(2)} = 0$ ;

$$g_0^{(n)} = \frac{[g_0^{(n-1)}]^2}{g_0^{(n-1)}} \quad (A-13)$$

if  $g_0^{(n-1)} \neq 0$ ; and

$$g_0^{(n)} = 2g_0^{(n-1)} \quad (A-14)$$

if  $g_0^{(n-1)} = 0$ .

Once the  $g_0^{(i)}$  have been set, tests are performed to ensure that

a. Depths of relative minimum  $v_0^{(i)}$  are not adjacent to those of relative maximum  $v_0^{(i)}$ , and

$$b. [g_0^{(i)}]^2 \geq g_0^{(i)} g_0^{(i+1)}.$$

If test (a.) is not satisfied, then an additional point (of inflection) is inserted at

$$z_0^{(i)'} = \frac{z_0^{(i)} + z_0^{(i+1)}}{2} \quad (A-15)$$

and

$$v_0^{(i)'} = \frac{v_0^{(i)} + v_0^{(i+1)}}{2}, \quad (A-16)$$

with

$$g_0^{(i)'} = 2g_0^{(i)}. \quad (A-17)$$

If test (b.) is not satisfied and  $|g_0^{(i)}| \leq |g^{(i)}| < |g_0^{(i+1)}|$ , then  $g_0^{(i+1)}$  is reduced according to

$$g_0^{(i+1)} = \frac{0.9999 [g^{(i)}]^2}{g_0^{(i)}}. \quad (\text{A-18})$$

If test (b.) is not satisfied and  $|g_0^{(i)}| > |g^{(i)}| \geq |g_0^{(i+1)}|$ , then  $g_0^{(i)}$  is reduced according to

$$g_0^{(i)} = \frac{0.9999 [g^{(i)}]^2}{g_0^{(i+1)}}. \quad (\text{A-19})$$

Finally, if  $|g_0^{(i)}| > |g^{(i)}|$  and  $|g_0^{(i+1)}| > |g^{(i)}|$ , an additional point (of inflection) is inserted according to equations (A-15) and (A-16), and  $g_0^{(i)}$  is given by the smaller value given by equations (A-18) and (A-19).

The next step is to compute  $g_2^{(i)}$ . It can be shown<sup>A1</sup> that for  $c(z)$  and  $dc(z)/dz$  to be continuous at  $z_0^{(i+1)}$

$$1 + [z_0^{(i+1)} - z_0^{(i)}] g_2^{(i)} = \frac{g^{(i)} \pm \sqrt{[g^{(i)}]^2 - g_0^{(i+1)} g_0^{(i)}}}{g_0^{(i+1)}} \quad (\text{A-20})$$

if  $g_0^{(i+1)} \neq 0$ , and

$$1 + [z_0^{(i+1)} - z_0^{(i)}] g_2^{(i)} = \frac{g_0^{(i)}}{2g^{(i)}} \quad (\text{A-21})$$

if  $g_0^{(i+1)} = 0$ . Only positive roots are acceptable, and, if tests (a.) and (b.) are met, at least one root will be positive. As the last step, the parameter  $g_1^{(i)}$  is given by

<sup>A1</sup> H. Weinberg, A Curve Fitting Technique for Acoustic Ray Analyses, NUSL Report 805, 14 March 1967.

$$g_1^{(i)} = \frac{g^{(i)} \left\{ 1 + \left[ \frac{z_0^{(i+1)} - z_0^{(i)}}{z_0^{(i+1)} - z_0^{(i)}} \right] g_2^{(i)} \right\}^2 - g_0^{(i)}}{z_0^{(i+1)} - z_0^{(i)}}. \quad (\text{A-22})$$

In practical applications, it is unnecessary to fit the input data exactly. Thus the number of breakpoints in the interpolation function can be reduced with a corresponding saving in computer execution time. The procedure, which continues until  $j$  equals  $n$ , is outlined below; but first the parameters  $v_0^{(i)}$  and  $g_0^{(i)}$ ,  $i=1,2,\dots,n$ , are assumed to have already been computed and modified so that tests (a.) and (b.) are satisfied:

- The index  $i$  is initially set to 1.
- The program determines the largest index  $j$  and parameters  $g_1^{(i)}$  and  $g_2^{(i)}$  such that a function in the form of equation (A-1) can fit the data specified at  $z_0^{(i)}$  and  $z_0^{(j)}$  while, simultaneously, the maximum deviation between the input velocities and the values of the fitting function at the intermediate depths  $z_0^{(i+1)}$ ,  $z_0^{(i+2)}$ , ...,  $z_0^{(j)}$  does not exceed 0.2 m/s.
- The intermediate data are discarded and the index  $i$  is incremented to  $j$ .

## Appendix B

### EVALUATION OF RAY-TRACING INTEGRALS

#### RANGE INTEGRAL

Upon substituting the velocity-interpolation function into the range integral,

$$\Delta x = \int_{z_a}^{z_b} \frac{c(z) |dz|}{\sqrt{c_v^2 - c^2(z)}} , \quad (B-1)$$

one obtains an expression that can be evaluated using elementary rules of integration. However, further algebraic manipulation is necessary to reduce computer-truncation errors. The results are summarized below; for notational convenience, the superscript (i) has been dropped and  $z_b$  is assumed greater than  $z_a$ .

Define the constants of integration  $\alpha$ ,  $\beta$ ,  $\gamma$ ,  $p$ ,  $q$ , and  $r$ , respectively, by

$$\alpha = v_o^2 - c_v^{-2} , \quad (B-2)$$

$$\beta = \alpha g_2 + \frac{1}{2} g_0 , \quad (B-3)$$

$$\gamma = \alpha g_2^2 + g_1 , \quad (B-4)$$

$$p = \gamma - g_2 \beta = g_1 - \frac{1}{2} g_0 g_2 , \quad (B-5)$$

$$q = \alpha \gamma - \beta^2 = \alpha r - \frac{1}{4} g_0^2 , \quad (B-6)$$

$$r = g_1 - g_0 g_2 , \quad (B-7)$$

and the variable  $Y$  by

$$Y = \alpha + 2\beta \Delta z + \gamma \Delta z^2 . \quad (B-8)$$



Then if

$$H = \int_a^{z_b} \frac{dz}{(Y)^{1/2}}, \quad (B-9)$$

it is shown by Weinberg<sup>B1</sup> that

$$\Delta x = \int_a^{z_b} \frac{1 + g_2 \Delta z}{c_v (Y)^{1/2}} dz = \frac{2D}{c_v} \left\{ 1 + g_2 (\Delta z)_{av} + p \left[ \frac{1}{\gamma} \left( \frac{H}{2D} - 1 \right) \right] \right\}, \quad (B-10)$$

where

$$\langle \Delta z \rangle_{av} = \frac{1}{2} (\Delta z_a + \Delta z_b), \quad (B-11)$$

$$D = \frac{z_b - z_a}{(Y_a)^{1/2} + (Y_b)^{1/2}}, \quad (B-12)$$

and

$$\left[ \frac{1}{\gamma} \left( \frac{H}{2D} - 1 \right) \right] = D^2 \left( \frac{1}{3} + \frac{\gamma D^2}{5} + \frac{\gamma^2 D^4}{7} + \dots \right), \quad (B-13)$$

if  $|\gamma D^2| < 10^{-4}$ ;

$$H = 2(-\gamma)^{-1/2} \tan^{-1} \left[ (-\gamma)^{1/2} D \right]. \quad (B-14)$$

if  $|\gamma D^2| \geq 10^{-4}$  and  $\gamma < 0$ ; and

$$H = 2(\gamma)^{-1/2} \tanh^{-1} \left[ \gamma^{1/2} D \right] \quad (B-15)$$

if  $|\gamma D^2| \geq 10^{-4}$  and  $\gamma > 0$ .

<sup>B1</sup> H. Weinberg, A Continuous Gradient Ray Tracing Technique, NUSL Report 829, 16 June 1967.

## TIME INTEGRAL

Upon substituting the velocity function into the time integral,

$$\Delta T = \int_{z_a}^{z_b} \frac{c_v |dz|}{c(z) \sqrt{c_v^2 - c^2(z)}}, \quad (\text{B-16})$$

one obtains

$$\Delta T = v_o c_v \Delta x + J, \quad (\text{B-17})$$

where  $\Delta x$  is given by equation (B-10) and

$$J = \int_{z_a}^{z_b} \frac{\Delta z (g_0 + g_1 \Delta z)}{(1 + g_2 \Delta z)(Y)^{1/2}} dz. \quad (\text{B-18})$$

Further analysis shows that if  $g_2 \neq 0$ , then

$$J = \frac{g_1 c_v \Delta x - 2pH + rI}{g_2}, \quad (\text{B-19})$$

where

$$\begin{aligned} I &= \int_{z_a}^{z_b} \frac{dz}{(1 + g_2 \Delta z)(Y)^{1/2}} \\ &= (r)^{-1/2} \tanh^{-1} \left[ (r)^{1/2} \frac{(Y_b)^{1/2} \left( \frac{1}{2} g_0 + p \Delta z_a \right) - (Y_a)^{1/2} \left( \frac{1}{2} g_0 + p \Delta z_b \right)}{-r(Y_a)^{1/2} (Y_b)^{1/2} + \left( \frac{1}{2} g_0 + p \Delta z_a \right) \left( \frac{1}{2} g_0 + p \Delta z_b \right)} \right] \end{aligned} \quad (\text{B-20})$$

if  $r > 0$ , and

$$I = (-r)^{-1/2} \tan^{-1} \left[ \frac{(-r)^{1/2} \frac{(Y_b)^{1/2} \left( \frac{1}{2} g_0 + p \Delta z_a \right) - (Y_a)^{1/2} \left( \frac{1}{2} g_0 + p \Delta z_b \right)}{-r(Y_a)^{1/2} (Y_b)^{1/2} + \left( \frac{1}{2} g_0 + p \Delta z_a \right) \left( \frac{1}{2} g_0 + p \Delta z_b \right)} \right] \quad (B-21)$$

if  $r < 0$ . There is no need to evaluate  $I$  when  $r = 0$  since the product  $rI$ , which appears in equation (E-19), approaches zero as  $r$  approaches zero.

### RANGE DERIVATIVE

The range derivative  $\partial x / \partial c_v|_{z=z_b}$  is obtained by differentiating  $\Delta x$ , as given by equation (B-10), with respect to the vertex velocity  $c_v$ . Since  $p$  is independent of  $c_v$ ,

$$\begin{aligned} \left. \frac{\partial x}{\partial c_v} \right|_{z=z_b} &= \left( \frac{1}{D} \frac{\partial D}{\partial c_v} - \frac{1}{c_v} \right) \Delta x \\ &+ \frac{2D}{c_v} \left\{ g_2 \frac{\partial \langle \Delta z \rangle_{av}}{\partial c_v} + p \frac{\partial}{\partial c_v} \left[ \frac{1}{\gamma} \left( \frac{H}{2D} - 1 \right) \right] \right\}. \end{aligned} \quad (B-22)$$

We now consider two cases. If the ray does not vertex in the layer,  $z_a$  and  $z_b$  are independent of  $c_v$ ,

$$\frac{\partial \alpha}{\partial c_v} = 2c_v^{-3}, \quad (B-23)$$

$$\frac{\partial \beta}{\partial c_v} = g_2 \frac{\partial \alpha}{\partial c_v}, \quad (B-24)$$

$$\frac{\partial \gamma}{\partial c_v} = g_2^2 \frac{\partial \alpha}{\partial c_v}, \quad (B-25)$$

$$\frac{\partial Y_a}{\partial c_v} = (1 + g_2 \Delta z_a)^2 \frac{\partial \alpha}{\partial c_v}, \quad (B-26)$$

$$\frac{\partial Y_b}{\partial c_v} = (1 + g_2 \Delta z_b)^2 \frac{\partial \alpha}{\partial c_v}, \quad (\text{B-27})$$

$$\frac{\partial \langle \Delta z \rangle_{av}}{\partial c_v} = 0, \quad (\text{B-28})$$

$$\frac{\partial D}{\partial c_v} = - \frac{D}{2(Y_a)^{1/2} + (Y_b)^{1/2}} \left( \frac{\partial Y_a / \partial c_v}{(Y_a)^{1/2}} + \frac{\partial Y_b / \partial c_v}{(Y_b)^{1/2}} \right), \quad (\text{B-29})$$

and

$$\begin{aligned} \frac{\partial}{\partial c_v} \left[ \frac{1}{\gamma} \left( \frac{H}{2D} - 1 \right) \right] &= \frac{1}{\gamma} \left\{ \frac{1}{1 - \gamma D^2} \left\{ \frac{DH}{2} - \left[ \frac{1}{\gamma} \left( \frac{H}{2D} - 1 \right) \right] \right\} \right. \\ &\quad \left. \cdot \left( \frac{1}{2} \frac{\partial \gamma}{\partial c_v} + \frac{\gamma}{D} \frac{\partial D}{\partial c_v} \right) - \frac{\partial \gamma}{\partial c_v} \left[ \frac{1}{\gamma} \left( \frac{H}{2D} - 1 \right) \right] \right\}. \end{aligned} \quad (\text{B-30})$$

However, if the ray does vertex at  $z_b$ , then  $z_b$  will be a function of  $c_v$  and  $Y_b$  will vanish identically. Equations (B-22) through (B-26) and (B-30) are still valid, but equations (B-27), (B-28), and (B-29) must be replaced by

$$\frac{\partial Y_b}{\partial c_v} = 0, \quad (\text{B-31})$$

$$\frac{\partial \langle \Delta z \rangle_{av}}{\partial c_v} = \frac{1}{2} \frac{\partial z_b}{\partial c_v}, \quad (\text{B-32})$$

and

$$\frac{\partial D}{\partial c_v} = - \frac{1}{2} \frac{D}{Y_a} \frac{\partial Y_a}{\partial c_v} + \frac{1}{(Y_a)^{1/2}} \frac{z_b}{c_v}, \quad (\text{B-33})$$

TR 4527

respectively, where

$$\frac{\partial z_b}{\partial c_v} = - \frac{(1 + g_2 \Delta z_b)^2}{2(\gamma \Delta z_b + \beta)} \frac{\partial \alpha}{\partial c_v} \cdot \quad (B-34)$$

## Appendix C

AMOS SURFACE DUCT EQUATIONS<sup>C1</sup>

The AMOS equations<sup>C2</sup> can be expressed in terms of the following variables:

R, horizontal range (kyd)

$Z_L$ , surface layer depth (ft)

$Z_x$ , source depth (ft)

$Z_t$ , target depth (ft)

f, frequency (kHz).

When the sound-speed structure of a surface duct is adequately represented by a linear sound-speed gradient  $\gamma$  and an average sound speed  $\bar{C}$ , then, in any consistent units, the range between successive surface reflections of the limiting ray is approximately  $2\sqrt{2\bar{C}/|\gamma|}Z_L$ . Hence in the typical situation where  $\gamma = 0.018 \text{ s}^{-1}$  and  $\bar{C} = 4900 \text{ ft/s}$ , and if R is interpreted as the number of kiloyards of range and  $Z_L$  is interpreted as the number of feet of layer depth, r is twice the number of surface reflections of the limiting ray out to range R, where

$$r = \frac{R}{\sqrt{Z_L}}.$$

Related scaled variables introduced for convenience are

$$z_x = \sqrt{Z_x/Z_L};$$

$$z_t = \sqrt{Z_t/Z_L};$$

<sup>C1</sup> This appendix was excerpted from references cited in footnotes C2 and C3.

<sup>C2</sup> H. W. Marsh and M. Schulkin, Report on the Status of Project AMOS (Acoustic, Meteorological, and Oceanographic Survey), 1 January 1953 - 31 December 1954, NUSL Report 255A, 23 March 1955.

<sup>C3</sup> W. H. Watson and R. W. McGirr, An Active Sonar Performance Prediction Model, NUC Technical Publication 286, April 1972.

and

$$r_1 = \begin{cases} \frac{1-z_x}{4} + \frac{1-z_t}{4}, & z_x \leq 1, z_t \leq 1, \\ \frac{1-z_x}{4} + \frac{\sqrt{z_t^2 - 1}}{5}, & z_x \leq 1, z_t > 1, \\ \frac{\sqrt{z_x^2 - 1}}{5} + \frac{1-z_t}{4}, & z_x > 1, z_t \leq 1. \end{cases}$$

When there is a surface duct, the near-surface propagation loss  $H$  is determined from equations (C-1) through (C-6).

#### DIRECT-RADIATION ZONE

When  $0 \leq r \leq r_1$  and both source and target depths are located within or at the bottom of the surface layer,

$$H = 20 \log (1000R/R_0) + \alpha R + (r/r_1) G(z_t, z_x), \quad (C-1)$$

where  $R_0$  is a reference range of 1 yd,  $\alpha$  is the absorption coefficient in decibels per kiloyard, and

$$G(z_t, z_x) = \begin{cases} 0.1 \times 10^{2.3(z_t - z_x)} (f/25)^{1/3}, & z_t - z_x < 1 \\ 20(f/25)^{1/3}, & z_t - z_x \geq 1 \end{cases} \quad (C-2)$$

For the direct-radiation zone, the smaller of the two propagation losses computed by equation (C-1) and by

$$H = 20 \log(1000R/R_0) + \alpha R + \left[ 25 - \sqrt{|Z_x - Z_L|} - \sqrt{|Z_t - Z_L|} + 5R \right] (f/25)^{1/3} \quad (C-3)$$

should be used. The quantity within brackets is taken as zero whenever negative.

## FIRST-ORDER SURFACE REFLECTION AND SHADOW ZONE

When energy has been reflected at least once off the surface, corresponding to  $r_1 \leq r \leq r_1 + 1/2$ , the following equation is used:

$$H = 20 \log(1000R/R_0) + \alpha R + 2(r-r_1) K(z_t, z_x) + [1 - 2(r-r_1)] G(z_t, z_x) + N_{co}, \quad (C-4)$$

where

$$K(z_t, z_x) = 0.4C_f [10^{z_x} + 10^{z_t} + 10^{(z_t-z_x)}], \quad (C-5)$$

with

$$C_f = \begin{cases} 1, & f < 8 \text{ (kHz)} \\ (f/8)^{1/3}, & f \geq 8 \text{ (kHz)}, \end{cases}$$

and  $N_{co}$  is the low-frequency-cutoff term described below. For this zone use either equation (C-3) or (C-4), whichever yields the lower propagation loss.

## SECOND- (OR HIGHER) ORDER SURFACE-REFLECTION ZONE

When energy has been reflected at least twice off the surface, corresponding to  $r > r_1 + 1/2$ , the following equation is used:

$$H = 10 \log(1000R/R_0) + \alpha R + K(z_t, z_x) + \alpha_s [R - \sqrt{Z_L}(r_1 + 1/2)] + 10 \log[1000 \sqrt{Z_L}(r_1 + 1/2)/R_0] + N_{co}, \quad (C-6)$$

where  $\alpha_s$  is the surface-reflection loss coefficient in decibels per kiloyard. For this zone use equation (C-3) or (C-6), whichever yields the lower propagation loss.



## SURFACE-REFLECTION LOSS COEFFICIENT

The expression for the surface-reflection-loss coefficient  $\alpha_s$  is given by

$$\alpha_s = \Gamma/R_b \text{ (dB/kyd)}, \quad (C-7)$$

where  $\Gamma$  is the surface-reflection loss in decibels and  $R_b$  is the bounce distance corresponding to the range between surface contacts for the surface-duct limiting ray. According to findings of Marsh and Schulkin,<sup>C4</sup>  $\Gamma$  is a function of the product of frequency and wave height, as given by

$$\Gamma = \begin{cases} 1.59\sqrt{fh}, & fh \geq 4.2691 \\ 10 \log [1 + (fh/4.14)^4], & fh < 4.2691, \end{cases} \quad (C-8)$$

$$(C-9)$$

where  $f$  is the frequency in kilohertz and  $h$  is the mean crest-to-trough wave height in feet. Figure C-1 illustrates surface loss per bounce as a function of the product of wave height and frequency.

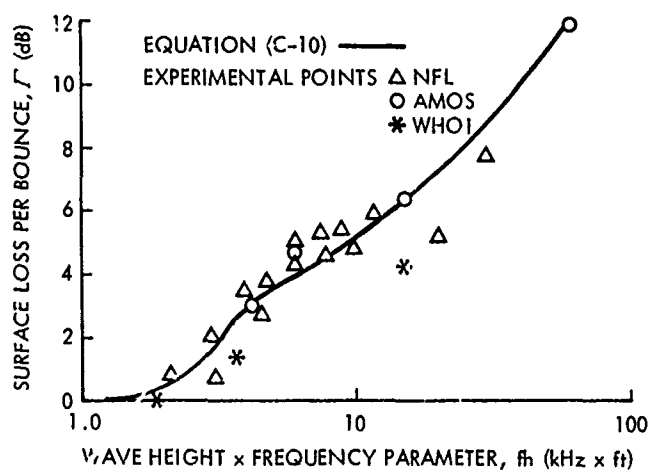


Figure C-1. Surface-Reflection-Loss Curve

<sup>C4</sup>Marsh and Schulkin, op. cit.

The bounce distance  $R_b$  is determined from

$$R_b = \sqrt{C_L^2 - C_s^2} / 1500 \gamma_0 \text{ (kyd) ,} \quad (\text{C-10})$$

where  $C_L$  and  $C_s$  are the sound velocities (ft/s) at the layer depth and the surface, respectively, and  $\gamma_0$  is the sound-velocity gradient ( $s^{-1}$ ) in the surface duct.

#### LOW-FREQUENCY-CUTOFF TERM

Arase and others<sup>C5-C11</sup> have reported the existence of low-frequency cutoff in surface-duct propagation. Thus an additive cutoff-loss term has been incorporated that is based on an approximation to the normal-mode surface-duct model

---

<sup>C5</sup> T. Arase, "Some Characteristics of Long Range Explosive Sound Propagation," Journal of the Acoustical Society of America, vol. 31, no. 5, May 1969, pp. 588-595.

<sup>C6</sup> M. A. Pedersen and D. F. Gordon, "Normal-Mode Theory Applied to Short-Range Propagation in an Underwater Acoustic Surface Duct," Journal of the Acoustical Society of America, vol. 37, no. 1, January 1965, pp. 105-118.

<sup>C7</sup> M. A. Pedersen and D. F. Gordon, Normal Mode Approach to Underwater Sound Propagation (U), NEL Report 1407, 27 September 1967 (CONFIDENTIAL).

<sup>C8</sup> C. S. Clay, "Sound Transmission in a Half Channel and Surface Duct," Meteorology International Incorporated, Project M-153, Technical Note Two 2:1-17, August 1968.

<sup>C9</sup> W. H. Furry, Theory of Characteristic Functions in Problems of Anomalous Propagation, Massachusetts Institute of Technology Laboratory Report 680, 1945; and Methods of Calculating Characteristic Values for Bilinear M Curves, Massachusetts Institute of Technology Report 795, 1946.

<sup>C10</sup> H. W. Marsh, Theory of the Anomalous Propagation of Acoustic Waves in the Ocean, NUSL Report 111, 12 May 1950.

<sup>C11</sup> D. F. Gordon and R. F. Hosner, "Underwater Sound Propagation in the Three-Layer Ducts Computed by Normal Modes," Naval Undersea Warfare Center Technical Paper 107, December 1968.

of Pedersen and Gordon, C12, C13 The  $n$ -th-mode amplitude  $A_n$  is closely approximated by

$$A_n = U_n(Z_x/Z_L) U_n(Z_t/Z_L) e^{-1000 \tau_n R}, \quad (C-11)$$

where  $U_n(Z_x/Z_L)$  and  $U_n(Z_t/Z_L)$  are depth-dependent functions of source and target depth and  $\tau_n$  is a mode-damping factor given by

$$\tau_n = (\pi f \gamma_0^2)^{1/3} \text{Im}(Mx_n) / C_s,$$

where  $\text{Im}(Mx_n)$  is the imaginary part of the  $n$ -th eigenvalue. Assuming that the empirical AMOS equations correspond to the fully ducted normal-mode situation, that  $U_n(Z_x/Z_L) U_n(Z_t/Z_L)$  is a slowly varying function of frequency near cutoff, and that contributions from second- (and higher) order modes are negligible, the cutoff term can be expressed as

$$N_{co} = 20 \log(e^{-1000 \tau_1 R}) \text{ (dB)}. \quad (C-12)$$

Figure C-2 shows the dependence of  $\text{Im}(Mx_1)$  on  $M$  and  $\rho$ . The parameters  $M$  and  $\rho$  are defined as

$$M = (8\pi^2 f^2 \gamma_0)^{1/3} Z_L / C_s, \quad (C-13)$$

and

$$\rho = -|\gamma_0 / \gamma_1|^{1/3}. \quad (C-14)$$

The quantity  $\gamma_1$  is the below-layer sound-velocity gradient ( $s^{-1}$ ). Cutoff effects start near  $M = 2.3$  and become extreme near  $M = 1.0$ . C14 A single curve corresponding to  $\rho = -0.48$  is used in the model. Thus in computing  $N_{co}$  the value for  $\text{Im}(Mx_1)$  is obtained by computing  $M$  and then interpolating from a curve of  $\text{Im}(Mx_1)$  versus  $M$ .

C12 Pedersen and Gordon, op. cit., footnote C6.

C13 Pedersen and Gordon, op. cit., footnote C7.

C14 Ibid.

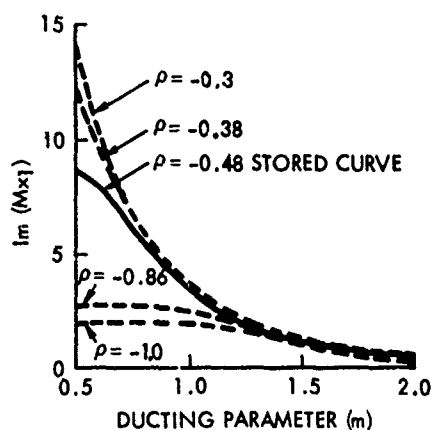


Figure C-2. Imaginary Eigenvalues  
for the First Mode

Propagation-loss computations over a wide range of frequencies for three different layer depths are shown in figure C-3. These computations were based on the normal-mode (total-energy) program of Watson and McGirr,<sup>C15</sup> the NISSM program, and the Fleet Numerical Weather Central (FNWC) approximate normal-mode expression<sup>C16</sup> as used in the Ship Helicopter Acoustic Range Pre-

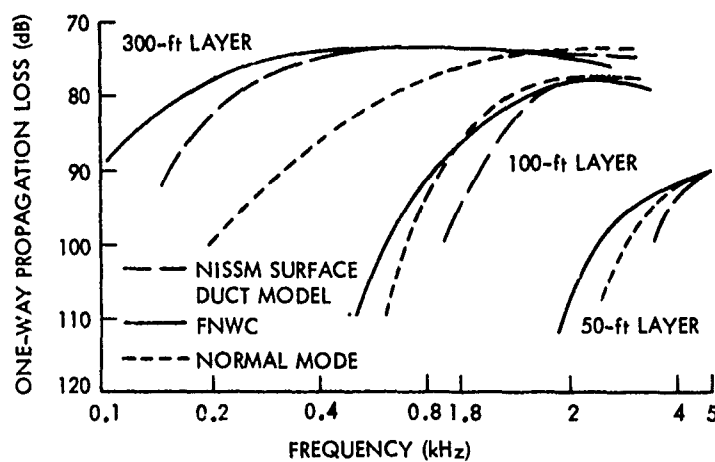


Figure C-3. Propagation Losses at 10 kyd Resulting  
from Surface-Duct Cutoff Adjusted to FNWC  
Maximum Propagation Losses

<sup>C15</sup>W. H. Watson and R. W. McGirr, "A Surface Channel Propagation Loss Model," NEL Technical Memorandum 921, 30 May 1966.

<sup>C16</sup>Clay, op. cit.

diction System (SHARPS) program. The results shown in figure C-3 are normalized with respect to the FNWC maximum values to better display the relative cutoff effects. This comparison shows that the FNWC cutoff is more gradual than the NISSM cutoff. However, this difference is expected, since the FNWC cutoff uses an asymptotic approximation to  $\text{Im}(Mx_n)$  that underestimates mode damping.